UNIVERSIDAD POLITÉCNICA DE VALENCIA

DEPARTAMENTO DE TECNOLOGÍA DE ALIMENTOS

Aplicación del análisis de imagen hiperespectral y tridimensional al control de procesos y productos en la industria harinera y sus derivados

Tesis Doctoral presentada por:

Samuel Verdú Amat

Directores académicos:

Raúl Grau Meló

José Manuel Barat Baviera

VALENCIA, FEBRERO 2016

AGRADECIMIENTOS

A mis tutores Raúl Grau y José Manuel Barat, por depositar su confianza en mí desde el primer minuto hasta el día de hoy y por su disponibilidad incansable. A mis compañeros María, Ana, Isabel, Carol, Arantxa, Joel…tanto por su ayuda como por su paciencia en multitud de momentos. A mis amigos Esteban, Francisco y Rafa, por estar ahí día a día. A Eugenio Ivorra y Antonio Sánchez, por su apoyo y esfuerzo en la materialización de mis ideas. A mi hermano Daniel, por mantenerse siempre tan fuerte. A mis tíos Alberto y Juana, y a mis primos Alberto, Verónica, José Antonio y Pablo, por estar ahí a pesar del paso del tiempo. A mis amigos impresentables David, Alejandro, Javi, Agustín, Nacho, José Antonio….por mantener intactos los niños que fuimos. A Francisco José Pérez Martínez, por enseñar a aquellos niños el pensamiento crítico, el respeto por la Naturaleza y la pasión por la ciencia y la razón en un entorno de oscuridad y adoctrinamiento. A los hombres serpiente que me llevan de viaje cada verano, ellos me enseñan a correr, nadar y trepar sin necesidad de tener brazos o piernas. A Patricia, por estar siempre ahí aguantando el chaparrón sin pedir nada a cambio. A todas las personas que han pasado por mi vida dejando o tomando algo y que es imposible citar aquí. A la Naturaleza, por dejarnos espiar sus intimidades. A mis padres Jesús y Milagros, por ser capaces de enseñarme tantas cosas en tan poco tiempo y a pesar de todo, nos veremos en el futuro.

Gracias!

“En los momentos de crisis, sólo la imaginación es más importante que el conocimiento”. **Albert Einstein**

“No voy a cambiar el mundo, pero puede que despierte a la persona que lo haga”. **Tupac Amaru Shakur**

ÍNDICE GENERAL *Pag.*

CAPÍTULO II: Relationship between fermentation behavior, measured with a 3D vision Structured Light technique, and the internal structure of bread

CAPÍTULO III: Study of high strength wheat flours considering their physicochemical and rheological characterisation as well as fermentation capacity using SW-NIR imaging

CAPÍTULO IV: Detection of adulterations with different grains in wheat products based on the hyperspectral image technique: the specific cases of flour and bread

CAPÍTULO V: Control of heat treatment process of wheat flour by SW-NIR image analysis

ÍNDICE DE TABLAS **Pag**

INTRODUCCIÓN

CAPÍTULO I

CAPÍTULO II

CAPÍTULO III

ÍNDICE DE FIGURAS

INTRODUCCIÓN

CAPÍTULO I

CAPÍTULO VII

CONSIDERACIONES PREVIAS

El trabajo realizado durante la tesis doctoral está dirigido al estudio y desarrollo de aplicaciones basadas en el análisis de imagen para el control de calidad y procesos en la industria harinera y de sus derivados. Las aplicaciones han sido enfocadas al análisis y control de materias primas (harinas), monitorización y caracterización de operaciones intermedias (fermentación, horneado, etc.), así como el análisis e inspección de producto terminado. Dichas aplicaciones también han sido aplicadas como herramienta de análisis en laboratorio para la caracterización de nuevos ingredientes y control de producto.

La tesis consta de siete capítulos divididos en dos bloques. El primer bloque recoge los capítulos 1, 2 y 3, los cuales están dedicados al desarrollo de las aplicaciones de imagen tridimensional basada en luz estructurada e imagen hiperespectral en relación a los procesos y materias primas utilizados. Instalación y calibrado de los equipos, estudio de la información obtenida y desarrollo de descriptores característicos. Todo ello en base al estudio de harinas de trigo destinadas a la producción en línea de pan de molde a escala industrial. El segundo bloque recoge los capítulos 4, 5, 6 y 7. En ellos se aplican conceptos y descriptores desarrollados en el primer bloque para objetivos diferentes, los cuales se enfocan a la caracterización de procesos concretos, análisis de producto acabado y estudio del comportamiento de nuevos ingredientes.

Los capítulos de la tesis corresponden a publicaciones independientes en diversas revistas internacionales (aceptados y en proceso de aceptación), por ello se presentan en inglés, el idioma original de estas. Al final del documento se presenta un anexo donde se recogen las publicaciones y participaciones en congresos realizados durante la elaboración del trabajo, tanto de la línea de investigación principal como de trabajos y colaboraciones complementarias durante del periodo.

RESUMEN

El presente trabajo está centrado en el estudio de los sistemas de análisis de imagen hiperespectral y tridimensional basado en luz estructurada para su aplicación en el control de procesos y calidad de la industria harinera y de sus derivados. El sistema de imagen tridimensional basado en luz estructurada fue la base para el desarrollo de un sistema de monitorización en continuo de la fase de fermentación de masas panarias. A partir de descriptores desarrollados relacionados con la variación de la forma del producto durante la operación, se establecieron diferencias entre lotes de harinas de trigo y describió el comportamiento de masas reformuladas con nuevos ingredientes. Dicho comportamiento fue analizado en conjunto con la estructura interna de la masa durante la operación, estableciendo relaciones concretas entre esta y la información obtenida a partir de las imágenes. Las diferencias de comportamiento durante la operación de fermentación también fueron estudiadas mediante el sistema de imagen hiperespectral. En este caso, las harinas fueron analizadas directamente mediante imágenes espectrales, obteniendo espectros de reflectancia difusa en el rango de longitudes de onda 400-1000, donde se observaron diferencias en determinadas bandas del espectro. Dichas diferencias fueron correlacionadas con determinados componentes fundamentales como el gluten. La caracterización espectral de la harina de trigo se utilizó posteriormente para la detección de cereales diferentes mezclados con esta. Adulteraciones de hasta un 2,5% de avena, sorgo y maíz fueron detectadas tanto en harina como

en panes de trigo. El análisis de imagen hiperespectral también ha sido aplicado al control del tratamiento térmico de harinas de trigo y avena, donde se ha conseguido relacionar la información espectral con las características del producto final.

ABSTRACT

This work is focused on studying of hyperspectral and structured light based tridimensional image analysis about their application on quality and process control of cereal flour industry and derived products. The structured light based tridimensional image analysis has been used to develop a bread dough dynamic fermentation control system. Descriptors obtained from dough shape evolution were used to describe differences between wheat flour batches during fermentation process. In the same way, that system was used to characterize the effect of new ingredients on fermentation process. Those behaviors were analyzed joint to the intern structure of dough during the process, establishing relationships between it and the tridimensional information. Differences in fermentation process were also studied using hyperspectral image analysis. Flours were analyzed using the obtained diffuse reflectance spectra, which contained information within 400-1000 nm of wavelength range. Differences in several spectral bands were correlated with fundamental components of flours such as gluten. That spectral characterization of flours was used to detect adulterations with different grains. Adulterations until 2, 5% of oat, sorghum and corn

were detected both flour and bread crumb. The hyperspectral image analysis was also used to control the heat treatment of wheat and oat flours, where spectral information was related to properties of end products.

RESUM

El present treball està centrat en l'estudi dels sistemes d'anàlisis d'imatge hiperespectral i tridimensional basat en llum estructurada per a la seua aplicació en el control de processos i qualitat de la indústria farinera i dels seus derivats. El sistema d'imatge tridimensional basat en llum estructurada va ser la base per al desenvolupament d'un sistema de monitoratge en continu de la fase de fermentació de masses panaries. A partir dels descriptors desenvolupats relacionats amb la variació de la forma del producte durant l'operació, es van establir diferències entre lots de farines de blat i es va descriure el comportament de masses reformulades amb nous ingredients. Aquest comportament va ser analitzat en conjunt amb l'estructura interna de la massa durant l'operació, establint relacions concretes entre aquesta i la informació obtinguda a partir de les imatges. Les diferències de comportament durant l'operació de fermentació també van ser estudiades mitjançant el sistema d'imatge hiperespectral. En aquest cas, les farines van ser analitzades directament mitjançant imatges espectrals, obtenint espectres de reflectància difusa en el rang de longituds d'ona 400-1000, on es van observar diferències en determinades bandes de l'espectre. Aquestes

diferències van ser correlacionades amb determinats components fonamentals com el gluten. La caracterització espectral de la farina de blat es va utilitzar posteriorment per a la detecció de cereals diferents barrejats amb aquesta. Adulteracions de fins a un 2,5% de civada, sorgo i dacsa van ser detectades tant en farina com en pans de blat. L'anàlisi d'imatge hiperespectral també ha sigut aplicat al control del tractament tèrmic de farines de blat i civada, on s'ha aconseguit relacionar la informació espectral amb les característiques del producte final.

1 INTRODUCCIÓN

1.1. La actualidad en la industria de producción de alimentos

Una parte importante de los avances presentados en los últimos años dentro del área de la producción y transformación industrial de alimentos ha estado centrada en la mejora tanto de procesos como de productos (Ostrouh & Kuftinova, 2011). Los avances científicos en materia de alimentos, tanto a nivel básico como en ciencia aplicada, han revelado un amplio abanico de conocimientos en base a los cuales se ha facilitado el desarrollo de nuevos productos y nuevas técnicas de procesamiento, así como a la optimización de procesos ya existentes o sustitución de estos por otros más eficientes (Shafie & Abdul, 2013).

En este sentido, es de notable importancia el campo de desarrollo relativo a técnicas de análisis y control de calidad antes, durante y después del proceso productivo.

La tendencia predominante al respecto es la de la experimentación y desarrollo de nuevos métodos de control de calidad que mejoren a los tradicionales en velocidad, precisión y exactitud (Caldwell, 2013). Así pues, uno de los objetivos ha sido el desarrollo de métodos rápidos, no destructivos, predominantemente con capacidad de trabajo en continuo a pie de línea. Por otra parte la sencillez en cuanto a fundamentos, adaptabilidad y robustez, así como un fácil manejo y mantenimiento, han sido algunas de las premisas básicas del área.

La finalidad de todo ello estriba en la necesidad de aumentar el rendimiento y con ello mejorar el aprovechamiento de las materias primas para así ofrecer al mercado productos con una calidad higiénica, nutricional y organoléptica acorde a la demandada (Huang, 2001). Todo ello fortalece otro pilar fundamental de las empresas, la competitividad, la cual produce una estimulación del desarrollo de tecnologías que aseguren las premisas anteriormente mencionadas.

Finalmente, a pesar de las generalidades que engloba la industria de alimentos, las necesidades específicas en cuanto a mejora de operaciones dentro de la cadena de procesado van a venir dadas por las propias peculiaridades del sector al que pertenezca el producto y sus especificaciones de presentación final.

1.2 Nuevas tendencias y mejoras: Análisis rápidos no destructivos

Los volúmenes de producción de alimentos actuales junto con el transporte de estos a través de fronteras nacionales, generan problemas a la hora de aplicar métodos tradicionales de control de procesos y calidad. La mayoría de estos métodos están basados en técnicas de muestreo estadístico y análisis destructivos, los cuales requieren de tiempos relativamente prolongados de análisis (Kondo, 2010) además, la mayoría de los métodos homologados para cualquier tipo de peligro (biológico, químico o físico) requieren de espacios y equipos de análisis específicos, así como reactivos,

elevando el costo de las operaciones económica y medioambientalmente. Los análisis no destructivos en general pretenden, no solo aumentar la velocidad de análisis, sino reducir la dependencia de reactivos, procesamiento y/o derivatización de las muestras, pudiendo llegar a analizar todas y cada una de las unidades de un lote de productos a través de la cadena de producción, evitando la incertidumbre intrínseca de los muestreos estadísticos tradicionales (Leemans et al., 2002). Así pues, dichas aplicaciones son susceptibles de ser aplicadas en cada operación de la cadena de producción. La monitorización de ciertas operaciones es clave en determinados sectores, pues permite la corrección en tiempo real de las condiciones para así reducir mermas, mantener los niveles de seguridad, reducir costos y en general optimizar el proceso (Bajd & Serša, 2011b).

Existen diversos principios a partir de los cuales se han desarrollado diferentes aplicaciones de análisis no destructivos. Los principales se podrían recoger en aplicaciones basadas en los ultrasonidos, electroquímicas y análisis de imagen. Por ejemplo los ultrasonidos han sido aplicados con éxito en el control en continuo del salado en jamones (De Prados et all., 2016). En el caso de las propiedades electroquímicas, diversos dispositivos han sido desarrollados en base a la potenciometría, impedancia o voltametría. Con ello, diferentes tipos de equipos de punción y de contacto superficial, tales como lenguas electrónicas, han sido aplicados en operaciones como el control del salado en carne de cerdo (García-Breijo et al., 2008; Gil-Sánchez et al., 2015) o detección de materia prima alterada

microbiológicamente en la elaboración de jamón curado (De Jesús et al., 2014). También desde el punto de vista de las propiedades dieléctricas se han realizado aplicaciones tales como el control de temperatura en el proceso de secado de vegetales (Ozturk et al., 2016) o la monitorización del proceso de congelación-descongelación de atún (Llave et al., 2014).

En el caso del análisis de imagen, el abanico de técnicas es muy amplio, probablemente por la versatilidad que presentan sus elementos y la posibilidad de combinarlos desde diferentes puntos de vista en función del objetivo. Así pues, en éste sentido, se dispone de diversas técnicas con fundamentos y aplicaciones diferentes. El tipo más sencillo es el análisis de imagen 2D, donde ésta es analizada en base a la matriz de píxeles que la forman, determinando sus colores y tonos, dependiendo del espacio de color utilizado y la cantidad de información de cada imagen. A partir de esta información se localizan áreas, circunferencias, contornos, perímetros y formas, las cuales corresponden a umbrales de color determinados, logrando de esta manera dividir la matriz en segmentos en función de la información requerida. Esta técnica ha dado buenos resultados en funciones como la determinación del tamaño y distribución de burbujas en pan durante la fermentación y horneado (Lassoued et al., 2007; Pérez-Nieto et al., 2010), así como en el estudio de la deformación del pan durante la masticación (Tournier et al, 2012). La información de los píxeles puede ser función de los colores que presentan los objetos capturados de la escena, si

se trata de trabajos en el espectro visible (el caso más sencillo), pero también puede ser función de la temperatura, si lo que se está analizando es la radiación infrarroja que emite un objeto por encima de 0K, obteniendo así un mapa de temperaturas de la superficie del mismo. En este último caso se trataría de termo-imágenes, las cuales han sido aplicadas con éxito en aplicaciones como la detección de cuerpos extraños en galletas (Senni et al., 2014) o la monitorización del secado de manzanas (Cuccurullo et al., 2012).

Otro tipo de análisis de imagen sería el de imágenes espectrales. En éste caso, se analiza de mismo modo la información de los paquetes de píxeles, así como su localización y forma, sin embargo, se añade una dimensión más, la longitud de onda, a través de la cual se determinan máximos y mínimos de una propiedad dada (absorbancia, reflencancia, transmitancia). En este grupo de técnicas las diferencias se basan en el rango espectral de trabajo (ultravioleta, visible, infrarrojo, etc.), la propiedad analizada, etc. Dichas técnicas ha sido aplicada para detectar fraude en carne picada (Ropodi et al., 2015) o detectar contaminaciones fúngicas en granos de maíz (Williams et al., 2009), entre otros. Los rayos X y resonancia magnética nuclear también son aplicados de forma común. En el caso de las imágenes de rayos X para el seguimiento de la evolución del tamaño de burbujas en masas panarias (Koksel et al., 2015) y la determinación de la densidad de diversos alimentos (Kelkar et a., 2015). En el caso de la imagen de resonancia magnética, las aplicaciones han sido principalmente de laboratorio o científicas de

base, esto es debido a su alto coste y a que su velocidad es relativamente limitada a día de hoy para su implementación dentro de una cadena de producción. A pesar de ello, dicha técnica ha dado buenos resultados en el estudio del efecto de nuevos componentes como la soja, en masas panarias congeladas (Simmons & Vodovotz, 2012) o la monitorización de la fermentación de masas (Bajd & Serša, 2011a).

Otro tipo de análisis de imagen es la tridimensional, el cual engloba varias técnicas basadas en diferentes tipos de sensores, fuentes de luz y algoritmos para generar la información 3D. Con ellas es posible determinar formas, volúmenes y texturas que resultan de gran utilidad dentro de la industria de alimentos. Algunas de las aplicaciones llevadas a cabo han sido en campos generales como el de la determinación de volúmenes en frutas (Omid et al., 2010) o más específicos tales como el estudio de propiedades térmicas de granos de café (Fabbri et al., 2011).

Finalmente, mencionar otros tipos de análisis de imagen que también han sido aplicados con éxito dentro de este campo, tales como la imagen de fluorescencia o la imagen obtenida a partir de ultrasonidos. Ambas se están aplicando con éxito en diferentes campos tales como el control de superficies en contacto con alimentos en espacios de procesamiento (Everard et al., 2016) o para el control de la evolución de las densidades en diferentes alimentos (Gan et al., 2006).

1.3 La automatización en la industria de cereales

La industria de cereales y derivados ha sufrido una constante modificación y mejora de sus procesos y operaciones. De modo que, aun teniendo una gran carga artesanal y desarrollo tradicional en determinados colectivos y zonas geográficas, la demanda masiva de sus derivados por el creciente número de habitantes, así como su importancia en el aporte energético y nutricional diario de la dieta humana y animal, genera la necesidad de aumentar los rendimientos tanto en producción primaria como en transformación.

Tanto las materias primas involucradas como las operaciones específicas en cada línea de procesado presentan propiedades y características que las hacen susceptibles de ser controladas y mejoradas mediante automatismos y mecanizaciones. A modo de ejemplo, el proceso de elaboración de pan de forma industrial ha sido modificado y automatizado al 100% en algunos casos, consiguiendo mejoras en rendimientos y aprovechamiento de recursos cada vez superiores. La Figura 1 muestra un esquema básico del proceso de elaboración de pan, en el cual se muestran variables fundamentales a tener en cuenta relacionadas con la materia prima, el proceso y el producto acabado.

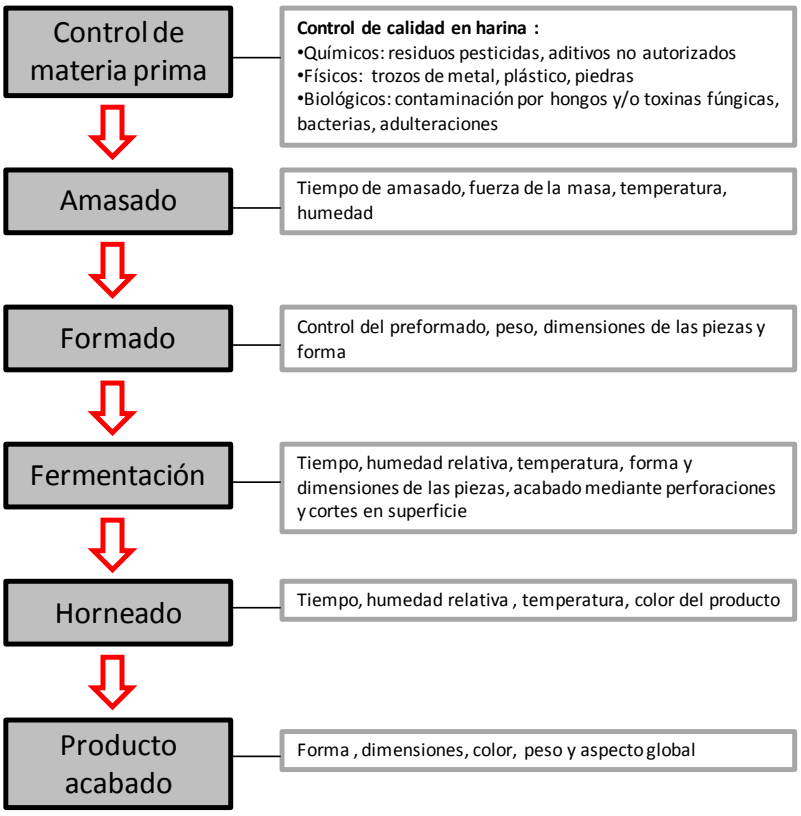

Figura 1. Esquema del proceso de fabricación de pan. Operaciones, variables principales y sistemas y técnicas de automatización utilizadas en la industria.

Existe la posibilidad, a día de hoy, de controlar todas ellas mediante automatismos basados en diversas técnicas que permiten tener un control total del proceso, asegurando el buen funcionamiento de este así como la calidad y seguridad del producto.

En este sentido, cada fabricante adapta la automatización de las líneas a sus necesidades y/o posibilidades, así como el proceso en sí. Además de las operaciones indicadas en el esquema, se puede encontrar otras diferentes tales como el control del almacenamiento de materias primas, abatimiento de temperatura, congelación del producto acabado, control de almacenamiento de producto acabado, control del envasado, etc. Todo ello hace que la oferta de nuevos dispositivos de control, tanto de aplicación en línea de producción, como en laboratorio, sea cada vez más amplia por parte de empresas tecnológicas. Del mismo modo, a nivel científico representa un amplio campo de investigación con expectativas de aplicación a corto plazo.

1.4 Visión tridimensional basada en luz estructurada

Una clasificación muy común para entender los sistemas de visión 3D es la referida a su interacción con la escena (Moreda et al., 2009) . Si no existe ninguna interacción se denominan pasivos, los cuales extraen la información a partir de una o más imágenes 2D e intentan estimar la forma de las superficies capturadas mediante la orientación de los puntos que la forman. La información en este tipo de sistemas es obtenida mediante diversas técnicas. Algunas de ellas son la estéreo-visión, imagen basada en generación de sombras, siluetas, contornos de oclusión, movimiento o geometría fractal. Con excepción de la técnica de estéreo-visión, el resto de técnicas basadas en el análisis de formas no pueden calcular directamente la profundidad de la escena, tan solo pueden hacerlo de forma relativa,

lo que conlleva a la asunción de un grado de error intrínseco difícilmente evitable. Del mismo modo, son sistemas monoculares que obtienen información tridimensional a partir de la imagen obtenida desde una sola dirección. Por el contrario, la técnica de estéreo-visión obtiene información a partir de dos imágenes capturadas desde dos direcciones diferentes. La información tridimensional se confecciona en base a la localización de puntos concretos de la escena en ambas imágenes, que por triangulación son combinados para acabar obteniendo datos de profundidad de la escena (Hryniewicz et al., 2005).

Los sistemas de visión tridimensional activos, tienen como principal característica su interacción con la escena y/o muestra. Dentro de este grupo se pueden encontrar técnicas basadas en interferometría, rayos X, campos magnéticos, luz estructurada o tiempo de vuelo. Estas técnicas son dependientes de la emisión de una señal la cual debe interactuar con la escena de una u otra manera, para así determinar las diferencias presentadas con respecto a la escena vacía. Dichas señales suelen ser radiación electromagnética pertenecientes a diferentes zonas del espectro, la cual interacciona con la muestra y devuelve información al sensor en cuestión.

Concretamente, Los sistemas de visión tridimensional basados en luz estructurada tienen como componentes fundamentales un láser y un sensor. La técnica se basa en la proyección del láser (luz estructurada) sobre el objeto u escena, el cual genera un patrón de luz de forma conocida, la cual varía en función de las geometrías que

interactúan con él. Así pues, la captura de dichos patrones de luz mediante imágenes y su posterior análisis permite obtener información acerca de la forma del objeto y con ello parámetros como el volumen (Feng et al., 2012). Existen diferentes tipos de láser en función de su patrón de luz, uno de los más utilizados es el lineal, aunque también existen punteros para los casos más simples y combinaciones lineales tipo cuadricula o malla, para casos donde se requiere mayor grado de exactitud o detalle. Tanto el láser como la cámara están dispuestos a distancias y ángulo conocidos de la escena (Figura 2) donde, por triangulación, se realiza un calibrado previo, el cual sirve para determinar las equivalencias en medida de profundidad y patrón de variación del láser.

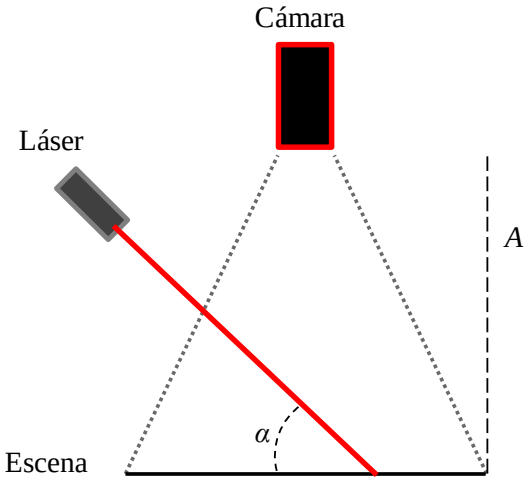

Figura 2. Esquema básico del sistema de imagen tridimensional basado en luz estructurada. A: distancia entre la escena y la cámara; α: ángulo entre el plano de la escena y el láser.

Otro factor fundamental es la existencia de movimiento y/o variación de la forma del objeto para interaccionar con el láser. Para ello, son usadas comúnmente cintas transportadoras que deslizan el objeto por la escena para así registrar las variaciones producidas en el patrón de luz con el tiempo. La Figura 3 muestra un esquema de un sistema tipo, donde t_1 es una captura de imagen con la escena vacía, en la cual el patrón de luz láser esta inalterado, es decir, proyectando el patrón original de la fuente luminosa, pues ningún elemento está interceptando su trayectoria. Así pues, la posición del láser se correlaciona con el valor en el eje Z (altura). La posición a tiempo 1 (t_1) de la Figura 3 por lo tanto indica altura igual a 0. Cuando la cinta transportadora mueve la muestra esta comienza a interceptar la trayectoria del láser. Este es el momento t_2, donde se produce una variación recogida por la imagen, la cual equivale a una altura concreta según la calibración previa. Dicha variación indica que el valor del eje Z deja de ser 0. En el momento t_3 ocurre lo mismo que en t_2, pero en este caso dos zonas de la muestra con alturas diferentes interceptan la trayectoria del láser. Así pues, el patrón de luz permite diferenciar dos valores diferentes en el eje Z. El esquema muestra un sistema con una muestra de forma simple, pero en situaciones reales pueden determinarse tantos valores en el eje Z como píxeles contenga la resolución de la imagen capturada, pudiendo obtenerse información muy precisa al respecto.

El conjunto de variaciones en el tiempo es integrado para obtener la información tridimensional, donde las variaciones en el eje X

determinan la anchura del objeto, la altura (eje Z) es la cantidad de desplazamiento de la línea láser respecto a un punto de referencia tal y como se ha explicado anteriormente, el cual suele ser uno de los límites laterales de la imagen, y finalmente la longitud (eje Y), la cual viene determinada por el tiempo total que la línea láser presenta interacción con el objeto.

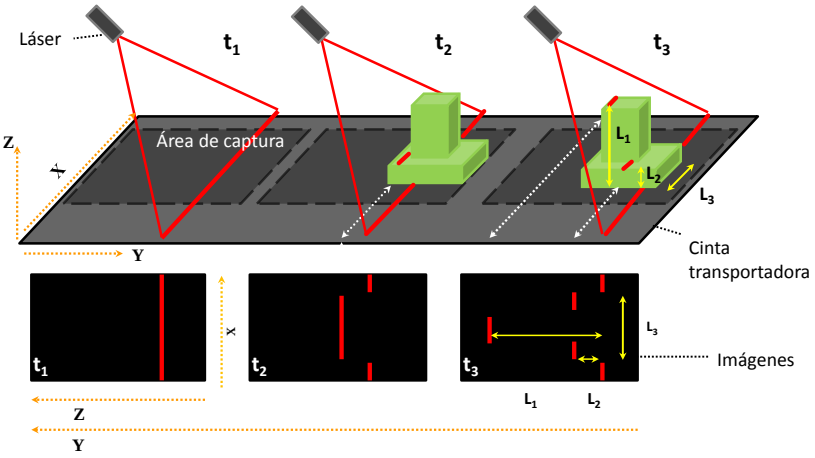

Figura 3. Esquema de funcionamiento básico de la técnica de imagen tridimensional basada en luz estructurada. XYZ: ejes cartesianos 3D; t_n: puntos de captura en el tiempo; L_n: medidas de la muestra.

1.5. Fundamentos de espectroscopía

La espectroscopía es una técnica muy extendida de gran peso dentro de los sistemas analíticos y quimiométricos actuales. Está basada en la interacción entre radiación electromagnética y materia, la cual tiene implicaciones directas sobre las características moleculares de los componentes que forman la muestra. Dos de las franjas más importantes del espectro electromagnético aplicadas en alimentos son la visible y la infrarroja (IR) (Safren et al., 2007). Aunque se encuentran en posiciones contiguas dentro del espectro electromagnético, sus longitudes de onda y frecuencias determinan mecanismos diferentes de interacción y por lo tanto diferencias considerables en su interpretación. La zona visible representa frecuencias capaces de inducir la excitación electrónica y transición de electrones enlazantes, mientras que la infrarroja produce vibraciones en los enlaces moleculares (Steinfeld, 1989).

Dado que ambas producen efectos diferentes, es importante destacar que no existe influencia de uno sobre el otro, pues los tiempos característicos de transición electrónica y de vibración molecular son muy desiguales. El principio de Frank-Condon establece que el tiempo de una transición electrónica es tan reducido, que los núcleos implicados no dejan de ser estáticos, y puesto que las vibraciones moleculares implican cambios en las distancias entre núcleos, se infiere que las escalas de tiempos no pueden ser comparables y por lo tanto, un fenómeno no se ve influido por el otro. Así pues, la información obtenida de cada zona del espectro se asume independiente.

En alimentos, la franja visible se suele analizar mayormente desde el punto de vista del análisis de espacios de color, mientras que el infrarrojo en forma de espectrometría clásica. Ésta última es la base de numerosos equipos de análisis químico de alimentos, los cuales incluso prescinden de la franja visible. Así pues, puesto que las transiciones electrónicas implican conceptos mecanocuánticos complejos que escapan al objetivo de la tesis, se pondrán de manifiesto las bases conceptuales de la espectroscopía de infrarrojos por su mayor aporte en el entendimiento de los resultados obtenidos.

La interacción entre radiación infrarroja y molécula depende de diversos factores. En primer lugar la presencia de momento dipolar, además de los grados de libertad vibracionales de la molécula en cuestión, los cuales van a determinar los modos y frecuencias de vibración posibles (Hollas, 1996). El segundo lugar la frecuencia de la radiación con la que interactúa. Así pues, la interacción de la radiación infrarroja con los estados vibracionales del momento dipolar de una molécula sólo es posible si el vector eléctrico de la radiación incidente oscila con la misma frecuencia que éste. Por lo tanto, dado que una molécula presenta un número finito de modos vibracionales (también llamados armónicos o sobretonos), su espectro infrarrojo puede presentar dicho número de bandas de actividad como máximo, cuyas frecuencias son proporcionales a la energía necesaria para la transición a cada uno de ellos (Svanberg,

1992). La Tabla 1 muestra algunos ejemplos de grupos funcionales y sus de bandas de absorción típicas.

Tabla 1. Bandas de absorción de diferentes grupos funcionales en el infrarrojo cercano (NIR)

Grupo Funcional	**1er sobretono (nm)**	**2do sobretono (nm)**	**3er sobretono (nm)**
CH	1680-1750	1175-1230	910-930
CH_2	1675-1750	1140-1220	890-930
CH_3	1625-1710	1120-1190	870-915
Ar-CH	1620-1650	1070-1100	850-870
R-HO	1410-1475	920-940	725-740
Ar-OH	1380-1420	930-960	725-730
H_2O	1850-1920	1400-1450	950-980
R-COOH	1875-1910		
R-COO-R´	1925-1975		
R-NH2	1480-1520	1020-1090	760-820
CONH2	1920-1925	1470-1490	
R-NH-R´			800-825

La interpretación práctica de todo ello se basa en el análisis de los espectros referentes a una propiedad concreta (absorbancia, reflectancia, transmitancia, interactancia,, etc.), en base a la cual, se interpretará la información con respecto a la presencia/ausencia de un determinado componente o la concentración de éste.

1.6. El sistema de imagen espectral

El análisis de imagen espectral se basa en la obtención de un conjunto de imágenes de una misma escena, objeto o muestra, cada una de las cuales pertenece a una longitud de onda diferente dentro de un rango específico del espectro electromagnético. El sistema está formado por una fuente luminosa o iluminante y una cámara. Dichos elementos pueden variar dependiendo del tipo de información que se desee adquirir. Las variantes en el sistema vienen dadas por la potencia y espectro de los iluminantes, tipo de captura de las cámaras, filtros ópticos, etc., en función de los requerimientos.

El conjunto de información obtenida se enmarca en un espacio tridimensional formado por los dos ejes del plano de la imagen (longitud (X) y anchura (Y)) y un tercero que es la longitud de onda (ʎ). El pixel es la unidad de información de la imagen, de modo que los píxeles en los que está dividida cada imagen en el plano contienen información en esas tres dimensiones. En primer lugar su posición en el plano de la imagen dentro de los ejes X e Y (constante para todas las imágenes a cualquier ʎ), y en segundo lugar el valor relativo a la propiedad medida (reflectancia, transmitancia, absorbancia, etc.), la cual es variable en función de cada ʎ. A éste conjunto de información también se le denomina “cubo espectral” o “hipercubo” y a los píxeles que lo forman “vóxeles”, haciendo referencia a píxeles tridimensionales o píxeles volumétricos con coordenadas en tres ejes diferentes. En resumen, el análisis de imagen espectral une las dos funciones básicas de los tradicionales espectrómetros IR y el análisis

de imagen 2D. Por un lado obtiene información espectral y por otro, a su vez es, capaz de situarla espacialmente sobre la imagen.

La Figura 4 muestra un esquema del concepto de imagen espectral. En el esquema se observa a modo de ejemplo la imagen original de una muestra de carne y las correspondientes a diferente ʎ a lo largo del espectro. La localización de los píxeles en X e Y permite conocer si éstos pertenecen a la zona de tejido magro o graso, de tal manera que una vez determinados los píxeles pertenecientes a dichos tejidos es posible aislar los espectros por separado de cada una de las partes de la imagen, o viceversa. En el caso de muestras sin partes diferenciadas, tales como alimentos pulverulentos (harinas), granulados (granos de cereal, tejidos triturados, etc.) o que contengan una sola fase desde el punto de vista macroscópico (quesos, emulsiones cárnicas, yogurt, etc.), la información de localización de píxeles en la imagen es a priori menos relevante, pues son muestras homogéneas, sin embargo resulta de gran utilidad para la discriminación del envase y rótulos de este en productos envasados. También resulta ventajoso desde el punto de vista de velocidad de obtención de datos, pues la información espectral de cada píxel de la imagen de una muestra homogénea puede considerarse como una réplica independiente tomada en diferentes zonas de esta, solo que mediante una sola captura.

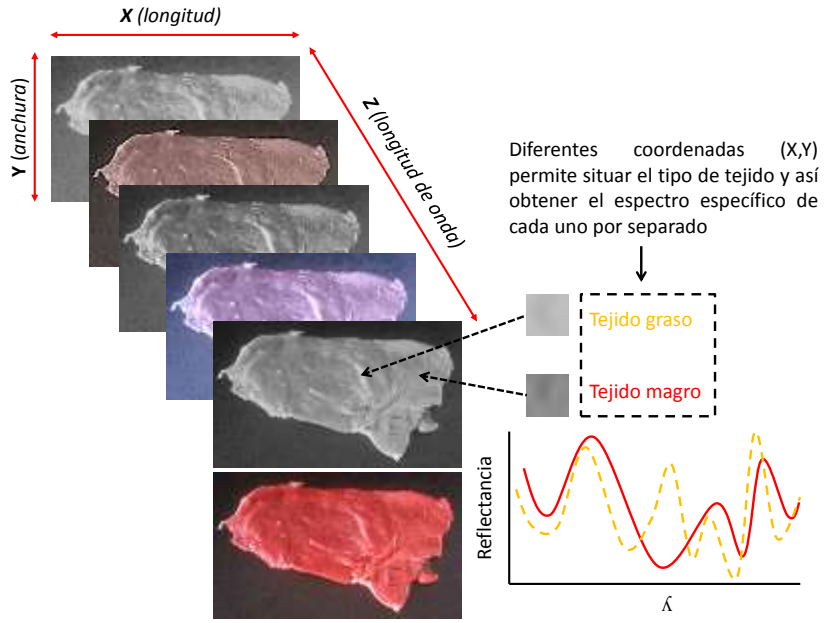

Figura 4. Esquema conceptual de imagen espectral

1.7. Tipos de imagen espectral

Dentro de esta técnica existen varios sistemas cuya diferencia radica en la cantidad de información obtenida y su disposición, es decir, el número de bandas espectrales dentro de un rango de longitudes de onda o frecuencias dadas. La imagen multiespectral recoge un número relativamente reducido de bandas espectrales, hasta de 20 como máximo, las cuales pueden o no ser contiguas. La imagen hiperespectral recoge un mayor número de bandas y siempre contiguas. Así pues, la información multiespectral se recoge en bloques discretos a lo largo del espectro, mientras que la

hiperespectral está en forma de espectro continuo de resolución considerablemente mayor (NASA/Headwall Photonics). Finalmente existen sistemas que mejoran la resolución hiperespectral llamados ultraespectrales, los cuales ofrecen una resolución máxima, aunque son menos utilizados por su alto costo y baja versatilidad. La figura 5 muestra un esquema conceptual del sistema multiespectral y el hiperespectral.

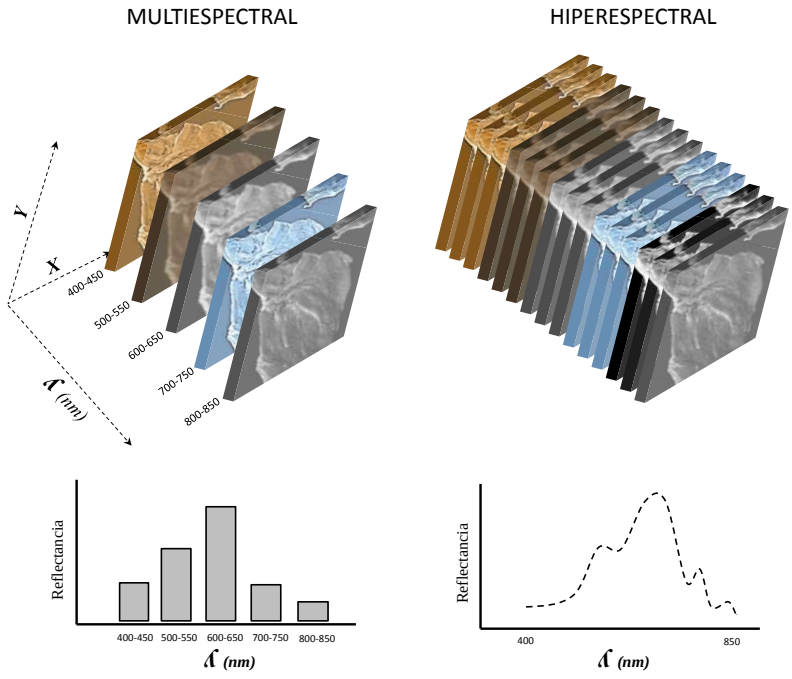

Figura 5. Esquema conceptual de los sistemas de imagen multiespectral e hiperespectral

1.8. Sistemas de adquisición de imagen espectral

El tipo de adquisición de imágenes también es un factor influyente sobre la cantidad de información obtenida en cada captura. Existen sistemas de adquisición diferentes dependiendo de la extensión de la escena que sea capaz de capturar, así como del rango de longitudes de onda disponibles para esta. La figura 6 muestra esquemáticamente los sistemas de captura disponibles y sus diferencias en función del eje o dimensión del hipercubo en el que trabajen. El sistema puntual es el más sencillo y trabaja tan solo en el eje de longitud de onda, de tal manera que recoge tan solo el espectro de este sin posibilidad de obtener espectros de diferentes posiciones a lo largo y ancho del plano de la escena. Dicho sistema ofrece la misma información que un espectrómetro tradicional pero sin necesidad de contacto, cuyo receptor captura el espectro de un punto aislado, sin tener en cuenta su posición, de forma automática. El sistema puntual puede recoger diferentes puntos de la muestra siempre que se desplace manual o automáticamente hasta diferentes zonas de la muestra. El sistema lineal captura información a lo largo de una linea recta de píxeles de longitud determinada. Así, éste sistema trabaja en dos dimensiones del hipercubo: X o Y y ʎ, donde se observa como la recta de captura recoge el eje X completo a lo largo de todo el eje de longitud de onda. La información espectral en este caso sí puede ser estudiada en función de su posición a lo largo del eje X, y por lo tanto en diferentes zonas de la muestra u escena capturada. En el caso de la captura en área, el alcance de la imagen obtenida es de todo el plano delimitado por X e Y, sin embargo no

existe movilidad a lo largo del espectro, es decir, recoge información espectral de todo el área pero tan solo a una longitud de onda o intervalo espectral específico. Por último, el sistema de captura única captura el hipercubo completo a lo largo sus tres dimensiones.

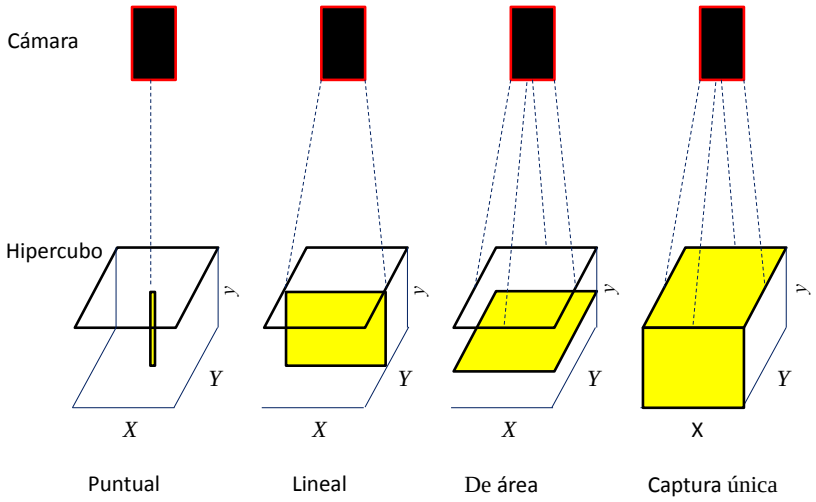

Figura 6. Sistemas de captura de cámaras espectrales

1.9. Modos de adquisición de imagen espectral

El modo en el que se dispone el iluminante en el sistema con respecto a la muestra y cámara es determinante sobre la interacción entre la radiación emitida por éste y el material de la muestra y con ello sobre el tipo de información obtenida. Así, el modo de detección está determinado por dicho factor y suelen ser tres los tipos más usados en la captura de imagen espectral. La figura 7 muestra el esquema de éstos tres modos. En el caso del modo de reflectancia, el

iluminante está situado en ángulo con la muestra de forma que se favorezca una reflexión, sea especular o difusa, que permita a la cámara capturar la radiación que no es absorbida por la muestra. Este modo es útil para determinar propiedades de superficie de las muestras o de la zona continua a ésta hacia el interior del material pero siempre las zonas más superficiales (Pan et al., 2016).

En el modo de transmitancia el iluminante es dispuesto en sentido opuesto a la cámara, de manera que la radiación emitida tenga que atravesar la muestra en cuestión para ser captada. A diferencia del modo de reflectancia, este modo permite obtener información acerca de las propiedades internas de la muestra a lo largo de todo su espesor (Leiva-Valenzuela et al., 2014). En el modo de interactancia, el iluminante está dispuesto en la misma dirección y sentido que el objetivo de la cámara. Podría considerarse un sistema intermedio entre el de reflectancia y transmitancia. La situación del iluminante no está pensada para favorecer la reflexión especular, sino que se pretende que la radiación penetre en mayor medida dentro del material de la muestra y el remanente vuelva a salir para ser detectado por la cámara. De este modo se obtiene información de zonas más profundas de la muestra en comparación con el modo de reflectancia y a su vez evita los problemas que pueden aparecer en el modo de transmitancia por la influencia del espesor de ésta, el cual puede llegar a anular la señal (Hu et al., 2016).

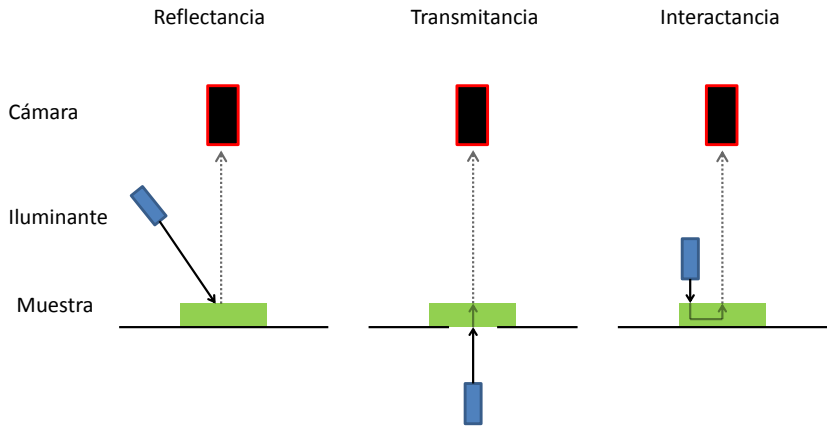

Figura 7. Modos de adquisición según la posición de los elementos del sistema: cámara, iluminante y muestra.

1.10. Bibliografía

Bajd, F., & Serša, I. (2011a). Continuous monitoring of dough fermentation and bread baking by magnetic resonance microscopy. *Magnetic Resonance Imaging*, *29*, 434–442.

Bajd, F., & Serša, I. (2011b). Continuous monitoring of dough fermentation and bread baking by magnetic resonance microscopy. *Magnetic Resonance Imaging*, *29*(3), 434–42.

Caldwell, D. Robotics and Automation in the Food Industry (2013), , Woodhead Publishing Ltd., AbingtonHall, Cambridge CB21 6AH, UK. ISBN: 978-1-8456-9801-0

Cuccurullo, G., Giordano, L., Albanese, D., Cinquanta, L., & Di Matteo, M. (2012). Infrared thermography assisted control for apples microwave drying. *Journal of Food Engineering*, *112*, 319–325.

De Jesús, C., Hernández-Coronado, G., Girón, J., Barat, J. M., Pagan, M. J., Alcañiz, M., … Grau, R. (2014). Classification of unaltered

and altered dry-cured ham by impedance spectroscopy: a preliminary study. *Meat Science*, *98*, 695–700.

De Prados, M., Garcia-Perez, J. V., & Benedito, J. (2016). Ultrasonic characterization and online monitoring of pork meat dry salting process. *Food Control*, *60*, 646–655.

Everard, C. D., Kim, M. S., & Lee, H. (2016). Assessment of a handheld fluorescence imaging device as an aid for detection of food residues on processing surfaces. *Food Control*, *59*, 243–249.

Fabbri, A., Cevoli, C., Alessandrini, L., & Romani, S. (2011). Numerical modeling of heat and mass transfer during coffee roasting process. *Journal of Food Engineering*, *105*, 264–269.

Feng, J., Liu, G., Wang, S., Zeng, L., Ren, W., (2012). A novel 3D laser vision system for robotic apple harvesting. In: ASABE Annual International meeting presentation. Paper Number: 12-1341025, St. Joseph, MI.

Gan, T. H., Pallav, P., & Hutchins, D. a. (2006). Non-contact ultrasonic quality measurements of food products. *Journal of Food Engineering*, *77*, 239–247.

García-Breijo, E., Barat, J. M., Torres, O. L., Grau, R., Gil, L., Ibáñez, J., Fraile, R. (2008). Development of a puncture electronic device for electrical conductivity measurements throughout meat salting. *Sensors and Actuators, A: Physical*, *148*, 63–67.

Gil-Sánchez, L., Garrigues, J., Garcia-Breijo, E., Grau, R., Aliño, M., Baigts, D., & Barat, J. M. (2015). Artificial neural networks (Fuzzy ARTMAP) analysis of the data obtained with an electronic tongue applied to a ham-curing process with different salt formulations. *Applied Soft Computing*, *30*, 421–429.

Hryniewicz, M., Sotome, I., Anthonis, J., Ramon, H., De Baerdemaeker, J., (2005). 3-D surface modeling with stereovision. In: Hertog, M.L.A.T.M., Nicolaï, B.M., (Eds.),

Proceedings of the 3rd International Symposium on Applications of Modeling as an Innovative Technology in the Agri-Food Chain; MODEL-IT 2005. ISHS Acta Horticulturae 674.

Hollas, M.Modern Spectroscopy, 3rd Edition, Wiley, New York (1996).

Hu, M., Dong, Q., Liu, B., Opara, U (2016). Prediction of mechanical properties of blueberry using hyperspectral interactance imaging. Postharvest Biology and Technology, Volume 115, May, Pages 122-131

Kelkar, S., Boushey, C. J., & Okos, M. (2015). A Method to Determine the Density of Foods using X-ray Imaging. *Journal of Food Engineering*, *159*, 36–41.

Koksel, F., Aritan, S., Strybulevych, A., Page, J. H., & Scanlon, M. G. (2015). The bubble size distribution and its evolution in Non-yeasted wheat flour doughs investigated by synchrotron X-ray microtomography. *Food Research International*. 12.005

Kondo, N. (2010). Automation on fruit and vegetable grading system and food traceability. *Trends in Food Science and Technology*, *21*, 145–152.

Lassoued, N., Babin, P., Della Valle, G., Devaux, M. F., & Réguerre, A. L. (2007). Granulometry of bread crumb grain: Contributions of 2D and 3D image analysis at different scale. *Food Research International*, *40*(8), 1087–1097.

Leemans, V., Magein, H., & Destain, M. F. (2002). AE--Automation and Emerging Technologies:: On-line fruit grading according to their external quality using machine vision. *Biosystems Engineering*, *83*, 397–404. doi:10.1006/bioe.2002.0131

Leiva-Valenzuela,G., Lu, R., Aguilera, J.M (2014). Assessment of internal quality of blueberries using hyperspectral transmittance and reflectance images with whole spectra or

selected wavelengths. Innovative Food Science & Emerging Technologies, Volume 24, Pages 2-13

Llave, Y., Terada, Y., Fukuoka, M., & Sakai, N. (2014). Dielectric properties of frozen tuna and analysis of defrosting using a radio-frequency system at low frequencies. *Journal of Food Engineering*, *139*, 1–9.

Omid, M., Khojastehnazhand, M., & Tabatabaeefar, a. (2010). Estimating volume and mass of citrus fruits by image processing technique. *Journal of Food Engineering*, *100*(2), 315–321.

Ostrouh, A., Kuftinova, N., (2012). Automation of Planning and Management of the Transportation of Production for Food-Processing Industry Enterprises. Automatic Control and Computer Sciences, , Vol. 46, No. 1, pp. 41–48.

Ozturk, S., Kong, F., Trabelsi, S., & Singh, R. K. (2016). Dielectric properties of dried vegetable powders and their temperature profile during radio frequency heating. *Journal of Food Engineering*, *169*, 91–100.

Pan, L., Zhang, Q., Zhang, W., Sun, Y., Hu, P., Tu, K (2016). Detection of cold injury in peaches by hyperspectral reflectance imaging and artificial neural network. Food Chemistry, Volume 192, 1, Pages 134-141

Pérez-Nieto, a., Chanona-Pérez, J. J., Farrera-Rebollo, R. R., Gutiérrez-López, G. F., Alamilla-Beltrán, L., & Calderón-Domínguez, G. (2010). Image analysis of structural changes in dough during baking. *LWT - Food Science and Technology*, *43*(3), 535–543.

Ropodi, a. I., Pavlidis, D. E., Mohareb, F., Panagou, E. Z., & Nychas, G.-J. E. (2015). Multispectral image analysis approach to detect adulteration of beef and pork in raw meats. *Food Research International*, *67*, 12–18.

Safren, O., Alchanatis, V., Ostrovsky, V., Levi, O., 2007. Detection of green apples in hyperspectral images of apple-tree foliage using machine vision. Trans. ASABE 50 (6), 2303–2313

Shafie, S., Abdul, F., Advanced Manufacturing Systems in Food Processing and Packaging Industry (2013). Materials Science and Engineering 46 012042

Senni, L., Ricci, M., Palazzi, A., Burrascano, P., Pennisi, P., & Ghirelli, F. (2014). On-line automatic detection of foreign bodies in biscuits by infrared thermography and image processing. *Journal of Food Engineering*, *128*, 146–156.

Simmons, A. L., & Vodovotz, Y. (2012). The effects of soy on freezable bread dough: A magnetic resonance study. *Food Chemistry*, *135*, 659–664.

Steinfeld, J. Molecules and radiation: An introduction to modern molecular spectroscopy, 2nd Edition, MIT Press, Londres (1989).

Svanberg, S. Atomic and Molecular Spectroscopy: Basic aspects and practical applications, 2nd Edicition, Springer (1992)

Tournier, C., Grass, M., Zope, D., Salles, C., & Bertrand, D. (2012). Characterization of bread breakdown during mastication by image texture analysis. *Journal of Food Engineering*, *113*(4), 615–622.

Huang, Y. Automation for food engineering : food quality quantization and process control. CRC series in contemporary food science,(2001). ISBN 0849322308

Williams, P., Geladi, P., Fox, G., & Manley, M. (2009). Maize kernel hardness classification by near infrared (NIR) hyperspectral imaging and multivariate data analysis. *Analytica Chimica Acta*, *653*(2), 121–30.

OBJETIVOS

El objetivo general de la tesis ha sido el desarrollo de aplicaciones basadas en el análisis de imagen hiperespectral en visible-infrarrojo cercano (SW-NIR) y tridimensional por luz estructurada, para el control de materias primas, procesos y productos acabados dentro de la industria harinera y de sus derivados. Todo ello llevado a cabo en base a los siguientes objetivos específicos:

- Adaptación del sistema de análisis de imagen tridimensional basado en luz estructurada para el control en continuo del proceso de fermentación de masas panarias.
- Estudio de la información tridimensional y obtención de descriptores del proceso de fermentación.
- Monitorización y caracterización del proceso de fermentación de masas mediante los descriptores tridimensionales obtenidos.
- Adaptación de la técnica de imagen hiperespectral para el análisis de muestras de harina.
- Estudio de la información espectral de las harinas en relación con su composición química y determinación de rangos espectrales descriptivos del producto.
- Aplicación de la imagen hiperespectral para detectar modificaciones en la composición química de harinas y panes.
- Control de las modificaciones sufridas por la harina durante un pre-tratamiento térmico mediante imagen hiperespectral.
- Caracterización espectral del producto modificado y estudio de sus relaciones con el procesado y producto final.

CAPÍTULO I

Continuous monitoring of bread dough fermentation using a 3D vision Structured Light technique

Journal of Food Engineering, Volume 130, June 2014, Pages 8-13.
Eugenio Ivorra, Samuel Verdú Amat, Antonio J. Sánchez, José M. Barat, Raúl Grau
Versión adaptada para la tesis doctoral

Abstract

Fermentation of the dough is an important phase in the bread-making process which is affected by several important factors related to raw materials and processing. Changes in fermentation affect parameters in the final product, such as texture, palatability and general quality. For this reason, it is important to develop dynamic methods to study this phase. In this work, a 3D vision system based on Structured Light (SL) was used to monitor the fermentation phase. The evolution of the dough was studied employing 10 wheat flours with non-physicochemical and rheological differences. However, differences in dough behaviours during fermentation were found based on SL method parameters. When the variation of the total transversal area was related to the maximum height at each fermentation time a set of peaks and valleys appeared. These sets were directly related to the fermentation capacity. Specifically, a lower number of peaks during the main fermentation time (100 minutes) is related to wheat flours with high fermentation capacity. Consequently, the proposed SL Technique could be used as a method to check the fermentation capacity of wheat flours according to their fermentation behaviour.

Keywords: Structured light, monitoring, fermentation, bread, behaviour.

1. Introduction

Several important factors affect productivity in the bread industry due to changes in the properties and behaviour of wheat flour during the bread-making process. Some of these are: the cultivation method, the variety of wheat, phytohealth products, environmental factors, climatic conditions, pests, stored kernel alterations and milling, all of which result in changes in the composition of the flour (Cocchi et al., 2005). Therefore, it is important to develop methods to study wheat flour properties and process phases to decide the best use for each batch of raw materials, and in turn to modify the process parameters when necessary. Fermentation of the dough is an important phase in the bread-making process which affects parameters in the final product, such as texture, palatability and general quality. This is an important temperature-dependent phase, in which the metabolism of yeasts transforms assimilable carbohydrates and amino acids into carbon dioxide and ethyl alcohol as the principal end products (Birch et al., 2013). Gluten plays a crucial role in creating the dough structure and baking the bread. It affects the stability of the dough and bread volume by forming a skeleton which combines the remaining ingredients and additives (Barak et al., 2013). The oxidation of cysteine amino acids from gluten proteins (gliadines and glutenines) by thiol groups generates a viscoelastic network which is capable of retaining carbon dioxide from which the gas cells develop. The growth of gas cells depends on cell size and dough composition (flour, water and other ingredients).

Several compounds are known to exert a stabilizing influence and retard unwanted phenomena such as coalescence (Gan et al., 1995). As a result, dough composition and yeast activity are manifested in dough bubble sizes and dough volume expansion.

Recently, empirical and physicochemical techniques (the majority of them based on destructive analysis) have been used to characterize the different phases of the bread-making process (Dobraszczyk and Morgenstern, 2003). In particular, the fermentation phase has been extensively studied from various points of view (many of them non-destructive) (Lassoued et al., 2007). All of them are aimed at obtaining information about the implicated fermentation and baking parameters, thereby explaining the process phenomena and improving knowledge as well as control over the final product. The evolution of parameters such as dough volume, density and gas cell sizes are important control variables, since their behaviour has an important influence on the quality of the final product.

Image analysis is an important tool for the characterization of the bread-making process which has been demonstrated to be an important research and industrial application (Calderón-Domínguez et al., 2008). Different techniques and methods based on multiple principles have been used to acquire and analyse images obtained during the process. Some examples are: Confocal laser scanning microscopy (Jekle et al., 2011, Upadhyay et al. 2012), magnetic resonance (Franci and Serša, 2011) and methods based on 2D (Pour-Damanab et al., 2011).

The structured-light method is another imaging technique. It is based on the projection of a pattern of light on a sample and the calculation of 3D dimensions from the deformation of the pattern using a camera (Verdú et al., 2013). This technique permits the monitoring of continuous processes and could be applied on-line. Accordingly, the aim of this work was to monitor bread dough fermentation of different wheat flour samples with developed computer vision based on Structured Light, in order to obtain useful information about the process and characterize the response of the raw material.

2. Material & methods

2.1 Dough preparation and the fermentation process

Ten types of flour obtained from different batches produced by Molí del Picó-Harinas Segura S.L (Valencia-Spain) were used in this study. The flour was sold as "high strength flour", for bakery products, sliced bread, plum cakes, etc. The doughs were made employing the following percentages: 56% wheat flour, 35% water, 2% refined sunflower oil (maximum acidity 0.2º.Koipesol Semillas S.L - Spain), 2% commercial pressed yeast (*Saccharomyces cerevisiae.*Lesafre Ibérica S.A - Spain), 4% white sugar (≥ 99.8 % sucrose. Azucarera Ebro, S.L – Spain) and 1.5% NaCl (refined marine salt ≥ 97 % NaCl. Salinera Española, S.A – Spain). All the doughs were made using the same procedure. The analyses of the samples were carried out according to the standard methods of the International Association for Cereal Science and Technology (ICC). Moisture was calculated based on the

weight loss suffered by the sample when dried at a temperature between 130 and 133 °C. Moisture content is taken to be the loss in weight, expressed as a percentage of the weight of the original sample (ICC standard No.110/1). Wet and dry gluten were isolated from the dough of a sample of flour, prepared previously by mixing the flour with a buffer of sodium chloride. Isolated wet gluten was dried at 100ºC until constant weight to remove moisture (ICC standard No.106/2). Falling number analysis was also carried out (FN 1500, Perten, Sweden) with the aim of evaluating alpha-amylase activity, as it affects the behaviour of starch and hence the commercial value of flour (ICC standard No.107/1). Rheological parameters were used to evaluate the resistance of the dough to stretch; its extensibility until the moment when it began to rupture was assessed based on the Chopin alveograph method (ICC standard No.121, Alveograph®, Chopin Technologies), France. The Kjeldahl method was used to analyse the protein content. The first step was to digest the wheat flour samples in H_2SO_4 to convert the protein N to $(NH_4)_2SO_4$. Ammonia was liberated by alkaline steam distillation and finally, it was quantified with standardized acid (AOAC Official Method 2001.11).

The doughs were made by combining all ingredients in a food mixer (Thermomix® TM31, Vorwerk, Germany) according to the following procedure. In the first step, the liquid components (water and oil), sugar and NaCl were mixed for 4 minutes at 37 °C. The pressed yeast was added in the next step and mixed at the same temperature for

30 seconds. Finally, the flour was added and mixed with the rest of the ingredients using a specific default program for dough mixing. In this step, the device mixes the ingredients with random turns in both directions of the mixer helix (550 revolutions/minute), in order to obtain homogeneous dough. This process was applied for 4.5 minutes at 37ºC. Then, 450 g of dough was placed in the metal mould (8x8x30cm) for fermentation. This process was carried out in a chamber with controlled humidity and temperature (KBF720, Binder, Tuttlingen, Germany), where a 3D Structured Light (SL) device was developed and calibrated. The conditions of the fermentation process were 37°C and 90% Relative Humidity (RH). The samples were fermented until the dough lost its stability and size, when growth depletion occurred. Four replicates were used for each dough.

2.2. Fermentation monitoring by ¨Structured Light¨ method (SL)

A 3D vision system, developed in a previous study (Verdú et al., 2013) and adapted specifically to monitor fermentation, was used. This vision system was composed of structured light and a camera. The structured light was generated employing a red lineal laser (Lasiris SNF 410, Coherent Inc. Santa Clara, California (USA)), and a network graycamera, with index protection of 67 (IP67) was used for image acquisition (In-Sight 5100, Cognex, Boston, Massachusetts (USA)). Both of them were installed in the fermentation chamber (Figure. I.1).

The laser had an angle β of 0.65 radians (Figure I.1) which in combination with the resolution of the camera (640x480) and its distance from the sample give a Z resolution of $1.4*10^{-4}$ m and X resolution of $2.1*10^{-4}$ m. This configuration was established to achieve a working range of 0.1 m in the X axis and 0.08m in the Z axis. The camera worked at an acquisition rate of 1 frame per second (fps) due to the length of time for the test (around 2 hours), but it can work at up to 60fps. Calibration of the equipment was performed by taking 10 regularly distributed points in 3D in the laser projection plane (Trobina et al., 1995). Using these points with known 3D coordinates and their correspondent points in the image, a homography transformation was calculated (Zhang et al., 2000).

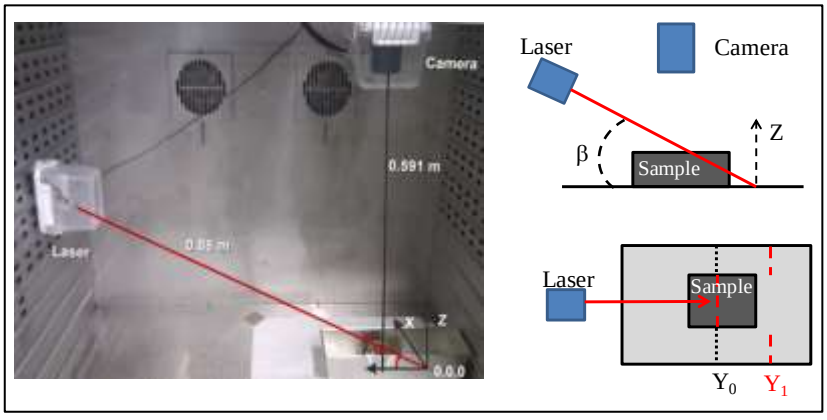

Figure I.1. Developed 3D vision system installed in the fermentation chamber and schematic 3D vision system.

2.3. SL method information extraction

The laser points projected on the image were extracted following these steps: first, the image was segmented using Otsu's global threshold (Otsu et al., 1979), then the image was filtered removing non connected pixels with an area lower than 100px and finally, row coordinates were calculated by weight mean. This weight mean value was calculated for each column using the intensity value in order to get subpixel precision. The 3D coordinates were then calculated using the homography from these pixel coordinates. The last step was the application of a rotation matrix in order to make the Z axis normal to the surface, as can be seen in the reference coordinate system of Figure I.1.

The sample was defined as a 3D curve composed of the 3D points which were between the known 3D points of the mould's borders. The following information about the growth of the samples during the fermentation was acquired from each image:

- Maximum height (H): The maximum Z value for the sample and its position.
- Transversal area (A): The integration of the Z values along the X direction of the sample.
- Arc correlation: A Pearson's correlation between a theoretical arc defined by two points (the two extreme sides of the sample along the X direction) and the radius (half the

modulus of the vector between the two points of the arc) and the 3D curve of the sample.

Acquisition and data processing was carried out using a code developed in the Matlab computational environment (The Mathworks, Natick, Massachussets, USA).

3. Results & discussion

Dough volume expansion, in which CO_2 production is associated with yeast activity (Bajd & Serša, 2011), was characterized from the data obtained employing the structured line method. Data were expressed as transversal area (*A*), the maximum height (*H*) at each time, and the relationship between both (*A/H*). Figure 2, as an example, shows the evolution of the dough transversal area with fermentation time. The X axis expresses the thickness of the bread, the Y axis the fermentation time and the Z axis the height.

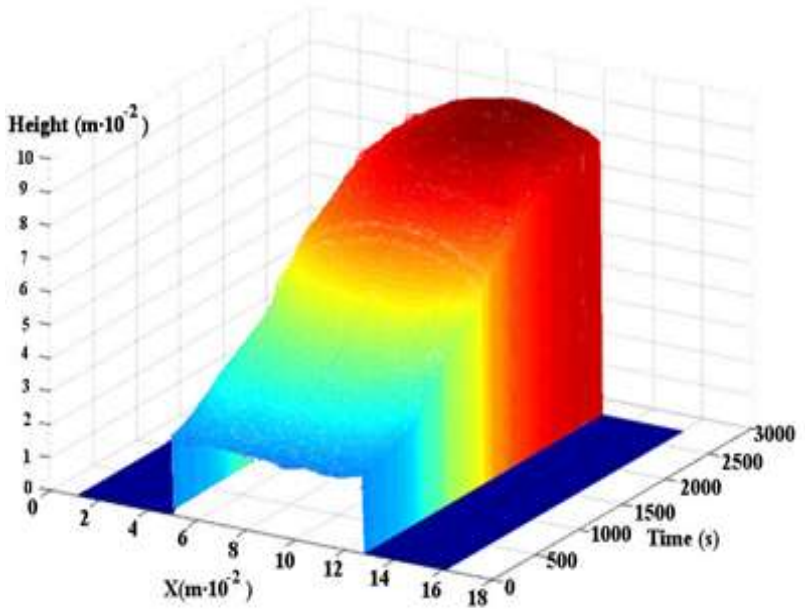

Figure I.2. 3D representation of transversal area (A) evolution with fermentation time for dough number 10.

Figure I.3 shows the evolution of the transversal area at each fermentation time (until growth depletion occurred) for the 10 doughs tested. Although the physicochemical analysis of the wheat flours used for making the doughs did not show any significant differences (Table I.1), the times to reach the maximum transversal area were different for the doughs tested (Figure 3). The maximum area value was 17.6 ± 1.9 m^2*10^{-4}, employing 187 minutes (dough number 10) and the lowest was 10.3 ± 0.5m^2*10^{-4} employing 108 minutes (dough number 1) (Table I.2).

Table I.1. Protein, alveograph parameters (P=maximum pressure (mm), L=extensibility (mm); W=strength (J-4), falling number, moisture, gluten and dry-gluten for the 10 batches of wheat flour employed. Experimental constituted of 3-4 determinations. The results are expressed in terms of average and standard deviation.

P	97 ± 2
L	104 ± 3
W	373 ± 12
P/L	0.93 ± 0.1
Falling number	413 ± 6
Moisture (%)	14.3 ± 0.2
Wet Gluten (%)	31.2 ± 0.2
Dry gluten (%)	13.5 ± 0.1

Similar behaviour was obtained when the maximum height at each fermentation time was compared (Table I.2). When the data about area and height at 100 min were compared, statistical differences were observed (Table I.2). The time of 100 min was the shortest time for a dough to reach its final fermentation and was similar to that employed by other authors as a fermentation time (Keskin et al*.,* 2004; Bajd and Serša, 2011; Rizzello et al*.,* 2012).

Table I.2. Transversal area and the maximum height of the tested doughs, at the end of each fermentation time (until no increase is observed) and at 100 minutes (time required for the dough which reached its final fermentation first).

	Until the end of fermentation time			At 100 min	
Dough	**Final time (Ft,min)**	**Transversal area (A) ($m^2.10^{-4}$)**	**MaximumHeight (H) ($m.10^{-2}$)**	**Transversal area (A) ($m^2.10^{-4}$)**	**MaximumHeight (H) ($m.10^{-2}$)**
1	108 ± 2 ^{a}	10.3 ± 0.5 ^{a}	4.4 ± 0.1	9.2 ± 0.5 ^{a}	4.6 ± 0 ^{a}
2	106 ± 4 ^{a}	10.6 ± 0.8 ^{a}	4.6 ± 0.1	9.2 ± 0.1 ^{a}	4.1 ± 0 ^{a}
3	100 ± 4 ^{a}	12.3 ± 0.3 ^{ab}	5.6 ± 0.1	11.7 ± 0.5 ^{bc}	5.3 ± 0.2 ^{cd}
4	138 ± 3 ^{c}	14 ± 0.7 ^{bc}	6.2 ± 0	11.1 ± 0.7 ^{abc}	4.8 ± 0 ^{bcd}
5	142 ± 5 ^{cd}	14.2 ± 1.5 ^{bc}	6.3 ± 0.5	10.2 ± 1.4 ^{abc}	4.7 ± 0.5 ^{abc}
6	123 ± 17 ^{bc}	14.3 ± 1.3 ^{bc}	6.4 ± 0	12.1 ± 0.7 ^{c}	5.4 ± 0.1 ^{d}
7	133 ± 4 ^{b}	14.4 ± 0.8 ^{bc}	6.3 ± 0.2	11.7 ± 0.9 ^{bc}	5.2 ± 0.3 ^{bcd}
8	155 ± 1 ^{de}	15 ± 1.9 ^{c}	6.7 ± 0.7	10 ± 1.1 ^{ab}	4.6 ± 0.5 ^{ab}
9	159 ± 3 ^{e}	16.3 ± 0.5 ^{cd}	7.3 ± 0.2	11.1 ± 1 ^{abc}	5.2 ± 0.2 ^{bcd}
10	187 ± 8 ^{f}	17.6 ± 1.9 ^{d}	7.5 ± 0.7	11.3 ± 1.3 ^{bc}	5.1 ± 0.5 ^{bcd}

Experimental constituted of 4 determinations. The results are expressed in terms of average and standard deviation. Different letters within columns mean significant differences at $p \leq 0.05$.

Differences between doughs could be related to the level of starch damage, the influence of gluten proteins and the number of bubbles and their size (Faridi, 1990; Barrera et al.. 2013; Mills et al., 2003; Boyaci et al. 2004).

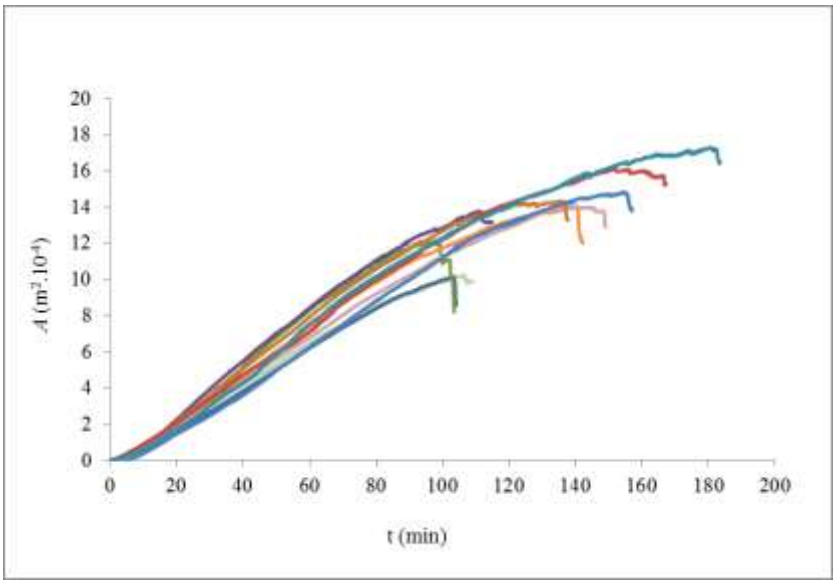

Figure I.3. Evolution of the dough's transversal area (*A*) with fermentation time (until growth depletion occurred). Doughs series are represented by followed colours: 1 – ; 2 – ; 3 – ; 4 – ; 5 – ; 6 – ; 7 – ; 8 – ; 9 – ; 10 – .

The fraction of starch damage is a consequence of the kind and time of milling of the wheat-kernels. These two factors have an influence on the rheological and functional properties of dough (Faridi, 1990) since they are able to modify flow regimes, processing variables and swelling proprieties (Barrera et al*.,* 2007). Excessive starch damage could overly hydrate the dough and permit accelerated enzymatic action (Boyaciet al*.* 2004), thus producing differences in the availability of yeast substrates and dough stability with time.

On the other hand, climatic fluctuations (Daniel & Triboi, 2000) and levels of several fertilizer compounds such as nitrogen, sulphur and

phosphorus (Altenbach et al*.,* 2002) may affect the enzyme activity kinetics during wheat growth, thus disturbing an optimal ratio generation of subfractions of gluten proteins (gliadin and glutenin). Higher glutenin levels make the dough more elastic, giving the dough its property of resistance to extension, while higher gliadin content increases the extensibility of the dough (Barak et al*.,* 2013). This ratio has a strong influence on the quality and technological proprieties of wheat flour (Radovanovic et al*.,* 2002). However, the analysis of starch damage or gluten protein composition requires specific techniques and devices that are not easy to carry out on a daily basis in the industry.

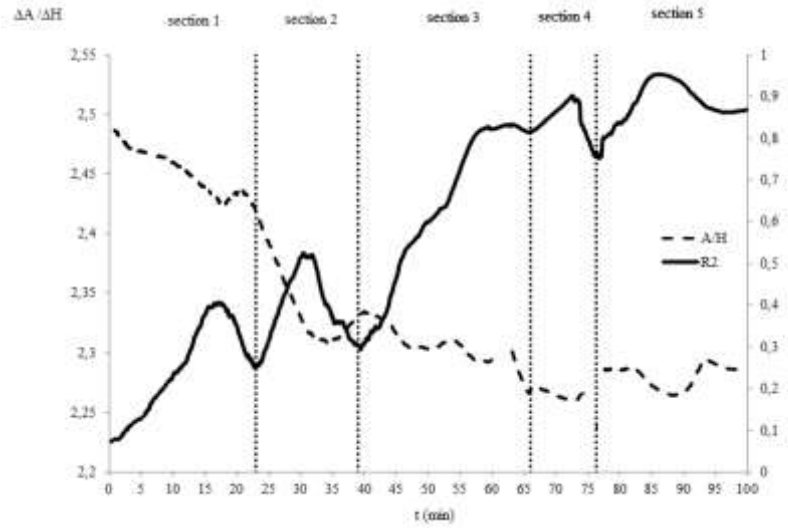

Figure I.4. Evolution with fermentation time (100 minutes) of the ratio between transversal area (A) and the height (H) increase (ΔA/ΔH) (broken line (- - - -)) and the arc correlation (continuous line (——)) for dough number 9.

When the ratio between total transversal area and maximum height increase *(ΔA/ΔH*) at each fermentation time was calculated, no stable evolution was observed (Figure I.4). The instability was related to the different velocities of *A* and *H*. In order to check this instability, the correlation between the arc described by the laser light when it is projected onto the dough surface (Figure I.5) and the theoretical arc was used. As it is possible to observe in Figure I.4, an example of a dough, in which the evolution of the ratio *ΔA/ΔH* and R^2 of Pearson are drawn, peaks and valleys could be identified (between broken lines). Peaks were considered when data from R^2 change their derivative sign from positive to negative (derivative zero value) and the function value is equal or higher than the previous peak. R^2 of Pearson and *ΔA/ΔH* had an inverse tendency with time. When *ΔA/ΔH* decreased, because the higher velocity of *H* changed, R^2 increased, evolving the shape of the dough surface to a theoretical arc. Inverse behaviour could be obtained when the *A* velocity was higher.

The recount of the number of peaks at 100 min (NP_{100}) (Table I.3) showed how this number is related to dough evolution and could be used to discern the final behaviour of doughs (Figure I.6). In doughs which did not have an important variation in their transversal area between 100 min and their final fermentation time (first doughs), the number of peaks did not increase, reaching their highest number of peaks.

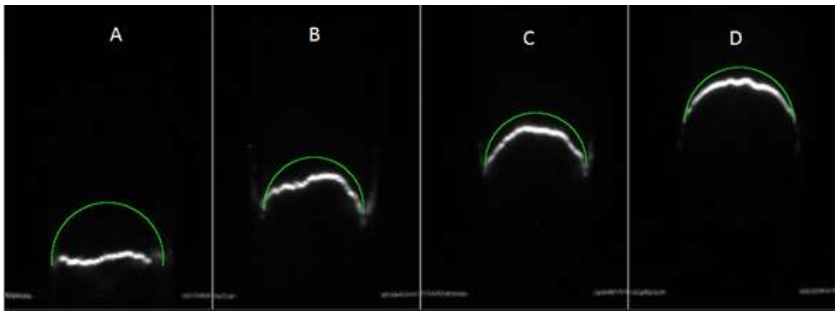

Figure I.5. Laser light projected onto the dough versus fermentation time (A: 5 min, B: 30 min, C: 60 min, D: 100 min) and the theoretical arc (green line).

On the other hand, doughs which increased their transversal area also increased their number of peaks (Table I.4). The failure of the gluten-network films separating some bubbles has been implicated in correct gas retention and therefore in the instability of the foam structure of bread (Gan et al., 1995), which could produce variations in the dough's evolution with time. This could be the reason why a reorganization or non-uniform distribution of bubbles could lead to total or partial collapse of the dough (Wang et al., 2011), making changes in the shape of doughs which could be related to the peaks and valleys.

Table I.3. Results of number of peaks at 100 min (NP_{100}) and at final fermentation time (NP_f).

Dough	NP_{100}	NP_f
1	7.5 ± 0 ^{de}	8 ± 1 ^{ab}
2	8.5 ± 1.4 ^{e}	8.5 ± 1 ^{ab}
3	7 ± 0.7 ^{cd}	7 ± 0 ^{a}
4	6 ± 0.7 ^{bc}	7.5 ± 1 ^{ab}
5	6 ± 0.7 ^{bc}	8 ± 1 ^{ab}
6	6 ± 0 ^{bc}	7.5 ± 1 ^{ab}
7	6 ± 0.7 ^{bc}	9.5 ± 1 ^{b}
8	4.5 ± 0.7 ^{a}	7 ± 1 ^{a}
9	5 ± 0 ^{ab}	8.5 ± 1 ^{ab}
10	4.5 ± 0.7 ^{a}	9 ± 1 ^{ab}

Experimental constituted of 4 determinations. The results are expressed in terms of average and standard deviation. Different letters within columns mean significant differences at $p \leq 0.05$.

Thus, according the experiments carried out in the present study and further analysis of obtained results it can be concluded that employing SL techniques it is possible to characterize wheat flours according to their fermentation capacity.

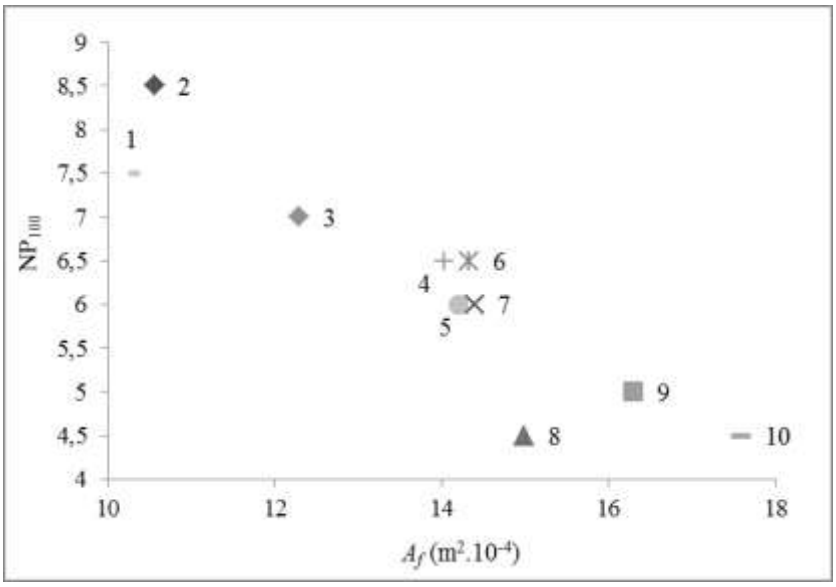

Figure I.6. Number of peaks at 100 minutes (NP_{100}) related to the transversal area at the end of each fermentation time (A_f) for the ten doughs tested.

4. Conclusion

The study demonstrated that the Structured Light method (SL) can provide useful information about the behaviour of dough during fermentation. Monitoring the fermentation of dough showed that wheat flours with similar moisture, protein, gluten, dry-gluten, falling number and alveograph parameters have different fermentation capacities. The peaks and valleys that take place during fermentation, when the variation of the total transversal area is related to the maximum height or to R^2 of Pearson (obtained when the curvature described by the laser light is adjusted to a theoretical arc when it is projected onto the dough surface), are directly related to the

fermentation capacity. A lower number of peaks during the main fermentation time (100 minutes) is related to wheat flours with high fermentation capacity. Hence the described technique could be used to check the fermentation capacity of wheat flours according to their fermentation behaviour.

5. Acknowledgements

We thank the Polytechnic University of Valencia and Generalitat Valenciana for the financial support provided (PAID-05-011-2870 and 226 GVPRE/2008/170 projects, respectively)

6. Bibliography

Altenbach, S.B., Du Pont, F.M., Kothari, K.M., Chan, R., Johnson ,E.L. & Lieu, D. (2003). Temperature, Water and Fertilizer Influence the Timing of Key Events During Grain Development in a US Spring Wheat. Journal of Cereal Science, 37, 9–20.

AOAC Official Method 2001.11. Protein (Crude) in Animal Feed, Forage (Plant Tissue), Grain, and Oilseeds.

Bajd, F. & Serša, I. (2011). Continuous monitoring of dough fermentation and bread baking by magnetic resonance microscopy. Magnetic Resonance Imaging, 29(3), 434-442.

Barak, S., Mudgil, D. & Khatkar, B.S. (2013). Relationship of gliadin and glutenin proteins with dough rheology, flour pasting and bread making performance of wheat varieties. Food Science and Technology, 51, 211-217.

Barrera, G. N., Pérez, G. T., Ribotta, P. D. & León, A. E. (2007). Influence of damaged starch on cookie and bread-making quality. Europe Food Research Technology, 225,1–7.

Barrera, G.N., Bustos M.C, Iturriaga, L, Flores, S.K., León, A.E. & Ribotta P.D. (2013). Effect of damaged starch on the rheological properties of wheat starch suspensions. Journal of Food Engineering, 116(1), 233-239.

Birch Anja N., Petersen Mikael A., Arneborg N. & Hansen Åse S. (2013). Influence of commercial baker's yeasts on bread aroma profiles. Food Research International, 52, 160–166.

Boyacı I.H., Williams, P.C. & Köksel, H. (2004). A rapid method for the estimation of damaged starch in wheat flours. Journal of Cereal Science, 39(1), 139-145.

Calderón-Domínguez, G.J., Chanona-Pérez, A.L. Ramos-Cruz, A.I., López-Lara, A.D., Tlapale-Valdivia, G.F. & Gutiérrez-López.(2008). Fractal and image analysis of Mexican sweet bread bubble distribution; influence of fermentation and mixing time. G.M. Campbell, M. Scanlon, L. Pyle, K. Niranjan (Eds.), Bubbles in food 2: Novelty, health and luxury American. Association of Cereal Chemists, St. Paul, MN, USA.

Cocchi, M., Corbellinib M, Focaa,G., Lucisanoc, M., Paganic, M. A., Lorenzo T. &Alessandro, U. (2005). Classification of bread wheat flours in different quality categories by awavelet-based feature selection/classification algorithm on NIR spectra. Analytica Chimica Acta, 544, 100–107.

Daniel, C. & Triboi, E. (2000). Effects of Temperature and Nitrogen Nutrition on the Grain Composition of Winter Wheat: Effects on Gliadin Content and Composition. Journal of Cereal Science, 32(1), 45-56.

Dobraszczyk, B.J. & Morgenstern, M.P. (2003). Rheology and the breadmaking process. Journal of Cereal Science, 38(3), 229-245.

Faridi, H. &Faubion, J.M. (1990).Dough rheology and baked product texture. Information Systems Division, National Agricultural Library (United States of America).

Gan, Z., Ellis, P.R. & Schofield, J.D. (1995). Gas Cell Stabilisation and Gas Retention in Wheat Bread Dough. Journal of Cereal Science, 21(3), 215-230.

ICC - International Association for Cereal Science and Technology (Vienna-Austria). Standard Methods.

Jekle, M. & Becker, T. (2011). Dough microstructure: Novel analysis by quantification using confocal laser scanning microscopy. Food Research International, 44(4), 984-991.

Keskin S. O., Sumnu G., Sahi S. (2004). Bread baking in halogen lamp–microwave combination oven. Food Research International, 37, 489–49.

Lassoued N, Babin P, Della Valle G, Devaux MF, Reguerre AL. (2007). Granulometry of bread crumb grain: contributions of 2D and 3D image analysis at different scale. Food Research International. 40, 1087–97.

Mills, E. N. C., Wilde, P. J., L. Salt, J. & Skeggs, P. (2003). Bubble formation and stabilization in bread dough. Food Bioproducts Process, 81, 189-193.

Pour-Damanab A.R. S, Jafary A. & Rafiee Sh. (2011). Monitoring the dynamic density of dough during fermentation using digital imaging method. Journal of Food Engineering, 107(1), 8-13.

Radovanovic, N., Cloutier, S., Brown, D., Humphreys, D. G., & Lukow, O. M. (2002). Genetic variance for gluten strength contributed

by high molecular weight glutenin proteins. Cereal Chemistry, 79(6), 843–849.

Rizzello, C.G., Coda, R., .Mazzacan, F., Minervini, D. & Gobbetti, M. (2012). Micronized by-products from debranned durum wheat and sourdough fermentationenhanced the nutritional.textural and sensory features of bread. Food Research International, 46, 304–313.

CAPÍTULO II

Relationship between fermentation behavior, measured with a 3D vision Structured Light technique, and the internal structure of bread

Journal of Food Engineering, Volume 146, February 2015, Pages 227-233
Samuel Verdú, Eugenio Ivorra, Antonio J. Sánchez, Jose M. Barat, Raúl Grau
Versión adaptada para tesis doctoral

Abstract

The bread-making process is a set of operations where could be relevant to use monitoring methods. Specifically, the fermentation phase is a crucial step in which the quality of the product can be affected. Several methods have been developed to monitor this stage based on different technologies. The aim of this study was to analyze and obtain information about the internal structure of bread dough during the fermentation process using a 3D vision system based on Structured Light (SL). The differences about fermentation behavior of two wheat flours classified as "high strength flour" by company providing were studied. The parameters of the internal structure of the baked product (final bubble size and their population density) were analyzed with 2D image segmentation. An important correlation (r=0.865) was observed between the 3D and 2D information, specifically between the transversal area and height (3D), and final bubble size and number of bubbles (2D). Although at the end of the dough fermentation process (Tf) the area (A) and maximum height (H) were different, the relationship between both parameters were similar, reaching a similar bubble size as a consequence of coalescence phenomena, independent of the bubble growth rate. This could be a base for the development of prediction models and devices to monitor the fermentation phase of the bread-making process.

Keywords: Structured light, bubble size, internal structure, monitoring, fermentation, bread dough, behavior.

1. Introduction

The preservation and improvement of product quality and properties is of utmost importance in the food industry. This must be as constant as possible to maintain competitiveness as well as to satisfy the expectations of consumers (Miralbes, 2004). Therefore, obtaining detailed information about the factors which influence the different phases in their processes is one of the main issues in the food industry. The present study is focused on this context, specifically the industrial bread-making process. Several factors affect productivity in the bread industry due to the modifications of wheat flour properties and hence their behavior during processing (Badj & Serša., 2011; Wang et al. 2011). In particular, chemical composition and rheological properties may seriously affect both the dynamics of the process and the final homogeneity of products (Barak et al. 2013; Cocchi et al. 2005). Process variables (time, temperature, humidity, proportions of ingredients, etc) and relevant quality attributes (texture, palatability, aroma profile) could be affected by these modifications (Le-Bail et al. 2009; Novotni et al. 2011). Specifically, one of the most influential phases, dough fermentation, is an easily alterable phase due to small changes in the characteristics of the raw

materials, which thereby brings out significant modifications in the usual development of production.

During fermentation, the gas produced by yeast activity expands the air bubbles previously incorporated into the dough system in the mixing phase (Ktenioudaki et al. 2009), therefore anything that modifies this phase could alter the final attributes of the product. These alterations occur because the variability in the gas phase distribution in the dough system plays a crucial role in crumb structure formation, since the stability and the growth of gas bubbles generated will determine the final volume of the loaf as well as the texture of the baked product (He & Hoseney, 1991). Thus, variables such as the volume and density of the dough, to control the fermentation process, as well as their relationship with the properties of the gas phase have been widely studied.

To improve the knowledge about the fermentation phase, many studies have been carried out using different points of view and techniques. Among them, there are static controls of variables like volume, density and bubble size (Perez-Nieto et al. 2010; Upadhyay et al. 2012). There are also studies addressing the development of applications to dynamically monitor the same variables (Falcone et al. 2005; Zúñiga et al. 2009; Lucas et al. 2010) based on ultrasound, MRI, 2D and 3D imaging analysis. Although 2D image analysis, in which segmentation images have been applied, is usually employed as a static control for checking the bubble size or bread crumb grain (Lassoued et al. 2007, Gonzales-Barron & Butler, 2008, Scanlon &

Zghal, 2001, Pérez-Nieto et al. 2010), in order to be related to different recipes or processing, mainly baking.

There are various techniques used to obtain 3D imaging, one of them based on structured light (Verdú et al. 2013). It is based on the projection of a pattern of light on a sample and the calculation of 3D dimensions from the deformation of the pattern using a camera (Verdú et al. 2013). This technique permits the monitoring of continuous processes and could be applied on-line. In a previous study (Ivorra et al. 2013), ten wheat flours, without physicochemical and rheological differences, were monitored and analyzed during their fermentation evolution, employing the Structured Light method. Results showed differences in their fermentation behavior (peaks and valleys that take place during fermentation, when the variation of the total transversal area is related to the maximum height) which were related with the fermentation capacity.

Thus, the objective of this work is to focus on that study, relating the fermentation behavior, measured with a 3D vision Structured Light technique, to the evolution of the internal structure of bread, measured with 2D image analysis.

2. Material & methods

2.1. Physicochemical characterization of flours

A battery of physicochemical analyses was carried out to obtain information about the general characteristics of the samples. Each analysis was realised according to the standard methods of the

International Association for Cereal Science and Technology (ICC). The analyzes performed were: moisture (ICC standard No.110/1), percentage of gluten (ICC standard No.106/2), falling number (ICC standard No.107/1, FN 1500, Perten, Sweden) and rheological parameters (ICC standard No.121, Alveograph®, Chopin Technologies). All analyses were carried out in triplicate. Table II.1 lists the average and standard deviation of the evaluated parameters.

Table II.1.Values and standard deviation of alveograph parameters and composition

Parameter	F1	F2
P	98 ± 1 [a]	97 ± 1 [a]
L	106 ± 1 [a]	105 ± 1 [a]
W	378 ± 5 [a]	369 ± 4 [a]
P/L	0.92 ± 0.01 [a]	0.92 ± 0.01 [a]
%Moisture	15 ± 0.1 [a]	14 ± 0.1 [a]
Dry Gluten (g/100 g)	12.9 ± 0.2 [a]	11.2 ± 0.4 [a]
Falling number	410 ± 5 [a]	417 ± 2 [a]

P=maximum pressure (mm), L=extensibility (mm); W=strength (J^{-4}), moisture, dry-gluten, and falling number of the two different wheat flours employed. Different letters in rows mean significant differences at $p \leq 0.05$.

2.2 Dough preparation and fermentation process

The wheat flours employed were obtained from two different batches produced by Molí del Picó-Harinas Segura S.L (Valencia-Spain). Both batches, without physicochemical and rheological differences (Table II.1), were selected from the previous study (Ivorra

et al. 2013).One had the lowest fermentation capacity (F1) and the other the maximum (F2). In addition a third batch (Fm), prepared mixing F1 and F2 (50%) was also used.

The ingredients and their percentages for the doughs were: 56% wheat flour, 35% water, 2% refined sunflower oil (maximum acidity 0.2º. Koipesol Semillas S.L - Spain), 2% commercial pressed yeast (*Saccharomyces cerevisiae.* Lesafre Ibérica S.A - Spain), 4% white sugar (≥ 99.8 % saccharose. Azucarera Ebro, S.L – Spain) and 1.5% NaCl (refined marine salt ≥ 97 % NaCl. Salinera Española, S.A – Spain). The three doughs were made using the same procedure.

The doughs were made by combining all the ingredients in a food mixer (Thermomix® TM31, Vorwerk, Germany) according to the following procedure. At the first step, the liquid components (water and oil), sugar and NaCl were mixed for 4 minutes at 37 °C. Then, the pressed yeast was added and mixed at the same temperature for 30 seconds. Finally, the flour was added and mixed with the rest of the ingredients using a specific default program for dough mixing. At this step, the device mixes the ingredients with random turns in both directions of the mixer helix (550 revolutions/minute), in order to obtain an homogeneous dough. Then, 450 g of the dough was placed in a metal mold (8x8x30cm) for its fermentation. This process was carried out in a chamber with controlled humidity and temperature (KBF720, Binder, Tuttlingen, Germany), where a 3D imaging Structured Light (SL) device was developed and calibrated. The conditions of the fermentation process were 37 °C and 90 % Relative

Humidity (RH). The samples were fermented until the dough lost its stability and size (*Tf*), specifically when growth depletion occurred. 4 replicates were carried out for each dough.

2.3 Fermentation monitoring by ¨Structured Light¨ method (SL)

The objective of the 3D vision system is to obtain the 3D sample profile during fermentation. In order to accomplish this objective a 3D vision system was developed specifically to monitor fermentation. This vision system was formed of a red lineal laser (Lasiris SNF 410, Coherent Inc. Santa Clara, California (USA)) and a network graycamera (In-Sight 5100, Cognex, Boston, Massachusetts (USA)). Both of them were installed inside the fermentation chamber (Figure. 1). This was possible because the camera has an index protection of 67 (IP67) and the laser is robust enough to work safely in these conditions.

The 3D visual system developed has a resolution of $2.1 \cdot 10^{-4}$m and $1.4 \cdot 10^{-4}$ m for the X and Z axes respectively. This resolution in derived from a laser angle β of 0.65 radians (Figure II.1) in combination with the resolution of the camera (640x480) and its distance from the sample. The working range achieved with this resolution is 0.1 m in the X axis and 0.08m in the Z axis.

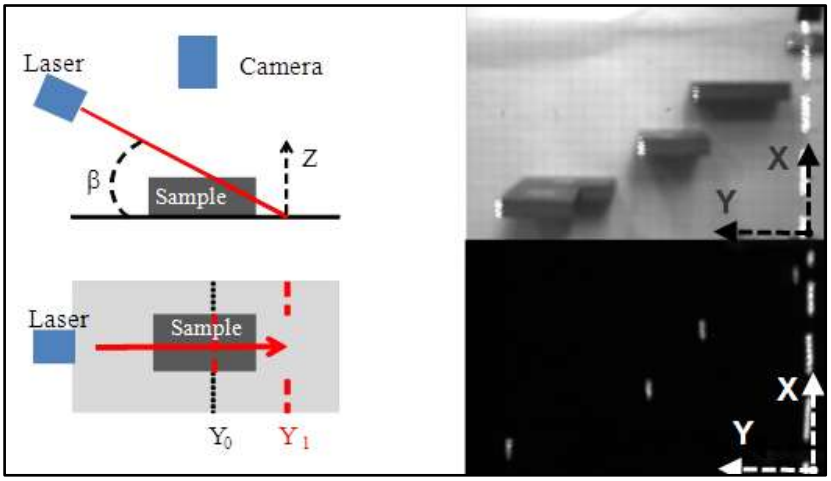

Figure II.1. Calibration of 3D vision system installed in the fermentation chamber. Calibration pieces capture with illumination (top right) and laser response under processing conditions (bottom right).

Although the camera can work at up to 60 fps, the acquisition rate was 1 fps due to the long period of time that fermentation requires (around 2 hours). Calibration of the equipment was firstly performed by taking 10 regularly distributed points in the laser projection plane with known coordinates (Trobina et al. 1995) and then using these 3D points and their correspondent points in the image to calculate an homography transformation (Zhang et al.. 2000).

2.4. SL method image processing

In order to obtain the 3D profile of the sample, the first step is the segmentation of the laser points captured by the camera. This segmentation was performed as follows: using a Otsu's global threshold (Otsu et al. 1979) the laser pixels were selected. Then, these pixels were filtered removing non-connected pixels with an area lower than 100px. Finally, exact row coordinates were calculated by weight mean for each column using the intensity value. Following this method, subpixel precision was achieved.

The second step is the transformation from image coordinates to a 3D local coordinate system. This was done using the homography transformation calculated in the calibration step. The last step is to change the local coordinate system using a rotation matrix which makes the z axis normal to the surface as can be seen in the world coordinate system of Figure II.1.

The 3D sample profile is a 3D curve composed of the 3D points which are between the known 3D points from the edges of the mold. The following information was extracted from each image in order to analyze the growth of the samples during fermentation:

- Maximum height (H): The maximum Z value for the sample and its position.
- Transversal area (A): The integration of the Z values along the X direction of the sample.

Acquisition and data processing were carried out using own code developed in the Matlab computational environment (The Mathworks, Natick, Massachussets, USA).

2.5. Sampling procedure to 2D image acquisition

The internal structure of the doughs was studied with 2D image segmentation. The aim was to obtain information about the final bubble size (*Bz*) and its population density (*Dp*) at different times during the fermentation process after they were baked. Sample times (T) were selected based on the final fermentation time of different doughs (Tf*)*. The first point (T1) was sampled at 50 minutes, as this was around ½ of the shortest *Tf* for the doughs (F1), in order to obtain information in the process early. The rest of the points were sampled at almost *Tf*, just before the depletion of each dough. Therefore, points T2, T3 and T4, were sampled at 100, 150 and 180 minutes for F1, Fm and F2 respectively (Figure II.4). Finally, different numbers of samples were obtained in function of the dough *Tf*. Hence, the number of sampling times for each dough was 2, 3 and 4 for F1, Fm and F2 respectively. Sampling was realized by stopping the fermentation and baking the doughs at each time at 180ºC/50 minutes. Each test was carried out in triplicate and 6 slices of 1 cm thickness were cut from the central zone of the breads.

2.6. 2D image acquisition and segmentation

Both sides of each slice of bread were captured with a scanner (Aficio™ MP C300-Ricoh, Tokyo, Japan) to be analyzed through image segmentation, so for each flour and time sample point information was extracted from 36 images. The images were acquired with a resolution of 300 dpi (Figure II.2 A). The use of the scanner directional and homogenous light is very suitable for bubble segmentation. In addition, a black background was used in order to enhance the measurement of the pore cell wall structure and porosity of the bread.

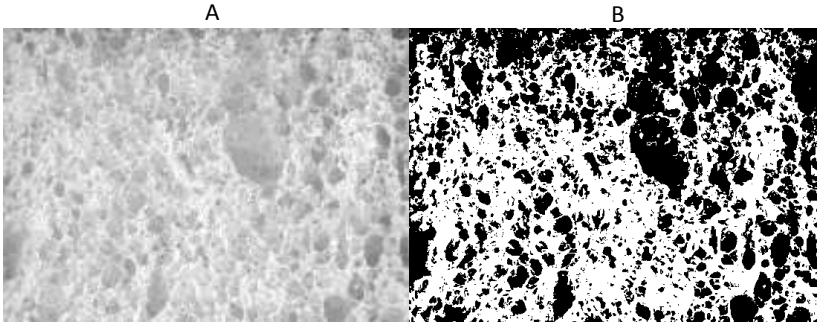

Figure II.2. (A) Gray image (dark areas represent bubbles and light areas represent structure); (B) segmented image (black pixels represent bubbles and white pixels are structure).

After trying several algorithms, a band thresholding method followed by a growing process was finally selected to segment the bubbles and structure pixels (Figure II.2 B). The band thresholding method was used to introduce flexibility to the global threshold selection decision.

Gray pixels, lower than a first threshold (Th_1), are classified as bubbles and pixels, higher than a second threshold (Th_2), are classified as structure (Figure II.3). These two thresholds were selected in order to obtain a high confidence for the first classification process. After this initial classification, pixels between these two thresholds were classed as undetermined at this first step. In order to classify the undetermined pixels a second growing step was performed. This second step consists of classifying undetermined pixels taking into account the previous classified neighbours in a growing process. This technique was previously used for detecting weed patches in cereal crops (Benlloch et al. 1995, Benlloch et al. 1996a, Benlloch et al. 1996b). Image processing was carried out using own code developed in the Matlab computational environment (The Mathworks, Natick, Massachussets, USA)

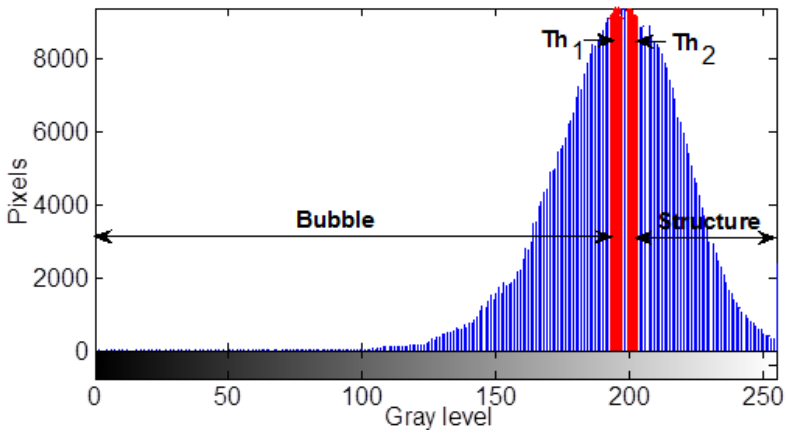

Figure II.3.Thresholds for classifying undetermined pixels.

3. Results & discussion

3.1 SL method results

The evolution of dough volume during fermentation was characterized from data obtained employing the structured light method. The dataset was expressed as the transversal area (*A*), the maximum height (*H*) and the ratio between both parameters *Q* at each time. Figure II. 4 shows the evolution of the transversal area (*A)* against the time of the fermentation process for F1, Fm and F2 until *Tf*, as this is the most representative parameter for the evolution of the process.

The results showed different values of *Tf*, *A* and *H* for the doughs. F2 attained the highest values (180 minutes, 17.2 $m^2 \cdot 10^{-4}$ and 7.7 $m \cdot 10^{-2}$ respectively). F1 presented the lowest values (100 minutes, 11.7 $m^2 \cdot 10^{-4}$ and 5.1 $m \cdot 10^{-2}$ respectively) and Fm reached intermediate values (Table II.2). It is interesting to note that behavior was similar until around 100 minutes, when statistical differences between the *A* and *H* of the doughs were not found, then F1 depleted, and Fm started to change its growth rate. Fm increased in size till around 150 minutes, then reduced its growth rate and attained intermediate values of *A* and *H* between F1 and F2 at its *Tf*. The reduction in Fm's growth rate could be due to features contributed by F1 and F2. Fm's behavior was quite logical as expected. This helped to confirm that

information about the behavior of F1 and F2 obtained by SL was reliable.

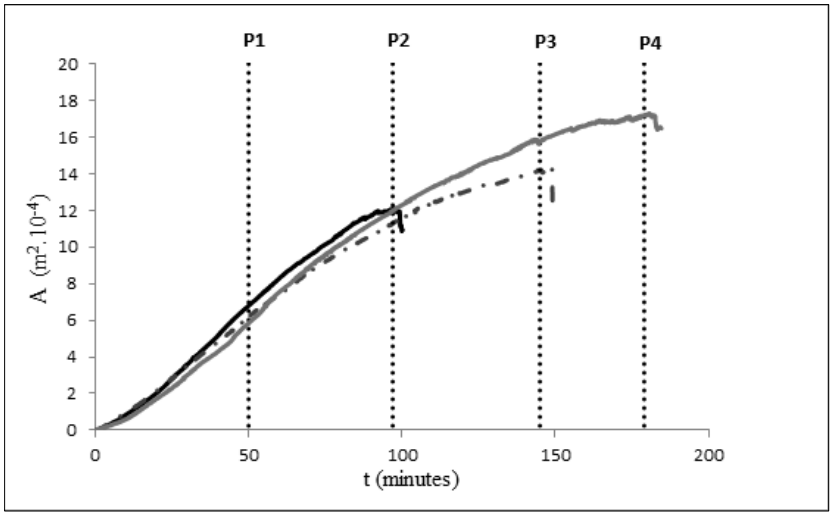

Figure II.4. Evolution of transversal area (*A*) of F1 (—), F2 (—) and Fm (---) during the fermentation process and sampling point times (T) to analyse image segmentation.

3.2 2D image segmentation results

Information about average final bubble size (*Bz*) and the population density (*Dp*) of samples was obtained through image segmentation. Table II.2 shows the results of different sampling times (T1, T2, T3 and T4) for each flour. *Bz* increased during fermentation, while *Dp* presented inverse behavior (Figure II.5 A). These behaviors agreed with studies realized previously by the authors, which showed that the rate of bubble size gain had a great influence on the structure of the dough during the fermentation process (Upadhyay et al. 2012;

Prud'homme and Khan, 1996; Wilde, 2003; Autio and Laurikainen, 1997). The results showed an increase of *Bz*, but with different rates between flours. At T1 and T2, F1 presented a greater *Bz* than Fm and F2. Furthermore at T2, F1 presented similar differences.

Table II.2. SL and 2D segmentation image analysis results.

Time	Sample	Area (A) ($m^2.10^{-4}$)	Height (H)($m.10^{-2}$)	Q(m)	Medium Bubble Size (Bz) ($m^2.10^{-6}$)	Density population (Dp)(bubbles/$m^2.10^{-4}$)
T1 (50 min)	F1	6.5 ± 0.1 ^{a}	2.9 ± 0 ^{a}	2.24 ± 0.1 ^{b}	2.7 ± 0.1 ^{b}	15.0 ± 0.8 ^{b}
	Fm	5.8 ± 0.6 ^{a}	2.6 ± 0.2 ^{a}	2.26 ± 0.04 ^{a}	2.0 ± 0.2 ^{a}	18.1 ± 1.2 ^{a}
	F2	5.8 ± 0.1 ^{a}	2.4 ± 0 ^{a}	2.36 ± 0.02 ^{a}	1.7 ± 0 ^{a}	19.6 ± 0.4 ^{a}
T2 (100 min)	F1	12.0 ± 0.3 ^{a}	5.4 ± 0 ^{a}	2.21 ± 0.07 ^{a}	3.3 ± 0.3 ^{c}	12.3 ± 0.7 ^{b}
	Fm	11.3 ± 0.6 ^{a}	5.1 ± 0.4 ^{b}	2.23 ± 0.05 ^{a}	2.4 ± 0 ^{b}	14.0 ± 1.0 ^{a}
	F2	11.7 ± 0.1 ^{a}	5.1 ± 0.2 ^{b}	2.29 ± 0.01 ^{a}	1.8 ± 0 ^{a}	19.2 ± 0.4 ^{a}
T3 (150 min)	Fm	14.1 ± 0.8 ^{b}	6.3 ± 0.1 ^{a}	2.23 ± 0.1 ^{a}	3.1 ± 0.2 ^{b}	9.3 ± 0 ^{b}
	F2	16.0 ± 0.3 ^{a}	7.2 ± 0.1 ^{b}	2.24 ± 0.02 ^{a}	2.3 ± 0.2 ^{a}	13.6 ± 1.1 ^{a}
T4 (180 min)	F2	17.2 ± 0.2	7.7 ± 0.2	2.22 ± 0.02	3.2 ± 0.1	12.8 ± 0.2

Different letters within columns mean significant differences at $p \leq 0.05$.

These results explained why F1 presented the lowest *Tf*, as bubble size at T2 was too high to resist dough structure so it reached coalescence and consequently overall depletion. Figure 5b shows the bubble sizes of all samples at T2, evidencing differences in the internal structure of the doughs based on significant differences between *Bz* and *Dp*, while differences between *A* were not found. Moreover, the same behavior of Fm and F2 in comparison with F1 at T2 were observed at T3 and T4. Figure 5c shows that just before the *Tf* of each dough, *Bz* and *Dp* presented the same tendency to reach similar values at the end. So, although *A* and *H* were different at *Tf*

for the doughs, the internal structure based on bubble number and size was not different for all samples before coalescence.

3.3 Joined analysis of SL and 2D image segmentation results

The data obtained by both image analysis techniques were compared and analyzed jointly. The objective was to see whether the SL results agreed with the image segmentation analysis. The evolution of the dough during fermentation was registered by SL, which provided information about dough growth kinetics, volume and shape at each second. SL parameters (*A* and *H*) were used in order to a further analyze of the dough shape, giving a ratio between both *Q* (*A/H*). This parameter linked the increment of height and transversal area. It was used as it is possible to find samples with non-different total volumes but different heights in function of flour properties as well as rheological features. The first study was to relate average final bubble size (*Bz*) to the transversal area of the doughs (*A*) at each sampling point (T). Figure 6 shows an example of the relationship presented between *A* and *Bz* at each T.

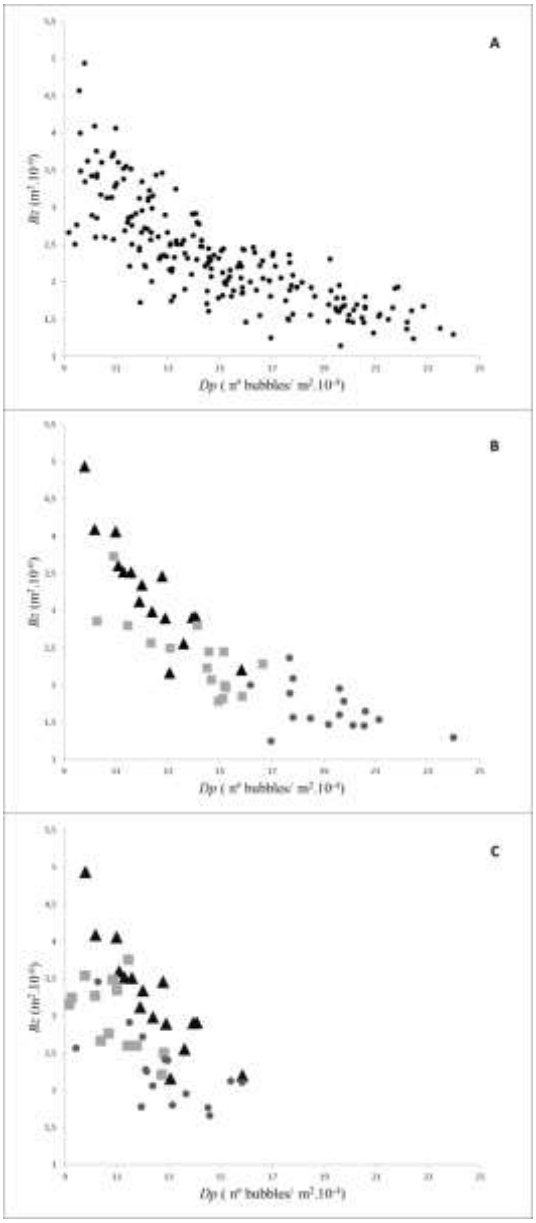

Figure II.5. Correlation between Population Density of bubbles (*Dp*) vs. Average bubble size (*Bz*) for (A) at all sampling times, (B) T2, and (C) *Tf* of each dough. (Series of B and C sections are: F1 (▲);Fm (■) and F2 (●)).

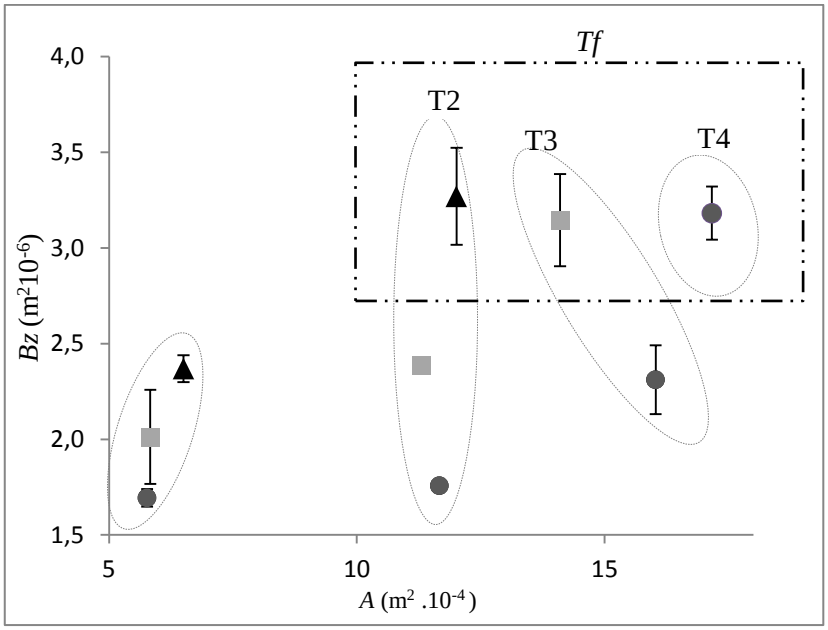

Figure II.6. Evolution of Average bubble size (*Bz*) against the increase of the transversal area of doughs (*A*) at each sampling point (P). (Series: F1 (▲); Fm (■) and F2 (●)).

A tendency can be seen about how *Bz* increases for each dough during the process. The kinetics of increase of Bz were similar because at the end all the doughs had a non-different value, however the doughs grew until reaching different values of *Tf* and *A*. Therefore, this variability could be interpreted as differences in the rate of bubble growth due to differences in rheological properties and chemical composition. Analysing each sampling point individually, it can be observed that *A* did not present differences between doughs at T1, and nor did *Bz*. At T2, the behavior was similar to T1. The *A* values were similar, but differences between *Bz* were

greater than at T1. T2 corresponded to the *Tf* of F1, which implied a maximum *Bz* and *A*, which meant that it was not able to endure the gas pressure resulting in coalescence and depletion. The values at T3 presented differences in both *A* and *Bz*. The process parameters of Fm should be between its precursor samples as it had a logically intermediate behavior between F1 and F2 during fermentation. Based on that theory, the results were successful. Fm presented a greater *Bz* than both, while it had the lowest *A*. Moreover, *Bz* at T3 presented non-different value with F1 at T2, as Fm reached coalescence at T3 so it also presented its maximum *Bz* as well as *A*. The differences between F1 and Fm were due to features proportioned by F2, which incremented its gas pressure resistance and thus coalesced later as well as a having a greater *A*.T4 correspond to the *Tf* of F2. It is the highest value of *A*, however *Bz* had a similar value to F1 at T2 and Fm at T3. Therefore F2 was able to resist greater amounts of gas for a longer time than the other two doughs. Variability between the *Tf* of doughs meant different levels of gas resistance in the dough matrix. An early *Tf* indicated that the gluten-starch matrix was not able to endure gas divided into small bubbles. So, smaller bubbles completely disappeared as a consequence of the mass transport of gas from small to large bubbles, causing an overall depletion of the structure with time (Mills et al. 2003).

The next step was to analyze the influence of *Bz* on the shape of the dough. The *Q* parameter at each T was studied jointly with *Bz*. Figure II.7 shows the behavior of the *Bz* vs. *Q* correlation at each T (r=0.865). The tendency of *Q* during the fermentation process was to decrease though the central zone of the dough had a higher increase rate than the lateral zones, while *Bz* presented the opposite behavior. Differences in *Q* indicated that doughs with non-different *A* presented different values of *H*.

This behavior could be a consequence of different growth kinetics for the bubbles and their distribution in the dough, as well as friction forces between the container and the dough, resulting in the typical curvature of the loaf (Pour-Damanab et al. 2011; Ktenioudaki et al. 2009). It is notable to observe the different location of doughs for each sampling time in Figure II.7.

Differences in *Q* values were observed for each dough at each P. The greatest difference was presented at T1, where F2 had an important difference in comparison with F1 and Fm. This meant that although all the doughs presented non-different *A* at T1, they had significant differences between both *Bz* and *Q*. Therefore, F2 had a lower increase of *H* than F1 and hence Bz too. The rest of P followed the same pattern. These behaviors suggested that the distribution of the larger F1 bubbles could accentuate the central zone of the dough, deforming it and increasing the *H* values but not *A*. Modification of the gluten-starch matrix during fermentation could also have an

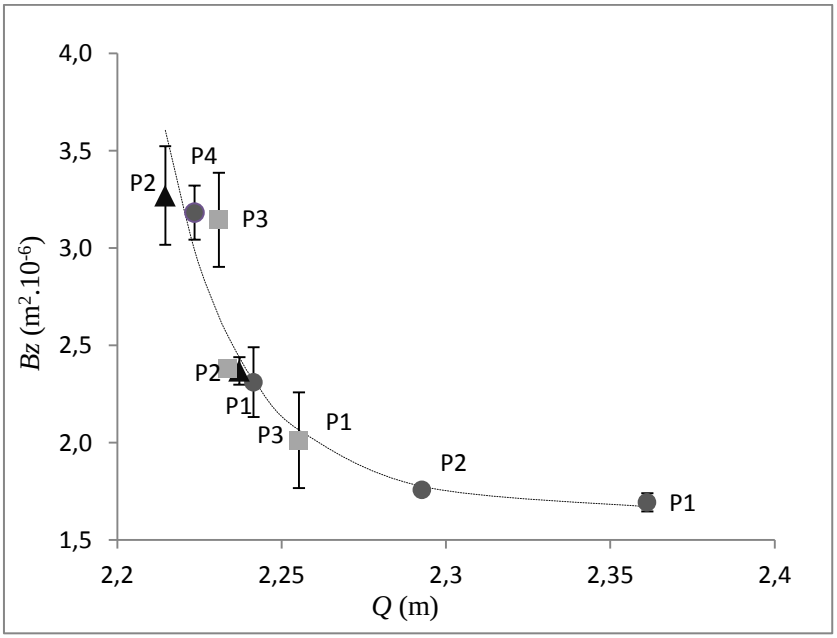

Figure II.7. Relationship between bubble size (Bz) vs. shape parameter of SL (*Q*) of each dough at each sampling point (P). (Series: F1 (▲); Fm (■) and F2 (●))

influence on shape changes. As doughs reached *Tf*, the gluten-starch matrix was weakened and gas pressure increased (Pyler et al. 1988b; Wieser et al. 2006; Dreese et al. 1988), consequently, as bubbles started coalescing, a decrease of dough surface resistance was produced and hence an increase *H* in the central zone of the dough. According to T2, T3 and T4, doughs followed the same tendency equalling their parameters at *Tf*. These results suggested that these experimental doughs could not achieve a *Bz* higher than 3-3,3$m^2.10^{-6}$ obtaining between 2.21-2.23 for *Q.* Differences in *Q* at *Tf* could be explained because sampling was carried out just before the *Tf* of each

sample, so small differences in this value could affect the results, increasing their dispersion. Furthermore, *Q* showed a strong sensibility to variations in *Bz* and *Dp*. However, it is difficult to attain better accuracy for this characteristic, so it is necessary to improve the system to obtain less dispersion of the data. The results could be explained by variability in the mass transport of gas from small to large bubbles, causing differences in the stability of the dough matrix, and in turn influencing dough shape. Therefore, retention of gas was affected more or less depending on the dough, thus retarding the overall weakening of the structure and resulting in higher yields of *A* (Shah et al. 1998;Gan et al. 1995).

4. Conclusions

Relationships between the information based on SL and the internal dough structure were found. It was possible to link the behavior of SL parameters to bubble growth kinetics using 2D image analysis as a tool. Although in the end, the dough fermentation capacity (Tf), the area (A), and maximum height (H) were different, the relationship between the parameters were similar, reaching similar final bubble size as a consequence of the coalescence phenomena, independent of the bubble growth rate.

The relationships obtained could be useful to determine the state of doughs during the fermentation process using the SL method, in order to improve the characterisation of different flour batches as well as improve monitoring of the processes. It could represent a

base to develop prediction models as well as devices to monitor the fermentation phase of the bread-making process.

5. Acknowledgements

We wish to thank the Polytechnic University of Valencia and Generalitat Valenciana for the financial support they provided through the PAID-05-011-2870 and GVPRE/2008/170 Projects, respectively.

6. Bibliography

Autio, K., & Laurikainen, T. (1997). Relationships between flour/dough microstructure and dough handling and baking properties. Trends in Food Science & Technology. Volume 8, Issue 6, June 1997, Pages 181–185.

Bajd, F. & Serša, I. (2011).Continuous monitoring of dough fermentation and bread baking by magnetic resonance microscopy. Magnetic Resonance Imaging, 29(3), 434-442.

Barak, S., Mudgil, D. &Khatkar, B.S. (2013).Relationship of gliadin and glutenin proteins with dough rheology, flour pasting and bread making performance of wheat varieties.Food Science and Technology, 51, 211-217.

Benlloch, J.V. , Sánchez, A., Agusti, M., Alberto, P. (1996b). Weed Detection in Cereal Fields Using Image Processing Techniques,Precision Agriculture. Precision agricu 3, 903-90. American Society of Agronomy, Crop Science Society of America, Soil Science Society of America.

Benlloch, J.V., Agusti, M., Sánchez, A., Rodas, A. (1995). Colour segmentation techniques for detecting weed patches in cereal crops. Proc. of Fourth Workshop on Robotics in Agriculture and the Food-Industry, 30-31.

Benlloch, J.V., Sánchez-Salmerón, A., Christensen ,S., Walter, M. (1996a). Weed mapping in cereal crops using image analysis techniques. Conference on Agricultural Engineering (AgEng '96), 1059-1060. Universidad Politécnica de Madrid

Cocchi, M., Corbellinib M, Focaa,G., Lucisanoc, M., Paganic, M. A., Lorenzo T. &Alessandro, U. (2005). Classification of bread wheat flours in different quality categories by awavelet-based feature selection/classification algorithm on NIR spectra.AnalyticaChimicaActa, 544, 100–107.

Dreese, P.C., Faubion, J.M., Hoseney, R.C., 1988. The effect of different heating and washing procedures on the dynamic rheological properties of wheat gluten. Cereal Food World 33, 225–228.

Falcone, P.M., Baiano, A., Zanini, F., Mancini, L , Tromba, G., Dreoss D. (2005). Three-dimensional quantitative analysis of bread crumb by X-ray microtomography. Journal of Food Science, 70(4):E265–72.

Gan, Z., Ellis, P.R. & Schofield, J.D. (1995).Gas Cell Stabilisation and Gas Retention in Wheat Bread Dough.Journal of Cereal Science, 21(3), 215-230.

Gonzalez-Barrón, U., Butler. F. (2008). Fractal texture analysis of bread crumb digital images. Eur Food Res Technol (2008) 226:721–729.

He, H., Hosene, R.C. (1991)Differences in gas retention, protein solubility, and rheological properties between flours of different baking quality. Cereal chemistry.68(5) 526-530.

Ivorra, E., Verdú, S, Sánchez A., Barat, J.M., Grau., R. Continuous monitoring of bread dough fermentation using a 3D vision Structured Light technique. Journal of Food Engineering 130 (2014) 8–13.

Ktenioudaki, A., Butler, F., Gonzales-Barron, U., Mc Carthy, U., Gallagher, E. (2009).Monitoring the dynamic density of wheat dough during fermentation.Journal of Food Engineering, 95, 332–338.

Le-Bail, A. Boumali, K., Jury, V., Ben-Aissa, F., Zuniga R. (2009). Impact of the baking kinetics on staling rate and mechanical properties of bread crumb and degassed bread crumb .Journal of Cereal Science, 50, 235-240.

Lassoued, N., Babin, P., Della Valle, G., Devaux, M.F., Reguerre, A.L., 2007. Granulometry of bread crumb grain: contributions of 2D and 3D image analysis at different scale. Food Res. Int. 40, 1087–1097.

Mills, E. N. C., Wilde, P. J., L. Salt, J. &Skeggs, P. (2003). Bubble formation and stabilization in bread dough. Food Bioproducts Process, 81, 189-193.

Miralbes, C. (2004).Quality control in the milling industry using near infrared transmittance spectroscopy. Food Chemistry, 88 621–628.

Otsu, N., (1979). A Threshold Selection Method from Gray-Level Histograms.2eeeTtransactions on Systrems, man, and cybernetics, smc-9(1).

Novotni, D., Ćurić, D., Galić, K., Škevin, D., Neđeral, S., Kraljić, K., Gabrić, D., Ježek, D. (2011).Influence of frozen storage and packaging on oxidative stability and texture of bread produced by different processes. LWT - Food Science and Technology, 44, 643-649.

Pérez-Nieto, A., Chanona-Perez, J.J, Farrera-Rebollo, R.R, Gutierrez-Lopez, G.F, Alamilla-Beltran, L., Calderon-Dominguez, G. (2010). Image analysis of structural changes in dough during baking. LWT Food Science and Technology. 43, 535-543.

Porosity in bread dough during proving. Food and bioproducts processing 87, 17–22

Pour- Damanab A.R.S, Jafary, A. & Rafiee, Sh. (2011). Monitoring the dynamic density of dough during fermentation using digital imaging method. Journal of Food Engineering, 107(1), 8-13.

Prud'homme, R.K., Khan, S.A., 1996. Experimental results on foam rheology. In: Prud'homme, R.K., Khan, S.A. (Eds.), Foams: Theory, Measurements, and Applications. Marcel Dekker, New York, pp. 217–241.

Pyler, E. J. (1988b). Physical chemistry and colloidal systems (3rd edition.)Baking science and technology, pp. 290–296). Kansans City, Missouri: Sosland Publishing Company.

Scanlon, M.G., Zghal, M.C. (2001). Bread properties and crumb structure. Food Res. Int. Volume 34, Issue 10, 2001, Pages 841–864

Wang, S., Austin, P., Bell, S. (2011). It's a maze: The pore structure of bread crumbs. Journal of Cereal Science, 54 203-210.

Shah, P., Campbell, G. M. ,. Mckee S. L, &. Rielly, C. D. (1998). Proving of bread dough: modelling the growth of individual bubbles. Trans IChemE, Vol 76, Part C, June.

Lucas, T., Grenier, D., Bornert, M., Challois, S., Quellec, S., (2010). Bubble growth and collapse in pre-fermented doughs during freezing, thawing and final proving. Food Research International. 43, 1041–1048

Trobina, M. (1995).Error model of a coded-light range sensor. Technique Report, Communication Technology Laboratory.

Upadhyay, R., Debjani, G. &Mehra, A. (2012). Characterization of bread dough: Rheological properties and microstructure Original Research Article. Journal of Food Engineering, 109(1), 104-113.

Verdú, S., Ivorra, E., J. Sánchez, A., Girón, J., Barat, J.M. & Grau, R. (2013). Comparison of TOF and SL techniques for in-line measurement of food item volume using animal and vegetable tissues. Food Control, 33(1), 221-226.

Wieser, H., Bushuk, W., &MacRitchie, F. (2006).The polymeric glutenins.InC.

Wilde, P., 2003. Foam formation in dough and bread quality. In: Cauvain, S.P. (Ed.)

Zhang, Z. (2000). A flexible new technique for camera calibration. Pattern Analysis and Machine Intelligence, IEEE Transactions on, 22(11), 1330- 1334. doi:10.1109/34.888718

Zuñiga, R., Le-Bail, A. (2009). Assessment of thermal conductivity as a function of porosity in bread dough during proving. Volume 87, Issue 1, March 2009, Pages 17–22

CAPÍTULO III

Study of high strength wheat flours considering their physicochemical and rheological characterisation as well as fermentation capacity using SW-NIR imaging

Journal of Cereal Science, Volume 62, March 2015, Pages 31-37

Samuel Verdú, Eugenio Ivorra, Antonio J. Sánchez, José M. Barat, Raúl Grau

Versión adaptada para la tesis doctoral

Abstract

The characterization of wheat flour destined for the bread-making process using Hyperspectral image analysis, based on Short Wave NIR imaging (SW-NIR), was studied. The first step was the characterization of batches of wheat flour considering physicochemical, rheological and fermentation kinetic parameters. The second step was to capture hyperspectral images of each batch. The results showed some significant differences in fermentation capacity related to gluten and its protein sub fractions. However, significant rheological differences were not observed. At first, the acquired images were analyzed by Principal Component Analysis, where a clustering tendency was observed. Consequently, a Partial Least Square analysis was carried out to study the relationship between the SW-NIR spectra response and the physicochemical, rheological and fermentation kinetic parameters. The results showed an important correlation between SW-NIR spectra (from 760 to 900 nm) and the fermentation capacity parameters of the batches. SW-NIR imaging analysis was able to obtain useful information about wheat flour which was possible to correlate with fermentation behaviour. Consequently, the studied technique may represent a useful, rapid and non-destructive method to help in the characterisation of wheat flour with non-different rheological parameters considering their behaviour during the fermentation process.

Keywords: SW-NIR image analysis, wheat flour, characterization, fermentation

1. Introduction

The production of wheat and derived products represents a large sector within the food industry. Both the kernels and their transformation have become a fundamental part of world economics. Additionally, cereals represent the principal energy and nutrient source in the food chain (Fava et al., 2013). Thus, the continuous improvement of processes and production methods is important to obtain better yields from raw materials and products. Although the processes used during transformations are quite well known, there are some factors that can still be improved. These factors have a great influence on processing, leading to repercussions in the final products. Variations in the raw material could represent a problem during transformation, producing final products with non-conformities and a corresponding loss in quality. Climatologic conditions during plant growth, methods of storing the kernels and the milling process all have an influence on the characteristics of the resulting flour. Moreover, the different cultivars are an important factor regarding the behaviour of flours. Therefore the identification of the best mixtures of wheat varieties is fundamental to guarantee the best performance of flours in production processes (Uthayakumaran et al., 1999). It is therefore necessary to analyse

each batch exhaustively to ensure accurate characterization and classification by the producer, who can thus offer a homogeneous product with optimal technological characteristics. Likewise, the transformation industry requires accurate classification to adapt its processes, both considering the product formula and process variables. For this reason, monitoring the raw material is an important phase in the productive processes of cereals and flour. For wheat flour in particular, there are standard characterization methods.

These methods are based on chemical composition (moisture, protein, dry gluten, ash, etc.) and rheological properties (Chopin alveograph, Brabender farinograph, RVA (Rapid Visco Analyser), etc). In short, a large amount of data is used to classify wheat flours. Although the relationships between the factors during processing are quite well known, there are many which are quite difficult to control, especially when they interact. These unexpected factors could result in alterations in processing and no-conformities in the final product, such as loaf dimensions, crumb texture and crust visual aspect and consistency of bread (Li Vigni et al., 2010).

It is therefore crucial to develop new studies to obtain advances which improve end product, being as constant as possible in order to satisfy the consumer's needs (Li Vigni et al., 2010). Moreover, traditional methods involve high economic investment in either laboratory equipment or external analysis, in addition to qualified

personnel and many man hours of work. Therefore, the development of quick analysis methods which facilitate the accurate characterization of wheat flour may be useful to improve production efficiency. In this field, several authors have reported research on new fast and non-destructive methods for monitoring wheat kernel production as well as processed wheat flour (Arazur, et al., 2012). This research has been carried out using many different technologies. One of the most important areas of applied technology is the analysis of infrared spectra (IR) using the whole range of wavelengths. For example Shao et al., (2011) predicted protein and starch levels in flour studying IR response with a spectrophotometer. Similarly, methods for the characterization of flours considering their properties during the bread-making process (Li Vigni et al., 2009), classification of different categories of flour batches (Cochi et al., 2005) and predictions about milling and baking parameters of different wheat varieties have been developed (Jirsa, et al., 2008). Characterisations through NIR technology of some phases of bread-making process, such as leavening phase, have also been reported. Concretely by Li Vigni & Cocchi (2013), where the existence of differences among the mixtures on the basis of NIR spectrum variability with respect to the leavening time were described. On the other hand, short near infrared image analysis of the raw material has been less studied. Manley et al., (2011) characterized water diffusion through wheat kernel tissues; Xing et al., (2011) compared the results from infrared spectrophotometry and hyperspectral

image analysis for their study of alpha-amylase activity determination; and Singh et al., (2009) used the same method to detect insect damage to wheat kernels. Furthermore, research into the relationship between hyperspectral image analysis and toxic metabolites of wheat fungus has been developed (Del Fiore et al., 2010). The present work is aimed at studying the capability of a SW-NIR camera for detecting differences among wheat flours which did not show differences in routine analysis at industry but showing different fermentation behaviour.

2. Material and methods

2.1 Assay development

The study was performed on 6 different batches of wheat flour sold as "high strength flour", employed for bakery products, sliced bread and sponge cakes (Molí del Picó-Harinas Segura S.L, Valencia-Spain). The batches were obtained in 6 different consecutive weeks (B1, B2, B3, B4, B5 and B6). First, wheat flour batches were characterized according to their physicochemical and rheological features, SW-NIR image captures and their kinetic fermentation parameters using the structured light (SL) vision technique. Then, according to the statistical results obtained from the SW-NIR image captured, data of batches B2 and B5 were regrouped and recoded as GA, and in the same way B4 and B6 as GB. In addition a new flour sample (50% mix) was generated mixing 25% of flour B2, B5, B4 and B6. For this last

flour sample news analysis with SW-NIR and SL techniques were carried out and statistical analysis was done again taking into account the new samples codification. Finally, according to the information from these two previous steps, statistical correlation between the physicochemical and rheological characteristics, and kinetic fermentation parameters with information from the spectra from the SW-NIR image captured was carried out.

2.2. Dough preparation and fermentation process

The ingredients employed and percentages used were: 56% wheat flour, 35% water, 2% refined sunflower oil (maximum acidity 0.2º Koipesol Semillas S.L - Spain), 2% commercial pressed yeast (Saccharomyces cerevisiae, Lesafre Ibérica S.A - Spain), 4% white sugar (≥ 99.8 % sucrose. Azucarera Ebro, S.L – Spain) and 1.5% NaCl (refined marine salt ≥ 97 % NaCl. Salinera Española, S.A – Spain). The dough was made by mixing all the ingredients in a food mixer (Thermomix® TM31, Vorwerk, Germany) according to the following method. In the first phase, the liquid components (water and oil), sugar and NaCl were mixed for 4 min at 37 °C. The pressed yeast was added in the next phase and mixed at the same temperature for 30 seconds. Finally, the flour was added and mixed with the rest of the ingredients using a default bread dough mixing program which provides homogeneous dough. This program is based on the mixing of ingredients with random turns of the mixer helix in both directions

(550 revolutions/minute). This process was applied for 4.5 min at 37ºC. Then, 450 g of dough (approximately 1cm thick) was placed in a metal mould (8x8x30cm) for fermentation. This was carried out in a chamber with controlled humidity and temperature (KBF720, Binder, Tuttlingen, Germany), where a 3D Structured Light (SL) device was developed and calibrated. The conditions of the fermentation process were 37 °C and 90 % Relative Humidity (RH). The samples were fermented until the dough lost its stability and size (Ft), when growth depletion occurred, which was assumed when the 3D imaging started to report dough area values describing both an asymptotic behaviour and a decrease of area values.

2.3 Characterisation of batches

2.3.1 Physicochemical analysis

Multiple physicochemical and rheological parameters were analysed for each wheat flour batch in order to characterize them. Each analysis was performed in triplicate, according to the standard methods of the International Association for Cereal Science and Technology (ICC), except the fractionation of gluten proteins, which was based on the method described by Graveland et al. (2000). The analysed parameters were the following: percentage of moisture (H), gluten (G), gliadin (GLI), glutenin (GLU), and alveograph parameters (P=maximum pressure (mm), L=extensibility (mm); W=strength (J^{-4})) (ICC standard No.121).

2.3.2 SW-NIR data acquisition & processing

Images of 12 samples in each batch were taken using a Photonfocus CMOS camera MV1-D1312 40gb 12 (Photonfocus AG, Lachen, Switzerland) and SpecimImSpector V10 1/2" filter (Specim Spectral Imaging, LTD., Oulu, Finland), which works as a linear hyperspectral camera. The illuminant was an ASD illuminator reflectance lamp (ASD Inc, Boulder, USA) which produces stable illumination across the full working spectral range.

Samples were placed in a glass Petri dish (10 cm diameter) and the spectra were collected directly at room temperature, without any sample treatment.

The position of the illuminant and camera relative to the sample was always constant, to control the lighting conditions and to obtain a constant image size. The distance between the illuminant and the sample was 0.525 m, with a distance of 0.225 m between the camera and the sample. The image (scanned line) obtained was composed of 256 grey levels (8 bits). The diffuse reflectance spectrum was collected using 53 different wavelengths (each wavelength was digitalized with 8 bits). These wavelengths were distributed at intervals of 11.2 nm in the range from 400 to 1000 nm. The scanned line was composed of 1312 points, so that an image was recorded with a resolution of 1312 x 1082 pixels.

The camera was operated by developed software based on the SDK Photonfocus-GigE_Tools using the programing language C++.

Reflectance calibration was performed to normalize the non-linear light source reflectance. This was done by applying equation 1 where *rW* is the reflectance value of a white pattern reflectance acquired under the same conditions, *rD* is the dark measure covering the camera's objective and *rS* is the sample reflectance.

$$R(\lambda) = \frac{(rS - rD)}{(rW - rD)} \quad (1)$$

Other operations carried out on the spectra for further statistical processing were Standard Normal Variety.

Image reflectance calibration and preprocessing were performed using a code developed with Matlab R2012a (The Mathworks, Natick, Massachussets, USA).

2.3.3 Monitoring fermentation with the ¨Structured Light¨ method (SL) and image processing

The purpose of the 3D vision system was to obtain the 3D profile of the samples during fermentation. In order to accomplish this objective the 3D vision system specifically developed in a previous study was used to monitor fermentation (Ivorra et al., 2013). This vision system was composed of a network graycamera (In-Sight 5100, Cognex, Boston, Massachusetts (USA)) and a red linear laser (Lasiris SNF 410, Coherent Inc. Santa Clara, California (USA)), both of them were inside the fermentation chamber.

The 3D visual system has a resolution of 2.1*10-4m and 1.4*10-4 m for the X and Z axes respectively. This resolution comes from the laser angle θ of 0.65 radians in combination with the resolution of the camera (640x480) and its distance from the sample. The working range was 0.1 m in the X axis and 0.08m in the Z axis.

The acquisition rate was 1 fps due to the long time that fermentation requires (around 2 hours). Calibration of the equipment was performed calculating a homography transformation (Zhang, 2000) taking 10 regularly distributed points in the laser projection plane with known coordinates (Trobina et al., 1995) and then using these 3D points and their corresponding points in the image.

The 3D sample profile is a 3D curve composed of the 3D points which lie between the known points of the mould's borders. In order to obtain these points, the first step was the segmentation of the laser points in the image captured by the camera using an Otsu's global threshold (Otsu, 1979). Then, these pixels were filtered removing non connected pixels with an area lower than 100px. The subpixel precision was achieved calculating the exact row coordinate by weight mean for each column using the intensity value.

The next step was the transformation from image coordinates to a 3D local coordinate system using the homography transformation previously calculated in the calibration step. The final step was to transform the local coordinate system using a rotation matrix which makes the z axis normal to the surface. The transversal area (A) (the integration of the Z values along the X direction of the sample) was

extracted continuously from the 3D sample profile to analyse the growth of the samples during fermentation with time, together with the time of the maximum transversal area (Ft).

Acquisition and data processing were carried out using a code developed in the Matlab 2012b computational environment (The Mathworks, Natick, Massachussets, USA).

2.3.4 Fitting of the dataset to the Gompertz prediction model

To model behaviour during fermentation, the dataset of the SL method, obtained from the 6 replicated doughs for each wheat flour batch, was fitted to the Gompertz prediction model. The Gompertz function is a nonlinear sigmoid growth function which was developed by Gompertz (1825) for the calculation of mortality rates of microorganisms. The equation is as follows:

$$A = a \cdot \exp((-\exp\left(\frac{V}{A} \cdot (Lt - t) + 1\right)) \quad (2)$$

Where *t* is time, *A* is the maximum area of the process, α is the area observed during process, *V* is the maximum rate of growth, and *Lt* represents the time of latency before the beginning of dough development.

The model parameters were determined using a nonlinear regression procedure and were obtained by minimizing the sum of squares of the prediction errors.

2.4 Statistical analysis

The physicochemical, rheological and fermentation parameters (H, G, Gli,Glu, Gli/glu, P, L, P/L, W and A, V, Lt and Ft) were studied with a one-way variance study (ANOVA). In those cases where the effect was significant (P-value < 0.05) the means were compared using Fisher's least significant difference (LSD) procedure. The relationship between data from physicochemical, rheological analysis, as well as fermentation kinetics was carried out using linear correlation. SW-NIR data spectra were analysed employing the multivariate statistical procedure employing Principal Component Analysis (PCA). The procedures were performed with PLS Toolbox 6.3 (Eigenvector Research Inc., Wenatchee, Washington, USA), a toolbox extension within the Matlab 7.6 computational environment (The Mathworks, Natick, Massachusetts, USA).

3. Results and discussion

3.1 Characterization of batches

3.1.1 Physicochemical analysis and fermentation kinetics

The 6 different batches of wheat flour were analyzed for different parameters. Table III.1 shows the results of the battery of analyses performed. The results indicated that there were no differences in H, Lt and alveograph parameters. However, significant differences in the amount of gluten, gliadin, glutenin, as well as in A, V and Ft were observed. The differences in gluten and its protein fractions could

help to understand the behaviour observed during the fermentation process, where differences between the kinetic parameters of dough development were observed (Ivorra et al., 2013). Figure III.1 shows the average of the evolution of A values for the 6 replicates of each flour processed (B1, B2, B3, B4, B5 and B6). It is important to observe the differences between them. B2 and B5 presented the highest non-different A values, followed by B3, and finally B4, B6 and B1 presented the lowest values. *Ft* followed the same behaviour as A. No significant differences were found for V and Lt.

To obtain a preliminary overall knowledge about the relationship between wheat flour composition and the fermentation capacity (maximum growth of dough), correlation map of both groups of data were performed (Table III.2).

Table III.1. Physicochemical, rheological and fermentation characterisation of flour batches.

	B1	B2	B3	B4	B5	B6
H (%)	14.3 ± 0.1a	14.2 ± 0.2a	14.5 ± 0.1a	14.6 ± 0.0a	14.2 ± 0.1a	14.6 ± 0.1a
G (%)	13.0 ± 0.1b	12.0 ± 0.1a	12.8 ± 0.2b	13.1 ± 0.2b	11.6 ± 0.2a	13.05 ± 0.2b
Gli (%)	7.2 ± 0.1a	7.3 ± 0.2a	7.3 ± 0.3a	7.1 ± 0.2a	7.3 ± 0.4a	7.2 ± 0.2a
Glu (%)	5.8 ± 0.4b	4.7 ± 0.1a	5.5 ± 0.2b	5.9 ± 0.2b	4.4 ± 0.1a	5.9 ± 0.3b
Gli/Glu	1.2 ± 0.1a	1.5 ± 0.1b	1.3 ± 0.1a	1.2 ± 0.0a	1.7 ± 0.1b	1.2 ± 0.1a
P	96.5 ± 2.1a	97.0 ± 1.6a	97.5 ± 1.7a	96.0 ± 1.4a	98.0 ± 1.8a	96.0 ± 1.9a
L	105.0 ± 1.4a	108.0 ± 1.0a	106.5 ± 1.2a	06.5 ± 0.7a	107.0 ± 1.2a	105.5 ± 1.3a
W	374 ± 5.7a	382 ± 5.4a	387 ± 5.2a	375 ± 5.7a	375 ± 5.5a	374 ± 4.3a
P/L	0.92 ± 0.1a	0.90 ± 0.2a	0.92 ± 0.1a	0.91 ± 0.2a	0.92 ± 0a	0.91 ± 0.2a
A ($m^2.10^{-4}$)	10.6 ± 0.7a	18.0 ± 1.0d	16.4 ± 0.8c	12.2 ± 0.7a	18.2 ± 0.5d	10.2 ± 1.0a
V ($m^2.10^{-4}$/min)	2.4 ± 0.2b	2.1 ± 0.4a	2.0 ± 0.1a	1.7 ± 0.0a	2.0 ± 0.1a	1.7 ± 0.2a
Lt (min)	1.7 ± 0a	1.6 ± 0a	2.0 ± 0a	1.8 ± 0a	2.0 ± 0a	2.1 ± 0.1a
Ft (min)	105.3 ± 3.5b	156.5 ± 4.0c	148.7 ± 5.0c	90.3 ± 1.4a	186.7 ± 5.0d	108,5 ± 4.8b

Values and standard deviation of composition parameters; H, moisture content; G, content of dry-gluten; Gli, gliadin content; Glu, glutenin content and Gli/Glu, ratio between gliadin and glutenin content. Alveograph parameters: P, maximum pressure; L, extensibility; W, strength. Fermentation parameters: A, maximum area ; V, maximum growth rate ; Lt, time of latency and Ft, final time. Values followed by different letters are significantly different at $P < 0.05$ between columns.

Analyzing the results of correlations, only A and Ft presented a high R^2 of correlation with several physicochemical parameters. Concretely, A was closely related to G (R^2 = -0.825), Glu (R^2 = -0.860) and Gli/Glu (R^2 = 0.859). Furthermore, it also presented a good correlation with P (R^2 = 0.882) and Gli (R^2 = 0.866). In the same way, Ft presented a strong correlation to G (R^2 = -0.907), Glu (R^2 = -0.922) and Gli/Glu (R^2 = 0.928). In this case Ft also correlated well with P (R^2 = 0.891) but less with Gli (R^2 = 0.756). Thus, it was evident that gluten

and its protein sub fractions had an effect on fermentation behaviour (Barak et al., 2013).

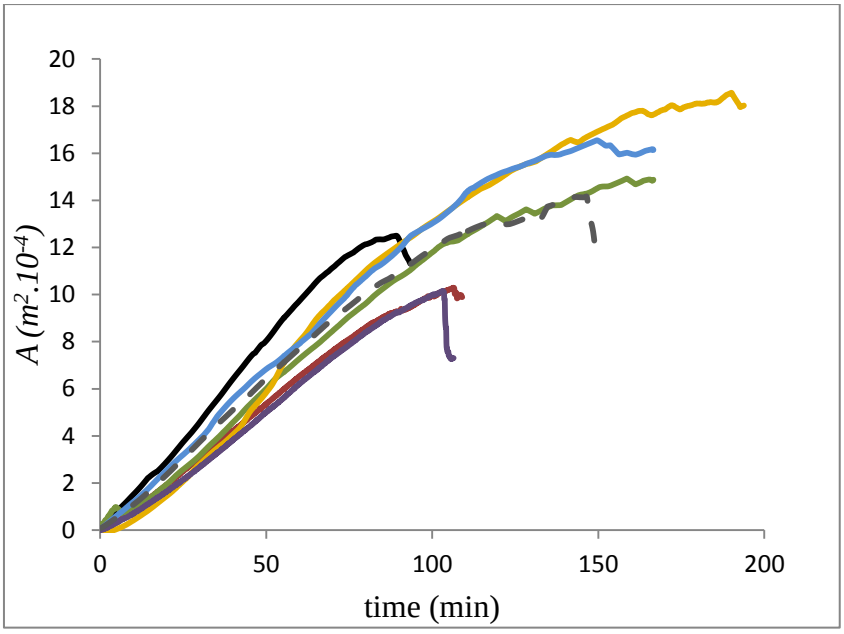

Figure III.1. Evolution of the transversal area of the dough (A) with fermentation time (until growth depletion occurred). Dough series are represented by the following colours: B1 –; B2 –; B3 –; B4–; B5 –;B6–; and 50% mix of GA (50% B2 + 50% B5)/GB (50% B4+ 50% B6) ––.

Table III.2. Coefficients of correlation (R^2) between rheological, chemical and kinetic parameters of the doughs, included scores of principal component 2 (PC2), obtained by SL technique, and physicochemical and rheological parameters of the flour batches.

	G	Gli	Glu	Gli / Glu	H	A	Ft	L	Lt	P	P / L	W	Score PC2
G	1												
Gli	-0.646	1											
Glu	0.995*	-0.711	1										
Gli / Glu	-0.995*	0.710	-0.998*	1									
H	0.814	-0.622	0.823	-0.815	1								
A	-0.825*	0.866*	-0.860*	0.859*	-0.842	1							
Ft	-0.907*	0.756	-0.922*	0.928*	-0.571	0.799	1						
L	-0.724	0.458	-0.727	0.714	-0.443	0.664	0.761	1					
Lt	0.093	0.013	0.093	-0.068	0.482	-0.329	0.166	-0.301	1				
P	-0.794	0.904*	-0.830*	0.845*	-0.645	0.882*	0.891*	0.496	0.145	1			
P / L	0.083	0.263	0.063	-0.025	0.231	0.100	0.027	-0.534	0.456	0.400	1		
W	-0.145	0.701	-0.222	0.210	-0.058	0.504	0.421	0.498	-0.062	0.467	-0.075	1	
Score PC2	-0.937*	0.791	-0.958*	0.948*	-0.787	0.885*	0.836*	0.671	-0.209	0.794	-0.111	0.317	1

*Correlation is significant at 0.05 level

The amount of G, Glu and Gli were the principal differences between the batches, so they could be the principal factor influencing fermentation parameters as resistance to gas pressure and dough stability depends largely on these characteristics (Park et al., 2006). Fermentation of B2 and B5 showed significant differences in comparison to B1, B4 and B6, which reached around 40% less A. Moreover, B6, B1 and B4 presented different characteristics concerning A and Ft values. Concretely, B1 and B6 reached a similar A value but B4 was significantly higher, while Ft was quite low in those the batches compared to the rest of the batches with high development. Furthermore, B2 and B5 also presented the lowest

amount of Glu and therefore higher Gli/Glu. Previous research performed by several authors postulate that the amount of gliadin and glutenin and an optimum ratio between them (Gli/Glu) are among the main factors which affected fermentation characteristics (Veraverbeke & Delcour., 2002). These factors possibly resulted in different capacities to retain gas and thus, provided different values of A and Ft. Probably, B1 and B4 (which presented the lowest *A* and *Ff* and the greatest amount of glutenin but not gliadin) had a decompensated ratio due to having too much glutenin, which offered an increase in the tenacity of the dough. This could have been an impediment to high values of A and Ft.

3.1.2 SW-NIR imaging analysis

Mean SW-NIR spectra for each wheat flour batch are represented in Figure III.2-A. It is possible to observe different activity zones for the spectra. Both the visible and infrared zone presented peaks which could offer information about the samples. Thus, to analyze this information and evaluate whether the spectra reported useful data about samples, complete spectra were processed. Principal Component Analysis (PCA), after Standard Normal Variety pre-treatment (SNV), was carried out.

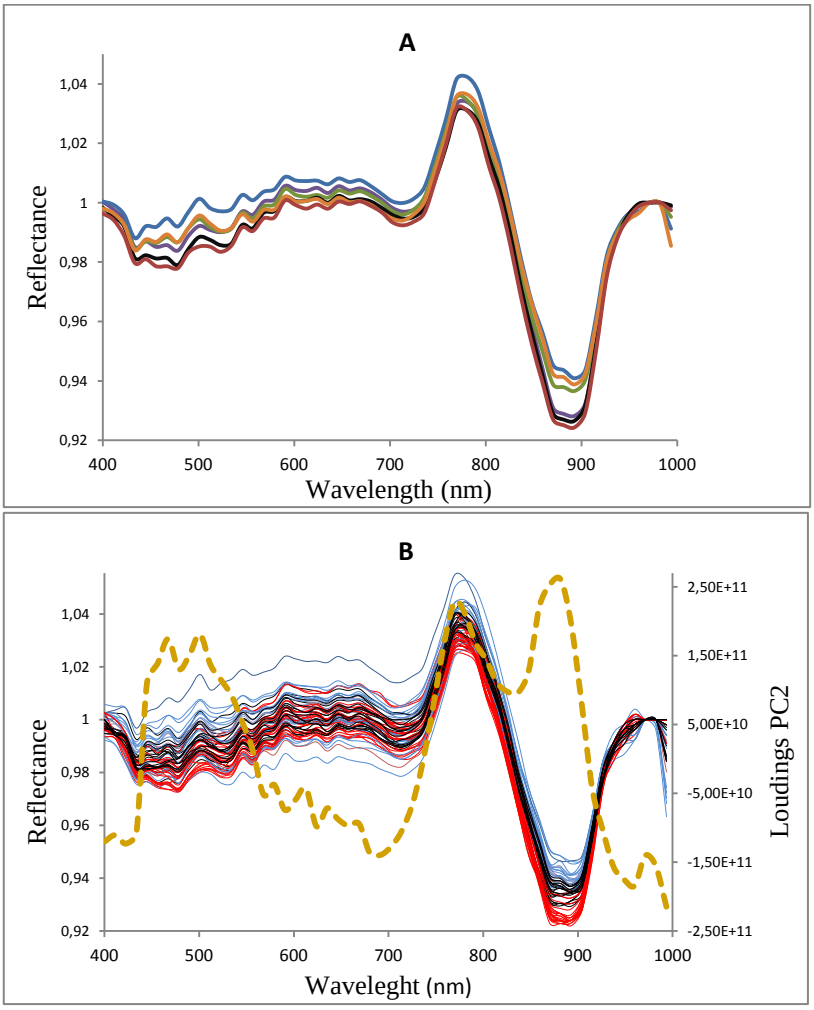

Figure III.2. **A**: Means of the spectra response for each wheat flour batch. B1 –; B2 –; B3 –; B4–; B5 –; B6–**.** **B**: Set of spectra responses of GA (B2+B5) –, GB (B4+B6) – and a 50% mix –**.** Loadings from the PC2 ---.

Figure III.3-A shows the PCA space obtained for the first and second PC (86.64% explained variance) of complete spectra. Only the first 2 PCs were taken into account as it was considered that they explained the variance sufficiently. A tendency of groups across PC2 is observable. This tendency shows how flour batches were positioned in different zones of PC2, maintaining the relationship regarding fermentation behaviour (Figure III.3). It can be observed that B2 and B5 are positioned in the positive values zone of PC2 and B4 and B6 were isolated in the negative values zone of PC2. However, B1 and B3 appeared in the middle of both zones without significant differences compared to the rest of the batches. Although B1 and B3 were not positioned in a specific zone like the rest of samples, it is possible to see that they have a tendency to cluster. Concretely, B1 tended toward the zone where B4 and B6 were placed, while B3 tended toward the zone of B2 and B5.

Following the results, extremely placed batches without differences between them were studied in conjunction as a single sample. This means that B2 and B5 datasets were recoded as a single sample called GA, and B4 and B6 as GB. Furthermore, with the aim of proving the observed phenomena, a new flour sample was created to be analyzed by imaging analysis as the initial flours. This new sample (50% mix) was the result of mixing 25% of B2 + 25% of B5 + 25% of B4 + 25% of B6. A new PCA was performed using the information from the recoded GA and GB and those from the new sample (50% mix).

Figure III.3-B shows the obtained PCA space where the same clustering tendency as the previous study can be observed, where samples were clustered mainly by PC2. GA (B2+B5) was placed in the positive zone of PC2 and GB (B4 + B6) was placed in its negative zone, however the 50% mix sample was placed in the middle. To assess the information from PC2, loadings of the component were plotted across the studied wavelength (dashed line in Figure III.2-B). Peaks of loadings were observed in both the visible and infrared zone of the spectra. However, the PCA analysis, carried out only employing information from visible spectra or from SW-NIR spectra, showed a higher value of explained variance for the last (78% and 90.5% of the total variance captured respectively). In order to compare the behaviour of the 50% mix wheat flour during its fermentation with those obtained for the wheat flours used to make up the mixture, a new fermentation study was realized. The result of its growth curve is included in Figure III.1 (discontinuous black line). Fermentation parameters, obtained fitting the curve to the Gompertz equation (Table III.3), had intermediate values between the GA and GB wheat flours.

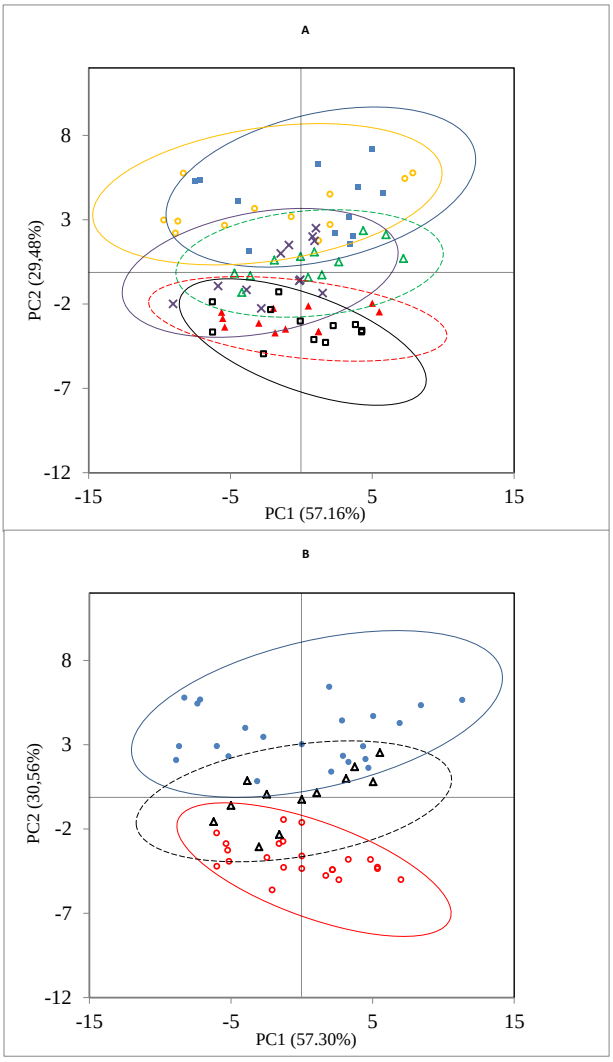

Figure III.3. PCA Studies. **A**: Scores plot of the first two PCs calculated by PCA based in the mean spectra from all the analyzed batches. B1x;B2■;B3Δ;B4□;B5○;B6▲. **B**: Scores plot of the unique two PCs calculated by PCA based in the mean spectra of GA (●), GB (○) and 50% mix of them (Δ). Circumferences mark significant differences.

So, according to the results expressed in Figure III.3-A and B and values of Table III.1 there is a parallelism between the physicochemical, kinetics parameters of fermentation and the information from the SW-NIR measurements. Therefore, comparing values of A and Ft (Table III. 1 and III.3) to the results from the PCA (Figure III.3-A and B) it is possible to observe that lower values of A and Ft were clustered in a different zone considering flour batches with higher values, furthermore flour batches with intermediate values were also positioned between the two previous zones. In order to evaluate this parallelism, correlations were carried out between the mean of the score, of each batch, from PC2 and the rest of the physicochemical and rheological parameters (Table III.2). The highest values of R^2 were obtained for the followed parameters: G, Gli, Glu, Gli/Glu, A and Ft.

The results show that the link between the fermentation behaviour and spectral response of the flour batches is probably mainly the amount of gluten and its sub fraction proteins, although other factors, such as starch, could also be affecting the process. It also proved that the amount of these components influences A and Ft directly and furthermore, they had an important relation to SW-NIR spectra response.

Table III.3. Fermentation characterisation of GA (B2+B5), GB (B4+B6) and a 50% mix (GA+GB) of flour batches.

	GA	*GB*	*50% mix*
A ($m^2.10^{-4}$)	18.1 ± 0.1a	11.2 ± 1.4c	14.1 ± 0.5b
V ($m^2.10^{-4}$/min)	2.1 ± 0.1a	1.7 ± 0a	2 ± 0.2a
Lt (min)	1.8 ± 0.3a	2.0 ± 0.2a	1.5 ± 0.3a
Ft (min)	171.6 ± 21.3a	107.6 ± 1.3b	143.4 ± 3.6ab

Fermentation parameters: A, maximum area; V, maximum growth rate; Lt, time of latency and Ft, final time. Values followed by different letters are significantly different at $P < 0.05$ between columns.

Thus, although the entire spectrum was analysed, the main information, which could differentiate the batches, was obtained around the interval from 760-900 nm approximately. Results conform to results of several previous studies, where relationships between both gluten and its sub fractions proteins to these absorption bands of spectra have been founded. As example of that, Chen et al. (2006) evaluating the NIR spectra of mixes with different proportions of gluten powder and starch observed that the absorbance of samples from 850 to 900 nm was increased together with the gluten concentration in the mixed formulation. Sinelli et al., (2011) reported that is possible to predict the amount of gluten in semolina for dried pasta analysing the spectra from 830 to 2700 nm and thus, to discern the technological quality of the raw material. The relationship between those absorption bands and functional groups is reported

by Murray (2004), who postulated that the groups R-NH_2 and R-NH-R among others have one of their maximum absorption peaks in the range of 770-850 nm. Therefore, the obtained response of spectra into that range of wavelengths could be associated to amine groups and peptide bonds of proteins and gluten concretely. In this sense, relationships observed in correlations with scores of PC2 could explain the differences between gluten and its sub fraction proteins of studied wheat flour batches.

4. Conclusions

In this work, a relationship between the SW-NIR spectra obtained by imaging analysis of non-different wheat flours considering the official quality analysis and their behaviour during the fermentation process was observed. Characteristics such as the amount of gluten and its sub fraction proteins influenced the spectral response, which could be differentiated through multivariate analysis (PCA). These variations were related directly to fermentation behaviour parameters obtained by SL technique, as was observed by the results of correlation map. Accordingly, SW-NIR imaging analysis may be the basis of a useful on-line tool to quickly obtain information about the behaviour of wheat flours, during fermentation, which show no differences in their characterization by rheological analysis. More research should be carried out to obtain robust models of prediction

with the aim of developing industrial on-line bread-making imaging applications.

5. Bibliography

Arazuri, S. Arana, J. I., Arias, N., Arregui, L. M., Gonzalez-Torralba, J., Jaren, C. (2012). Rheological parameters determination using Near Infrared technology in whole wheat grain. Journal of Food Engineering 111 (1), pp. 115-121.

Barak, S., Mudgil, D. & Khatkar, B.S. 2013.Relationship of gliadin and glutenin proteins with dough rheology, flour pasting and bread making performance of wheat varieties (2013). Food Science and Technology, 51, 211-217.

Chen, Z., Morris, J., Martin, E. (2006). .Extracting chemical information from spectral data with multiplicative light scattering effects by optical path-length estimation and correction. Analitical Chemistry, 78, 7674-7681

Cocchi, M., Corbellinib M., Focaa, G., Lucisanoc, M., Paganic, M. A., Lorenzo T. & Alessandro, U. (2005). Classification of bread wheat flours in different quality categories by a wavelet-based feature selection/classification algorithm on NIR spectra.AnalyticaChimica Acta, 544, 100–107.

Cocchi, M., Corbellini, M., Foca, G., Lucisano, M., Pagani, M.A., Tassi, L., Ulrici. A. (2005). Classification of bread wheat flours in different quality categories by a wavelet-based feature selection/classification algorithm on NIR spectra. Analytica Chimica Acta 544 100–107.

Del Fiore, A., Reverberi, M., Ricelli, A., Pinzari, F., Serranti, S., Fabbri, A.A., Bonifazi, G., Fanelli, C. (2010). Early detection of toxigenic

fungi on maize by hyperspectral imaging analysis. International Journal of Food Microbiology, 144 64–71.

Fava, F., Zanaroli, G., Vannini, L., Guerzoni, E., Bordoni, A., Viaggi, D., Robertson, J., Waldron, K., Bald, C., Esturo, A., Talens, C., Tueros, I., Cebrián, M., Sebok, A., Kuti, T., Broeze, J., Macias, M and Brendle, H. (2013). New advances in the integrated management of food processing by-products in Europe: sustainable exploitation of fruit and cereal processing by-products with the production of new food products (NAMASTE EU). New Biotechnology. Volume 30, Number 6, September.

Gompertz, B. (1825). On the nature of the function expressive of the law of human mortality, and a new mode of determining the value of live contingencies. Philosophical Transactions of the Royal Society, 182, 513–585.

Graveland, A., Henderson, M.H., Paques, M., Zandbelt, P.A. (2000).Composition and structure of gluten proteins. In: Schofield, J.D. (Ed.), Wheat Structure, Biochemistry and Functionality. Royal Society of Chemistry, Cambridge, MA, pp. 90–99.

ICC – International Association for Cereal Science and Technology (Vienna-Austria).

Ivorra, E., Girón, J., Sánchez A., Verdú, S., Barat, J.M., Grau, R. (2013). Detection of expired vacuum-packed smoked salmon based on PLS-DA method using hyperspectral images. Journal of Food Engineering 117 342–349.

Ivorra, E., Verdú, S, Sánchez A., Barat, J.M., Grau., R. (2014). Continuous monitoring of bread dough fermentation using a 3D vision Structured Light technique. Journal of Food Engineering 130 8–13.

Jirsa, O., Hrušková, M., Švec, I., (2008). Near-infrared prediction of milling and baking parameters of wheat varieties, Journal of Food Engineering, 87 (1), pp. 21-25

Li Vigni, M., Durante, C., Foca, G., Marchetti, A., Ulrici, A., Cocchi, M. (2009). Near Infrared Spectroscopy and multivariate analysis methods for monitoring flour performance in an industrial bread-making process. Analytica Chimica Acta. 642 69–76.

Li Vigni M., Durante, C., Foca, G., Ulrici, A., Møller Jespersen, B.P., Bro, R., Cocchi, M. (2010). Wheat flour formulation by mixture design and multivariate study of its technological properties. Journal of Chemometrics, Volume 24, Issue 7-8.

Manley, M., du Toit, G., Geladi, P. (2011). Near infrared spectroscopy and multivariate analysis to evaluate wheat flour doughs leavening and bread properties. Analytica Chimica Acta 686, 64–75.

Murray, I. (2004). Scattered information: philosophy and practice of near infrared spectroscopy. Proceedings of the 11th International Conference on Near Infraredspectroscopy.NIR Publications 2.

Nobuyuki Otsu. (1979). A Threshold Selection Method from Gray-Level Histograms. 2EEE TRANSACTIONS ON SYSTREMS, MAN, AND CYBERNETICS, SMC-9(1).

Park, S. H., Bean, S. R., Chung, O. K., &Seib, P. A. (2006).Levels of protein and protein composition in hard winter wheat flours and the relationship to breadmaking. Cereal Chemistry, 83, 418-423.

Shao, Y., Cen, Y., Yong He, Y., Liu, F. (2011). Infrared spectroscopy and chemometrics for the starch and protein prediction in irradiated rice. Food Chemistry 126 1856–1861.

Sinelli, N., Pagani, M.A., Lucisano, M., D'Egidio, M.G., Mariotti.M.(2011). Prediction of semolina technological quality by FT-NIR spectroscopy. Journal of Cereal Science 54 218-223.

Singh, C.B., Jayas , D.S., Paliwal, J., White N.D.G. (2009). Detection of insect-damaged wheat kernels using near-infrared hyperspectral imaging. Journal of Stored Products Research 45 151–158.

Uthayakumaran S., Gras P.W., Stoddard F.L., Bekes F. (1999). Effect of varying protein content and glutenin-to-gliadin ratio on the functional properties of wheat dough. Cereal Chemistry, 76(3): 389–394.

Veraverbeke, W. S., &Delcour, J. A. (2002). Wheat protein composition and properties of wheat glutenin in relation to breadmaking functionality. Critical Reviews in Food Science and Nutrition, 42, 179-208.

Xing, J., Symons, S., Hatcher, D., Shahin, M. (2011). Comparison of short-wavelength infrared (SWIR) hyperspectral imaging system with an FT-NIR spectrophotometer for predicting alpha-amylase activities in individual Canadian Western Red Spring (CWRS) wheat kernels. Biosystems engineering, 108 303-310.

Zhang, Z. (2000). A flexible new technique for camera calibration. Pattern Analysis and Machine Intelligence, IEEE Transactions on, 22(11), 1330– 1334. doi:10.1109/34.88871

CAPITULO IV

Detection of adulterations with different grains in wheat products based on the hyperspectral image technique: the specific cases of flour and bread

Food Control, Volume 62, April 2016, Pages 373-380
Samuel Verdú, Francisco Vásquez, Raúl Grau, Eugenio Ivorra, Antonio J. Sánchez, José M. Barat
Versión para la tesis doctoral

Abstract

The objective of this study was to test the capability of a SW-NIR hyperspectral image technique to detect adulterations in wheat flour and bread with cheap grains, such us sorghum, oats and corn, and to compare the hyperspectral information with the physicochemical alterations in the properties of products. Wheat flour was adulterated at four different degrees (2.5, 5, 7.5 and 10%) with sorghum, oat and corn flours. Flours were prepared and used to make bread. Flours and breads were characterized according to several physicochemical parameters (pasting properties, water activity, mass loss during the baking process and texture profile analysis). Crumbs were extracted from breads and conditioned. Hyperspectral image captures were taken of both flours and conditioned crumbs. The data analysis was based on multivariate statistical process control method (MSPC), where the differentiation of adulterated samples was observed in all cases for both flours and crumbs. Finally, in order to relate the image analysis results and the adulterated sample properties, a correlation significance map was created between the physicochemical properties of samples and the multivariate statistical parameters. The SW-NIR image technique was capable of detecting adulterations in each case and high correlation significances were observed ($\alpha = 0.01$) between wavelengths from specific spectra zones and the physicochemical properties of samples.

***Keywords*:** bread, adulteration, image analysis, MSPC, hyperspectral

1. Introduction

Adulteration of food products (raw materials, intermediate products, authorized additives, end products, etc.) is of primary concern for consumers, food processors, regulatory agencies and industries. Adulteration typically involves replacing or diluting high-cost ingredients with cheap low-quality products (Kalivas et al., 2014). The history of food adulteration reports not only economic motives, but even criminal ones. Thus food frauds and adulterations may have economic implications for local authorities due to increased work load and costs to governments through loss of value-added taxes made from sales (Tähkäpää et al., 2015). Therefore, rapid qualitative analyses are required to separate adulterated samples, followed by a quantitative analysis of this adulterant, if necessary.

The development of non-destructive rapid analysis methods is an area in which interest increased a few years ago. Within this area, numerous methods based on different chemical and physical principles have been proposed to carry out both qualitative and quantitative determinations in laboratories and process chains. The methods which have demonstrated high versatility and robustness are those based on the simultaneous analysis of the large number of wavelengths of electromagnetic spectra, and in all their modes (reflectance, absorbance, interactance, etc.) (Wu & Sun, 2013).

Specifically, the study of infrared spectra (IR) has been used for a vast number of determinations from multiple food matrices and analytes.

Two of the main techniques used for this purpose are IR spectroscopy and spectral imaging analysis. Several recent IR spectroscopy applications for detecting adulterations, fraud and contaminants have included the detection of pork adulteration in veal products based on FT-NIR spectroscopy (Schmutzler et al., 2015), minced lamb meat adulteration (Kamruzzaman et al., 2013), minced beef adulteration with turkey (Alamprese et al., 2013), fraudulent adulteration of chili powders with Sudan dye (Haughey et al., 2014), adulteration of oil used in animal feed production (Graham et al., 2012), etc. Concretely, into the area of grain product adulterations, (Cocchi et al., 2006), developed a method to quantify the degree of adulteration of durum wheat flour with common bread wheat flour based on near-infrared spectroscopy assisted by different multivariate calibration techniques. Although fewer works have been carried out using the spectral imaging analysis technique, it has also been used in a large number of applications to detect adulteration of beef and pork in raw meats (Ropodi et al., 2015), melamine in milk powders (Fu et al., 2014), gelatin adulteration in prawn (Wu et al., 2013), and for the pattern recognition for the categorization and authentication of red meat (Kamruzzaman et al., 2012), etc.

The objective of this work was to study the feasibility of an SW-NIR hyperspectral image technique to detect adulterations in wheat flour

and bread with other cheap grains, such as sorghum, oat and corn, and to compare the hyperspectral information with the adulteration repercussions for flour and bread properties.

2. Material and Methods

2.1 Flour types and raw materials

The commercial wheat flour (WF) used was obtained from a local producer (Molí de Picó-Harinas Segura S.L. Valencia, Spain), whose chemical composition was: 12.7±0.6% of proteins, 1.0±0.03% of fat, 13.09±0.5% of moisture, and 0.32±0.1% of ash (w.b). The alveographic parameters were also facilitated by the company, which were P = 94±2 (maximum pressure (mm)), L = 128±5 (extensibility (mm)), W = 392±11 (strength (J-4)) and P/L= 0. 73. Oat and corn flours were obtained from a local supermarket (La Carabasseta, Valencia, Spain). Their composition was 11.3±0.1% of proteins, 8.0±0.1% of fat, 12.6±0.6% of moisture and 0.92±0.1% of ash (w.b), and 8.3±0.1% of proteins, 2.8 ±0.1% of fat, 12.89±0.6% of moisture and 0.38±0.1% of ash (w.b), respectively. Sorghum flour was obtained from a commercial bakery (Integral Food S.A. Barcelona, Spain), whose composition was 10±0.1% of proteins, 1.7±0.5% of fat, 12.6±0.6% of moisture and 1.74±0.1% of ash (w.b). In order to maintain particle size homogeneity, grain flours were analyzed and remilled in a stainless steel grinder, whenever necessary (Retsch GmbH, ZM 200, Haan, Germany), until particle size distribution with

no significant differences was achieved with the wheat flour used. The particle size of flours was measured 6 times by laser scattering in a Mastersizer 2000 (Malvern, Instruments, UK), equipped with a Scirocco dry powder unit. The results were expressed as a maximum size in µm at 10%, 50% and 90% (d (0.1), d (0.5) and d (0.9), respectively) of the total volume of the analyzed particles as their averages (D [4, 3]). The average results were d (0.1) = 25.5±1.1, d (0.5) = 92.0±0.6, d (0.9) = 180.6±0.8 and D [4, 3] = 99.4±1.2. Having ensured homogeneous particle size, in order to simulate possible adulterations, binary mixes were made by adding different percentages of sorghum, oat or corn to wheat flour. Specifically, adulterations were 2.5, 5, 7.5 and 10% (w/w) of wheat flour with all the different flour grain types.

The other ingredients to make bread were sunflower oil (maximum acidity 0.2º Koipesol Semillas, S.L., Spain), pressed yeast (Saccharomyces cerevisiae, Lesafre Ibérica, S.A., Spain), white sugar (≥ 99.8% of saccharose, Azucarera Ebro, S.L., Spain) and salt (refined marine salt ≥ 97% NaCl Salinera Española S.A., Spain), which were purchased in local stores.

2.2 Bread-making process

The formulation used to prepare bread dough was based on previous works (Verdú et al., 2015) and was as follows: 56% flour (pure wheat flour or the adulterated versions), 2% refined sunflower oil, 2%

commercial pressed yeast, 4% white sugar 1.5% salt and 34.5% water. The process was carried out by mixing all the ingredients in a food mixer (Thermomix® TM31, Vorwerk, Germany) according to the following method: in the first phase, liquid components (water and oil), sugar and salt were mixed for 4 minutes at 37 ºC. Pressed yeast was added in the next phase to be mixed at the same temperature for 30 seconds. Finally, flour was added and mixed with the other ingredients according to a default bread dough mixing program, which makes homogeneous dough. The program system centers on mixing ingredients with random turns of the mixer helix in both directions (550 revolutions/minute) to obtain homogeneous dough. This process was applied for 4.5 minutes at 37 ºC. Then 450 g of dough were placed in the metal mold (8x8x30cm) for fermentation. Height was approximately 1 cm.

Dough fermentation was carried out in a chamber with controlled humidity and temperature (KBF720, Binder, Tuttlingen, Germany). The fermentation process conditions were 37 °C and 90% relative humidity (RH). Samples were fermented for 1 h. The baking process was carried out at the end of fermentation. Metal molds were placed in the middle of the oven (530x450x340, grill power 1200W, internal volume 32L, Rotisserie, DeLonghi, Italy) plate, which was preheated to 180 ºC. Baking time was 35 minutes.

2.3 Crumb conditioning

Having baked the breads, crumbs were extracted and processed to be analyzed as so: crumbs from central bread zones (the middle third of total bread length) were removed from the crust and dried in a food dryer (Excalibur 3900B Deluxe Dehydrator) at 50 ºC to obtain the same moisture of raw flours (approx. 13% of moisture). Dried crumbs were milled in a stainless steel grinder (Retsch GmbH, ZM 200, Haan, Germany) until particle size distribution with no significant differences was achieved with the flours used.

2.4 SW-NIR data acquisition and processing

Images of both groups of samples (flours and crumbs from pure wheat and adulterated versions) were taken with a Photonfocus CMOS camera, model MV1-D1312 40gb 12 (Photonfocus AG, Lachen, Switzerland), and using a SpecimImSpector V10 1/2" filter (Specim Spectral Imaging, LTD., Oulu, Finland), which works as a linear hyperspectral camera. The illuminant was an ASD illuminator reflectance lamp (ASD Inc, Boulder, USA), which produces stable illumination over the full working spectral range. Fifteen grams of sample were placed into a glass Petri dish (10 cm diameter) and a homogeneous surface and height were maintained (approx. 0.75 cm). Spectra were collected directly at room temperature. Four samples of each flour, mix and crumb flours were prepared. Five images of each were acquired by rotating 1.04 radians each time around its normal axis. Twenty image acquisitions of each case were obtained.

The position of the illuminant and camera in relation to the sample was always constant in order to control lighting conditions and to obtain a constant image size. In order to avoid any heat transfer to the sample, the distance between the illuminant and the sample was 0.5 m. The distance between the camera and the sample was 0.15 m. The obtained image (scanned line) comprised 256 gray levels (8 bits). The diffuse reflectance spectrum was collected with 53 different wavelengths (each wavelength was digitalized with 8 bits). These wavelengths were distributed at intervals of 11.2 nm within the 400-1000 nm range. The scanned line comprised 1312 points, so an image was recorded with a resolution of 1312 x 1082 pixels. Image reflectance calibration and preprocessing were performed as described in (Verdú et al., 2015). The camera was operated by a software, developed based on SDK Photonfocus-GigE_Tools, and programming language C++ was used.

2.5 Physico-chemical parameters

2.5.1 Pasting properties of flours

For the purpose of evaluating the influence of different adulterations on flours, pasting properties were analyzed using the viscosity profile obtained by the RVA (Rapid Visco Analyser Super 4, Newport Scientific) viscometer. To this end, the method was approved by the AACC (America Association of Cereal Chemists), whose reference is the “General Pasting Method for Wheat or Rye Flour of Starch Using the RVA. AACC 2000 number 76-21” was used. Samples of 3 g±0.01g

were weighed and 25 g±0.01g of water were incorporated. The test started at 50 °C and 960 RPM, and was then slowed down to 160 RPM at 10 s. Temperature was maintained during the first minute, and went from 50 °C to 95 °C to then increase during the next 4 minutes to reach 95 °C at minute 5 in a second step. The third step involved maintaining the temperature at 95 °C until minute 7.5. The fourth step was to lower the temperature to 50 °C, which was reached at minute 11. The last step entailed maintaining a temperature of 50 °C until minute 13. Measurements were taken in triplicate. The obtained pasting parameters were pasting temperature (*Tp*), peak viscosity (*Pv*), trough viscosity (*Tv*), breakdown viscosity (*Bv*), final viscosity (*Fv*), setback viscosity (*Sv*) and peak time (*Pt*).

2.5.2 Baking loss, water activity and texture profile analysis of breads

To evaluate the effect of adulteration on the end product, some of most relevant bread properties were studied. In this phase, mass loss during the baking process (ΔM_b) was concluded by the difference between the pre-baking dough weight and the finished bread weight (both bread products were cooled at room temperature for 1 h). This parameter was called “baking loss”. The water activity of raw crumbs (a_w) was determined in an Aqualab® dew point hygrometer (DECAGÓN Aqualab CX-2, Pullman, WA, USA). The texture profile

analysis (*TPA)* was performed following the method used by (Miñarro et al., 2012), where two 12.5-mm-thick cross-sectional slices were obtained from the center of each bread product. The texture profile analysis was carried out in a TA-TX2 texture analyzer (Stable Micro Systems, Surrey, UK). A 25-kg load cell (35-mm diameter) was used. The assay speed was set at 1.7 mm/s to compress the bread crumb center at 50% of its previous height. The time between compressions was 5 s. The studied parameters were hardness (*D*), springiness (*S*), cohesiveness (*C*), gumminess (*G*), chewiness (*Ch*) and resilience (*R*).

2.5 Statistical analysis

The study of the hyperspectral results was based on Multivariate Statistical Process Control (MSPC). This method derives from the Univariate Control Process, and offers the possibility of including a large number of variables and the interactions among them at the same time. The objective of MSPC is to create a model based on the required features of samples and the generation of thresholds (confidence limit), which determines the conformity of new samples according to the pre-established specifications (normal conditions) to then maintain the system under control (Bersimis, Psarakis, & Panaretos, 2007). The process can used by including new multivariate data in the created model, and evaluating the distance of any new samples from the model by studying T^2-statistic (Hotellings), and Q-statistic (Q-residuals). The situation of these parameters within the confidence limit indicates samples according to the pre-established

requirements, and then under control (samples of pure wheat flour and pure wheat flour breads). On the contrary, any samples situated beyond the confidence limits imply that something occurred under the controlled conditions which caused a deviation from the model (adulterated samples, if applicable). Any T^2-statistic beyond the control is interpreted as both new samples that present an unusual distance from the center of the model, and alterations in the values of some of their variables. Any Q-statistic beyond the control represents samples that the model is incapable of describing, which means the presence of some irregularities in the control variables that first allow the identification and then separation from the samples under the control.

The physicochemical parameters obtained from flours (Tp, Pv, Tv, Bv, Fv, Sv, Pt) and breads (ΔMb, a_w and TPA (*H, S, C, G, Ch*)) were studied by a one-way variance study (ANOVA). In those cases in which the effect was significant (P-value < 0.05), means were compared with Fisher's least significant difference (LSD) procedure.

Procedures were performed with PLS Toolbox, 6.3 (Eigenvector Research Inc., Wenatchee, Washington, USA), a toolbox extension in the Matlab 7.6 computational environment (The Mathworks, Natick, Massachusetts, USA).

3. Results

3.1 MSPC results

Figure IV.1 provides the MSPC statistical analysis results in Q-residuals terms applied to spectra data. This statistic was used to observe the capability of the created models (based on pure wheat flour and pure wheat flour bread crumbs) to place the adulterated samples beyond the confidence limit. Both the flours and adulterated bread crumbs were located beyond the 95% confidence limit of their respective pure wheat models, regardless of the cereal type used for adulteration and percentage. The percentage of adulteration revealed evolution across the Q-residuals axis following the degree, where the cases with 2.5% came close to the limit, while those with 10% were the most distant ones. Of the adulterated flours, sorghum and corn presented a clear differentiation among the obtained adulteration percentages, but oat showed more agglomeration in its points. The behavior of crumbs was the same as the adulteration degree, but cereal type appeared to have an influence. Crumbs from the breads adulterated with sorghum remained well beyond the model limit in all cases, with even a wider separation compared to its analog flour, and the same occurred with oat, but its position was closer to the limit compared to sorghum. Crumbs from the bread adulterated with corn showed more differences compared to their analog flours. The degrees of 2.5% and 5% came into contact with the limit line, and even caused problems for detecting some samples.

Then the baking process influenced the response of the hyperspectral technique. Sorghum and oat presented minor differences between the flour and crumb results, but the bread-making process apparently made it difficult to detect corn in some bread crumbs at low adulteration percentages, although corn was detected in most samples.

The results showed that the used technique has reached a detection sensibility until 2.5% of adulteration for all grains. In early works, durum wheat flour adulterer with soft wheat flour was detected with a sensibility of 0.5% using NIR spectroscopy (Cocchi et al., 2006). In the same way, detection of soft wheat had also been addressed using other methods as the determination of alkylresorcinol composition in pasta, obtaining a sensibility of 5% (Knödler et al., 2010), as well as DNA microsatellite region method, where until 1% of adulteration was detected in durum wheat semolina, pasta and bread (Sonnante et al., 2009). Moreover, adulterations with other flours have been detected at 0.1%, concretely in the case of lupin seed flour, by real-time PCR method (Scarafoni, Ronchi, & Duranti, 2009). In comparison to works reported previously, the sensibility of the present method is within high intermediate place, taking into account that it was configured as online inspection tool.

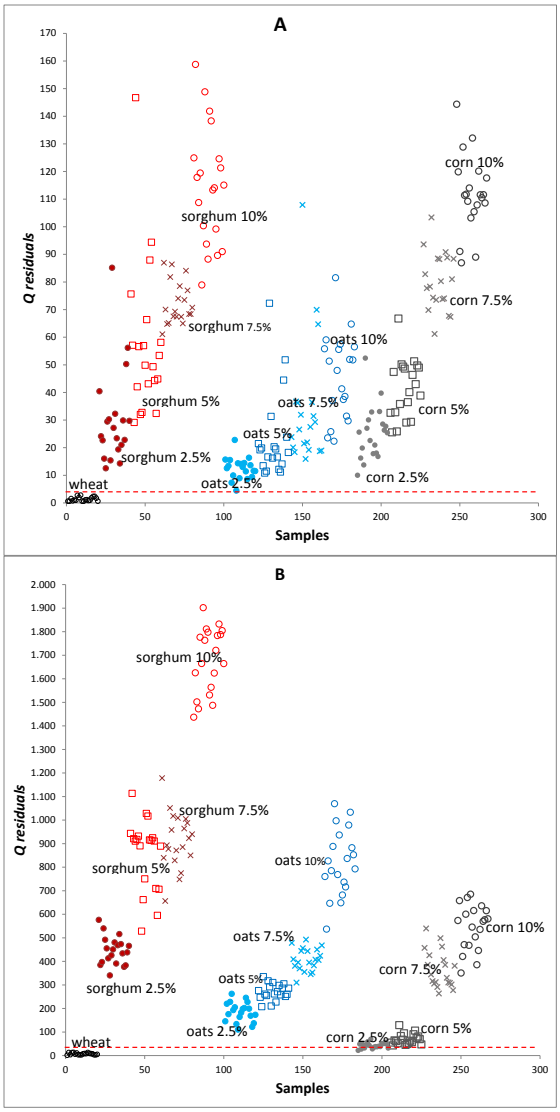

Figure IV.1. The Q-residuals results for adulterated flour samples (A) and crumb samples (B). The dashed horizontal red line indicates a 95% confidence limit. Red corresponds to sorghum, blue to oat, gray to corn and black to wheat. The series of shapes are arranged according to the percentage of adulteration: ● 2.5%, □ 5%, **x** 7.5% and ○ 10%.

To study the exclusion process of adulterated samples, the Q-contributions of each variable (wavelength) per sample were compared. The Q-contribution plots report information about the causes of the disturbance to the process in terms of the original variables' influence. A high absolute Q-contribution value for a given variable means a problem with that specific variable (Westerhuis et al., 2000). Figure VI.2 shows the plotted mean results of the Q-contributions based on each adulteration of cereal. The Q-contributions for the pure flours of sorghum, oat and corn were included in the adulterated flours plots to compare their results with the adulterated wheat flour and their main peaks within the spectra. First, a main peak across spectra appeared in both the visible and the infrared zones for all the cereal types. Flours presented an increment in contributions following the increase in the degree of adulteration for all the cereals (Figure IV.2 (left plots)), which brought about the most marked peaks for sorghum, while corn obtained the least marked one. There were common spectra zones with high values for all the cereals, but with different intensities. The corresponding variables of these peaks were wavelengths 490, 556, 612, 792 and 904 nm for sorghum and oat. Corn presented the same wavelengths, but by adding 859 nm and removing 612 nm.

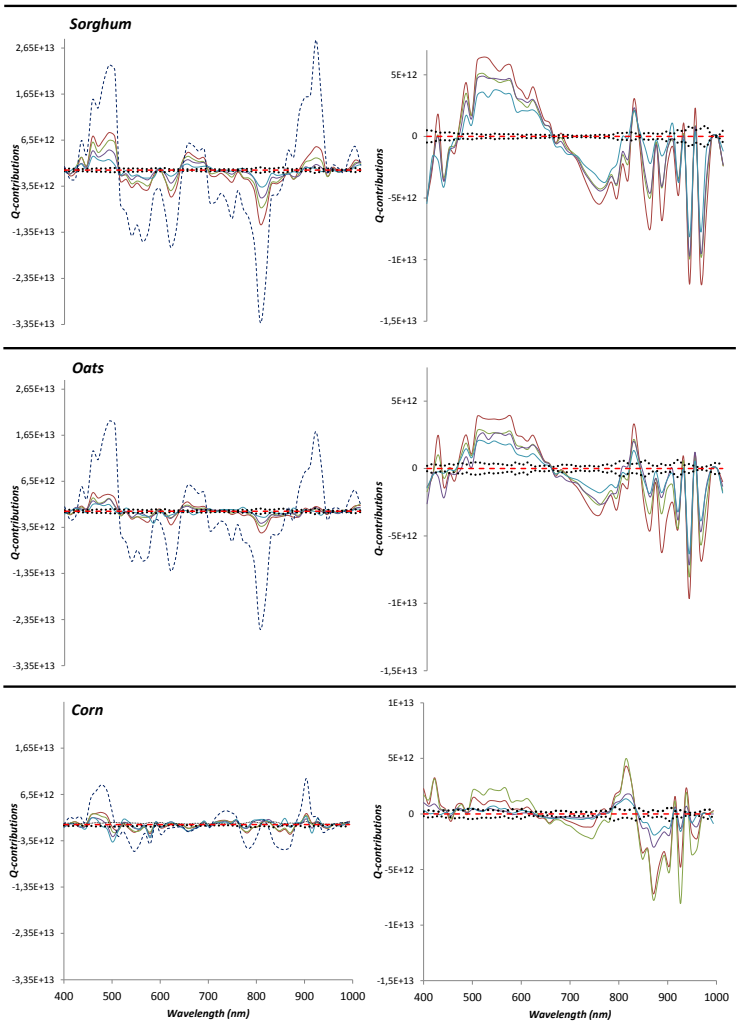

Figure IV.2. The Q-contributions plots for the adulterated flours (left) and crumbs (right) for each cereal. The dashed red lines represent pure wheat, while the dashed black lines denote the standard deviation of the pure wheat contributions. The dashed blue lines correspond to pure cereal flour adulteration. The red line indicates 10% of adulteration, the green line corresponds to 7.5%, the purple line to 5% and the blue line to 2.5%.

For the crumb results (Figure IV.2 (right plots)), the degrees of adulteration also followed the position order in the plot. Peaks presented differences in regard to flours. In this case, the common variables with a heavy weight were wavelengths 523, 747, 848, 926 and 948 nm. In the same way as flours, sorghum presented the most marked peaks and corn the least marked one. However, wavelength 814 showed the inverse behavior as it achieved considerable importance for oat and corn.

Although the fundamental composition of the adulterated flours and crumbs was the same, the bread-making process influenced the response of the hyperspectral image device.

3.2 Repercussions of adulteration on flour and bread properties, and its relationship with hyperspectral detection

Adulteration can be detected by the hyperspectral image technique. Nevertheless, in order to ensure that the observed statistical results were related to the real effect of adulteration on the product, and was not produced by any uncontrolled factor, some physicochemical properties of both flours and breads were tested and related with the MSPC results.

First, a battery of physicochemical analyses was carried out to characterize pure wheat flour and bread, and their adulterated versions with the different cereals. On the one hand, flours were characterized according to their pasting properties with the RVA. On

the other hand, whole breads were analyzed in terms of baking loss, water activity and texture properties based on the TPA. Table IV.1 contains the physicochemical analysis results.

Table IV.1. Results of the physicochemical characterization of flours and breads

		Flours						Breads						
Cereal	%	Tp	Pv	Tv	Bv	Fv	Sv	Pt	ΔM_b	a_w	D	S	C	G	Ch	R
Wheat	0	68.9±0.6a	2245±15a	1421±4a	823±10a	2660±5a	1238±10a	6.1±0.2a	33.5±3.5a	0.955±0.003a	9.3±0.1a	0.98±0.04 a	0.81±0.01a	7.5±0. 7.4±0.8a		0.44±0.01a
Sorghum	2.5	68.9±0.5a	2164±7a	1308±48a	856±26b	2614±58a	1306±10b	6.04±0.05 a	36,1±2.8a	0.956±0.003b	8.2±0.1a	0.98±0.02 a	0.80±0.01b	6.5±0. 6.4±0.9a		0.43±0.01a
	5	87.2±0.1b	2225±19b	1369±7b	856.5±26b	2742±6b	1373±13c	6.13±0.01a	37±2.5a b	0.958±0.003b	9.3±0.2a	0.96±0.04 a	0.79±0.01b	7.4±0. 7.2±0.9a		0.43±0.01 a
	7.5	87.2±0.1b	2214±18b	1339±12b	875±5b c	2833±6c	1494±19d	6±0.04a	38,2±3.7b	0.959±0.003c	9.6±1.4a	0.98±0.02a	0.80±0.01b	7.7±1. 7.6±1.0a		0.44±0.01 a
	10	87.±0.5b	2306±199c	1422±7b	884±26c	3029±47d	1607±54e	6.07±0.09a	38,6±4b	0.960±0.002c	10.5±1.5a	0.97±0.03a	0.78±0.07b	8.2±1. 8.0±1.1a		0.43±0.01 a
Oats	2.5	69.3±1.1a	2194±26a	1396.5±37a	798±11a	2564±54a	1168±16a	6.17±0.05a	38,3±2.9b	0.957±0.002a	6.3±1.0b	0.94±0.07a	0.82±0.01a	5.2±0. 4.9±0.9b		0.45±0.01ab
	5	70.18±0.1a	2245±31a	1426±9a	819±41a	2658±45a	1232±55a	6.17±0.05a	38,8±3.2b	0.961±0.008a	6.7±0.7b	0.98±0.01a	0.82±0.01b	5.5±0. 5.4±0.6b		0.45±0.01ab
	7.5	84.73±0.1b	2246±44a	1429±45a	817±1a	2675±25a	1246±19a	6.14±0.09a	37,8±3.5b	0.961±0.001c	6.1±0.9b	0.97±0.08a	0.82±0.01b	5.0±0. 4.9±1.0b		0.45±0.01ab
	10	85.15±0.1b	2266±12a	1476±36a	790±24a	2715±14a	1239±22a	6.2±0.1b	39,2±0.7b	0.969±0.002d	4.8±1.0c	0.92±0.11a	0.83±0.01b	4.0±0. 3.7±0.9c		0.45±0.01b
Corn	2.5	69.33±0.1a	2210±10a	1363.5±14a	847±4b	2577±26a	1214±11a	6.07±0.01b	37,9±3.6ab	0.957±0.008a	7.2±0.1b	0.96±0.04a	0.81±0.01a	5.9±0. 5.7±0.6b		0.44±0.01ab
	5	85.95±0.1b	2219±14a	1374.5±7b	844±21b	2651±12a	1277±19b	6.04±0.05c	38,2±1.6b	0.960±0.002a	5.2±1.1c	0.95±0.05a	0.83±0.01a	4.3±0. 4.1±0.9b		0.45±0.01 ab
	7.5	85.15±0.5b	2201.5±31a	1374±35b	867±3c	2669±44a	1335±9c	5.93±0.02d	40,2±2bc	0.960±0.002a	4.7±1.3c	0.94±0.07a	0.84±0.01a	4.0±1. 3.8±1.1b		0.45±0.01ab
	10	84.83±0.4b	2260±14a	1379.5±24b	890±10d	2728±25b	1358.5±50d	5.97±0.14d	40,4±1.1c	0.966±0.005b	5.6±0.8c	0.95±0.05a	0.85±0.05b	4.8±0. 4.6±0.7b		0.45±0.01b

Tp: pasting temperature, Pv: peak viscosity, Tv: trough viscosity, Bv: breakdown viscosity, Fv: final viscosity, Sv: setback viscosity, Pt: peak time. ΔMb: baking loss, a_w: water activity, D: hardness, S: springiness, C: cohesiveness, G: gumminess, Ch: chewiness, R: resilience. Letters in columns mean significant differences at a p-value < 0. 05 of each adulteration cereal compared only to wheat flour.

The physicochemical analysis results verified the influence of degree of adulteration and the type of cereal used. The effects of pasting properties led to differences depending on the cereal used. In general terms, some pasting properties, e.g. pasting temperature, was affected by them all from 7.5% of adulteration, and even from 5% for sorghum and corn. Some properties had no influence in any case, such as peak viscosity, breakdown viscosity or setback for oat. Breads also presented significant modifications to ΔM_b, a_w and to some textural properties, such as hardness and cohesiveness. However, some textural properties were not affected by any cereal or degree of adulteration, such us springiness. Having collected the information about the physicochemical properties of samples, a study of whether these results agreed with the previously observed hyperspectral results was conducted. Here the objective was not to find dependencies between hyperspectral data and physicochemical properties to develop a prediction model, but to ensure that the imaging analysis response was in accordance with the measurable influence of adulteration on products.

For this purpose, a correlation coefficient was calculated between the Q-contribution values from all the wavelengths and the studied physicochemical variables of flours and breads for each degree of adulteration. By way of example, Figure IV.3 shows the correlation of several variables from flours and breads for the Q-contributions of the wavelengths for sorghum adulteration. The correlation level differed for each variable. Setback viscosity (Sv) and pasting

temperature (Tp) maintained a similar correlation level for each wavelength, and setback viscosity was slightly high. Although peak viscosity (Pv) tended to obtain a high correlation coefficient at the same wavelengths, it presented a high or equal correlation at the 0.80 level in only a few cases (Figure IV.3-A). Bread variables also exhibited irregular behavior, where the same peaks and zones with the maximum correlation level across the spectra for baking loss (ΔMb) and water activity (a_w) were observed, while hardness (D) presented quite less peaks above the 0.80 level (Figure IV.3-B).

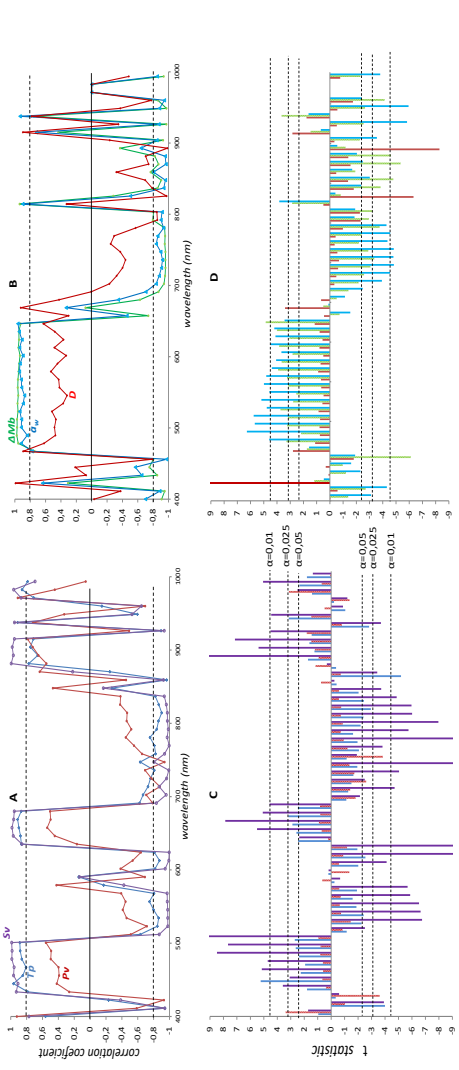

Figure IV.3. The correlation coefficient spectra between the Q-contributions of each wavelength and some physicochemical parameters of flour (A) and bread (B) adulterated with sorghum flour; Tp: pasting temperature, Pv: peak viscosity, Sv: setback viscosity, ΔMb: baking loss, aw: water activity, D: hardness. The dashed black line in A and B marks the positive and negative threshold for the correlation level = 0.80. Lower images (C and D) represent the level of significance based on the t-statistic test for each correlation coefficient of the previous correlations. The dashed black lines represent confidence levels of 95, 97.5 and

The results showed that the hyperspectral information indeed was influenced by the variations caused by the adulteration effects. In order to ensure the observed relationships, a decision was made to determine the degree of significance for each correlation. The results were studied at three degrees of significance (α=0.05, α=0.025 and α=0.01) based on the t-statistic. Figure IV.3-C and 3-D graphically depict the results of the level of significance for the physicochemical variables used as an example of sorghum adulteration (Figure IV.3-A and 3-B). We can see how the significance of the correlations presented variability for the coefficients that presented no differences. This procedure was carried out for each cereal and physicochemical variable to obtain a correlation significances map and to observe the differences among them. Figure IV.4 shows a map of the level of significance map for correlation according to the gray tones.

The correlation results influenced cereal type and whether the analyzed matrix was flour or bread from the same degree of adulteration. With flours, the cereal with higher correlations, and at the same time, higher correlation significances at the 99% confidence level, was sorghum, followed by corn and oats, and presented fewer significant correlations. With breads, the adulteration with oats presented the highest correlation levels of significance, followed by sorghum and corn. In general, the common correlations observed for the pasting properties of all the adulterated flours lay inside the visible and infrared zones. The common visible wavelengths zones

were around 422, 467 and 523 nm, while the infrared wavelengths zones were about 724-792, 860-915 and 982 nm. Breads also presented common zones within the visible and infrared zones. Specifically, 411, 456-478, 501-568 nm for the visible and the infrared zones presented almost all the wavelengths from 700 to 980.

Not all the physicochemical variables and cereal types had the same number of high correlations with spectra, although the results sufficed to conclude that the relationship between the hyperspectral data and the physicochemical data was observed. This means that the recognized pattern based on MSCP was produced neither randomly nor by uncontrolled factors, but was due to the influence of the adulteration levels on products.

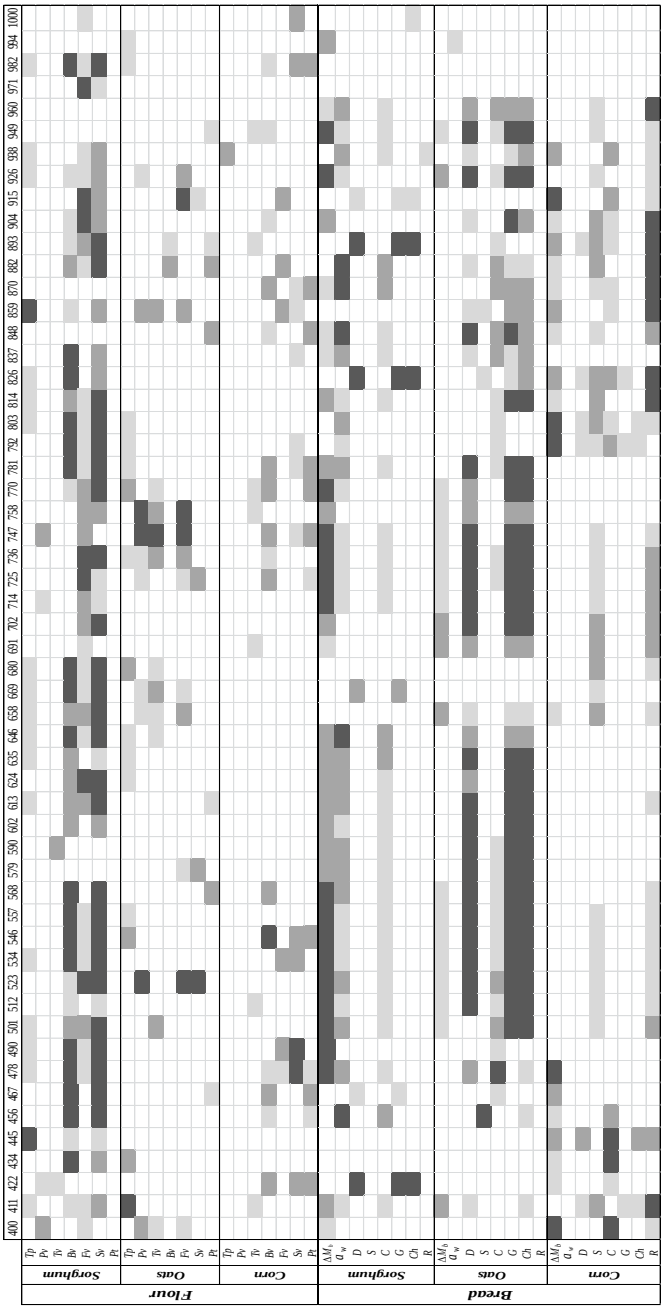

Figure IV.4. Correlation map. Gray marks the correlation's level of significance: ■ 95%, ■ 97.5%, ■ 99%. The positions in white indicate a non-significant correlation. Tp: pasting temperature, Pv: peak viscosity, Tv: trough viscosity, Bv: breakdown viscosity, Fv: final viscosity, Sv: setback viscosity, Pt: peak time. ΔMb: baking loss, aw: water activity, D: hardness, S: springiness, C: cohesiveness, G: gumminess, Ch: chewiness, R: resilience.

4. Conclusions

The capability of the hyperspectral imaging technique used herein to detect adulterations in the tested products at the proposed levels was successful. The bread-making process did not affect detection, but could generate false-negatives in low adulteration percentages in bread with corn. Sorghum was the least affected by this process. The relationship between the hyperspectral data and the physicochemical data indicated that detection was actually based on the modifications produced by adulteration. The results proved that a tool based on this principle could be useful for detecting adulterations of this type. Experiments that include more grain types and other flour products would be interesting to help advance in developing a plausible inspection tool.

5. Bibliography

Alamprese, C., Casale, M., Sinelli, N., Lanteri, S., & Casiraghi, E. (2013). Detection of minced beef adulteration with turkey meat by UV-vis, NIR and MIR spectroscopy. *LWT - Food Science and Technology*, *53*, 225–232.

Bersimis, S., Psarakis, S., & Panaretos, J. (2007). Multivariate statistical process control charts: An overview. *Quality and Reliability Engineering International*.

Cocchi, M., Durante, C., Foca, G., Marchetti, A., Tassi, L., & Ulrici, A. (2006). Durum wheat adulteration detection by NIR spectroscopy multivariate calibration. *Talanta*, *68*, 1505–1511.

Fu, X., Kim, M. S., Chao, K., Qin, J., Lim, J., Lee, H., … Ying, Y. (2014). Detection of melamine in milk powders based on NIR hyperspectral imaging and spectral similarity analyses. *Journal of Food Engineering*, *124*, 97–104.

Graham, S. F., Haughey, S. A., Ervin, R. M., Cancouët, E., Bell, S., & Elliott, C. T. (2012). The application of near-infrared (NIR) and Raman spectroscopy to detect adulteration of oil used in animal feed production. *Food Chemistry*, *132*, 1614–1619.

Haughey, S. A., Galvin-King, P., Ho, Y. C., Bell, S. E. J., & Elliott, C. T. (2014). The feasibility of using near infrared and Raman spectroscopic techniques to detect fraudulent adulteration of chili powders with Sudan dye. *Food Control*.

Kalivas, J. H., Georgiou, C. A., Moira, M., Tsafaras, I., Petrakis, E. A., & Mousdis, G. A. (2014). Food adulteration analysis without laboratory prepared or determined reference food adulterant values. *Food Chemistry*, *148*, 289–293.

Kamruzzaman, M., Barbin, D., Elmasry, G., Sun, D. W., & Allen, P. (2012). Potential of hyperspectral imaging and pattern

recognition for categorization and authentication of red meat. *Innovative Food Science and Emerging Technologies*, *16*, 316–

Kamruzzaman, M., Sun, D. W., ElMasry, G., & Allen, P. (2013). Fast detection and visualization of minced lamb meat adulteration using NIR hyperspectral imaging and multivariate image analysis. *Talanta*, *103*, 130–136.

Knödler, M., Most, M., Schieber, A., & Carle, R. (2010). A novel approach to authenticity control of whole grain durum wheat (Triticum durum Desf.) flour and pasta, based on analysis of alkylresorcinol composition. *Food Chemistry*, *118*, 177–181.

Miñarro, B., Albanell, E., Aguilar, N., Guamis, B., & Capellas, M. (2012). Effect of legume flours on baking characteristics of gluten-free bread. *Journal of Cereal Science*, *56*(2), 476–481.

Ropodi, a. I., Pavlidis, D. E., Mohareb, F., Panagou, E. Z., & Nychas, G.-J. E. (2015). Multispectral image analysis approach to detect adulteration of beef and pork in raw meats. *Food Research International*, *67*, 12–18.

Scarafoni, a., Ronchi, a., & Duranti, M. (2009). A real-time PCR method for the detection and quantification of lupin flour in wheat flour-based matrices. *Food Chemistry*, *115*(3), 1088–1093.

Schmutzler, M., Beganovic, A., Böhler, G., & Huck, C. W. (2015). Methods for detection of pork adulteration in veal product based on FT-NIR spectroscopy for laboratory, industrial and on-site analysis. *Food Control*, *57*, 258–267.

Sonnante, G., Montemurro, C., Morgese, A., Sabetta, W., Blanco, A., & Pasqualone, A. (2009). DNA Microsatellite Region for a Reliable Quantification of Soft Wheat Adulteration in Durum Wheat-Based Foodstuffs by Real-Time PCR. *Journal of Agricultural and Food Chemistry*, *57*(21), 10199–10204.

Tähkäpää, S., Maijala, R., Korkeala, H., & Nevas, M. (2015). Patterns of food frauds and adulterations reported in the EU rapid alarm system for food and feed and in Finland. *Food Control*, *47*, 175–184.

Verdú, S., Ivorra, E., Sánchez, A. J., Barat, J. M., & Grau, R. (2015). Study of high strength wheat flours considering their physicochemical and rheological characterisation as well as fermentation capacity using SW-NIR imaging. *Journal of Cereal Science*, *62*, 31–37.

Verdú, S., Vásquez, F., Ivorra, E., Sánchez, A. J., Barat, J. M., & Grau, R. (2015). Physicochemical effects of chia (Salvia Hispanica) seed flour on each wheat bread-making process phase and product storage. *Journal of Cereal Science*, *65*, 67–73.

Westerhuis, J. A., Gurden, S. P., & Smilde, A. K. (2000). Standardized Q-statistic for improved sensitivity in the monitoring of residuals in MSPC. *Journal of Chemometrics*, *14*, 335–349.

Wu, D., Shi, H., He, Y., Yu, X., & Bao, Y. (2013). Potential of hyperspectral imaging and multivariate analysis for rapid and non-invasive detection of gelatin adulteration in prawn. *Journal of Food Engineering*, *119*, 680–686.

Wu, D., & Sun, D.-W. (2013). Advanced applications of hyperspectral imaging technology for food quality and safety analysis and assessment: A review — Part I: Fundamentals. *Innovative Food Science & Emerging Technologies*, *19*, 1–14.

CAPÍTULO V

Control of heat treatment process of wheat flour by SW-NIR image analysis

Samuel Verdú, Eugenio Ivorra, Antonio J. Sánchez, José M. Barat, Raúl Grau

Abstract

The capability of the SW-NIR (short wave near infrared) hyperspectral imaging system to characterize the heat treatment process of cake wheat flour was studied. Combinations of heat treatments of flour were run at different temperatures (80, 100 and 130ºC) and for various times (10, 20 and 30 min). The resulting treated flours were analyzed by the imaging technique. The hyperspectral results, studied by multivariate statistical methods, showed a pattern evolution of the flours treated by different heat treatments. The wavelengths that contributed the most, and implied in the differentiations, were detected. The selection of wavelengths allowed us to optimize the analysis, which reduced from 54 to 6 wavelengths. To ensure that the SW-NIR information depended on the heat treatment influence on flours, cakes were produced and characterized according to height, mass loss during the baking process, crumb structure and textural properties. The SW-NIR imaging analysis was capable of following the changes that occurred during the different heat treatments of flours. SW-NIR was applied to determine and adjust the heat treatment process variables to improve the features of flours during the cake production process.

Keywords: heat treatment, wheat flour, SW-NIR hyperspectral, image analysis, process control

1. Introduction

Cake is a good example of a food product obtained from a foam structure into which air has been introduced by a mixing process, which finally expanded and was fixed by the baking process (Wang et al. 2013). Consumer acceptance is based not only on a sweet taste as sponge texture is extremely important (Scanlon and Zghal 2001). Cake texture depends on a cake batter's gas-retention capability during and after mixing (Chesterton et al. 2013). Depending on this property, internal structure and maximum rising can considerably alter. Variations in gas-retention capacity terms are: size of the bubbles generated; total number of bubbles; distribution of bubbles across the liquid phase of the cake batter (Shibata et al. 2011). The above-cited differences relate to the properties of the raw material used in the formula, where polymeric molecules, such as proteins and starch, and their physicochemical state and amount, have a direct impact (Sağol et al. 2006). One main influential factor is the formation of a functional network based on proteins provided by several components like egg, milk, flour, etc., and starch provided principally by flour. This network can have quite different properties depending on the types of these components. Apart from the role of proteins, the state of flour starch and its physicochemical features are other direct factors in network structures, as is their behavior during the process. Therefore, the amount of proteins and starch in selected formula, plus the changes produced by pre-treatments

under physicochemical conditions, cause variations that could be interesting for improving or optimizing some processes and product variables.

In line with this, one of the most widely used procedures is to heat treat flours at different temperatures and from distinct moisture contents. This is a physical treatment method utilized to modify the functional properties of native starch, and includes pasting characteristics, granule morphology, amylose leaching, textural properties, etc., which are particularly favorable for food applications (Jiranuntakul et al. 2011; Lee et al. 2012; Sun et al. 2014). Studies into the effect of heat treatment on the physical and chemical features of wheat flours have been published by Guerrieri and Cerletti (1996), Ozawa and Seguchi (2006) and Ozawa et al., (2009). Hypotheses about the modification of starch granules and the gluten fraction have been included, but the precise mechanism by which heat treatment affects flour behavior has not yet been identified (Meza et al. 2011).

The main effects observed in cakes made with heat-treated wheat flour are increased gas retention and, hence, maximum caking rising, bubble size reduction and homogenization, which can also induce an increase water-holding capacity while baking/treating cake batter. All this, in turn, contributes to the overall quality of the appearance and mouth sensation of end products (Neill et al. 2012). For all these reasons, heat treatment of wheat flours is an important technique to

improve wheat flour properties, and to match them to the requirements of each production process and end product standard. Works conducted to date have studied the influence of different heat treatments, temperatures and flour moisture combinations on the aforementioned effects to predict flour improvement models, and to avoid using other chemical additives to achieve this aim. Therefore, studying the changes undergone by wheat flour during heat treatment can be interesting for optimizing this process if we take into account the required necessities of the production process.

When changes in wheat flour occur during heat treatment, near infrared reflectance imaging techniques offer interesting capabilities that can be applied to study them (Toit 2009). Specifically, SW-NIR (the short wavelength near infrared imaging analysis) has been used in many works to study the variability and properties of flours based on both protein and starch in the cereal processing science area (Singh et al. 2009; Xing et al. 2011). This technique could represent a rapid non destructive method to study the changes that wheat flour undergoes during heat treatment. The main purpose of this work was to study the capability of the SW-NIR imaging system to characterize the effect of the heat treatment process on cake wheat flour prior to cake making, and to secondarily select the most influential wavelengths to optimize hyperspectral information.

2. Material and Methods

2.1 Heat treatment of wheat flour

Wheat flour was obtained from a producer (Molí del Picó-Harinas Segura S.L, Valencia, Spain), which is sold as a "high-strength flSeg" for bakery products, sliced bread, plum cakes, etc. On a wet basis, it contained 15% of moisture, 10% of protein and 31% of wet gluten. Its alveographic parameters were W= 145 (strength (J^{-4})), P= 46 (maximum pressure (mm)), L=143 (extensibility (mm)), P/L = 0.31. Heat treatment was performede with forced convection hot air at three different temperatures (80, 100 and 130ºC) and times (10, 20 and 30 min). The work of Neil et al., (2012) was taken as a reference. The time for stabilizing oven temperature was 1.5 minutes as a maximum for the lower heat treatment (80ºC). Temperature was monitored with a digital thermometer (range 0-300ºC, resolution 0.1ºC, precision ± 0.2ºC). Each treatment was carried out by spreading 300 g of untreated flour on a layer of a maximum thickness of 0.5 cm, which was placed onto a metal plate covered with baking paper. During this process, moisture reduced from 15% to 10.5% (wet basis) as a maximum for 130ºC/30 min. Loss of moisture was calculated according to the mass difference between weights from after and before the process. In order to recover the original moisture values, flours were placed into a chamber (KBF720 Binder Tuttlingen Germany) with controlled humidity and temperature (15% R.H. and 25ºC). Flours remained inside the chamber for 48 h as this

time was required to recover moisture if maximum loss occurred, which was 130ºC/30 min. Finally, samples were softly milled in a food mixer blender (Thermomix® TM31, Vorwerk, Germany) to homogenize any oversized particles produced during the process.

2.2. SW-NIR data acquisition and processing

Images of the wheat flour samples treated by different heat treatments were taken with a Photonfocus CMOS camera MV1-D1312 40gb 12 (Photonfocus AG, Lachen, Switzerland) and a SpecimImSpector V10 1/2" filter (Specim Spectral Imaging, LTD., Oulu, Finland), which works as a linear hyperspectral camera. The illuminant was an ASD illuminator reflectance lamp (ASD Inc, Boulder, USA), which produces stable illumination over the full working spectral range. Samples were prepared by placing 35 g of flour into a glass Petri dish (10 cm diameter) to form an approximately 1-cm thick layer. Images were collected directly at room temperature from the samples of the treated flours after the moisture conditioning process. Four samples of each treated flour were prepared. Five images of each were acquired by rotating 1.04 radians each time around its normal axis. Twenty image acquisitions of each case were obtained. The position of both the illuminant and camera in relation to the sample was always constant to control the lighting conditions and to obtain a constant image size. In order to avoid any heat transfer to the sample, the distance between the illuminant and sample was 0.5

m. The distance between the camera and sample was 0.15 m. The obtained image (scanned line) was composed of 256 gray levels (8 bits). The diffuse reflectance spectrum was collected with 54 different wavelengths (each wavelength was digitalized with 8 bits). These wavelengths were distributed at intervals of 11.2 nm within a range from 400 to 1000 nm. The scanned line comprised 1312 points, thus an image was recorded with a resolution of 1312 x 1082 pixels. The spatial resolution achieved with this setup was 7 $m.10^{-5}$. Image reflectance calibration and preprocessing were performed as described in Verdú, Ivorra, Sánchez, Barat, & Grau, 2015b, but it essentially acted as a reflectance calibration to normalize the nonlinear light source reflectance and Standard Normal Variety statistical preprocessing. The camera was operated by software that was developed based on SDK Photonfocus-GigE_Tools using the C++ programming language.

2.3. Cake processing

Sponge cakes were made by employing the heat-treated and non heat-treated wheat flours as a pattern. The components employed and percentages used were based on previous studies (Meza et al. 2011), with some modifications. The formula is included in Table V.1.

Table V.1. Cake formula

Raw materials	**%**
white sugar	36
wheat flour	27
water	14.5
whole liquid egg	14
skimmed milk powder	4
refined sunflower oil	2.8
baking powder	1
salt	0.6

The skimmed milk powder composition was 32.5% of proteins, 54.5% of carbohydrates, 1% of lipids and 1.3% of salt (Central Lechera Asturiana, SAT. Asturias, Spain). The whole liquid egg composition was 11% of proteins, carbohydrates were negligible, 9.5% of lipids, and the rest was water (Grupo Maryper de Alimentacion, SL, Spain). The refined sunflower oil had a maximum acidity of 0.2º (Koipesol Semillas S.L., Spain). The commercial baking powder was composed of sodium bicarbonate, disodium diphosphate, rice flour and monocalcium phosphate (Royal, Kraft Foods Inc. Germany), white sugar presented ≥ 99.8% sucrose (Azucarera Ebro, S.L., Spain) and refined marine salt ≥ 97% NaCl (Salinera Española, S.A., Spain). Cake preparation was based on Chesterton et al. (2015) and was as follows:

1. Dry ingredients (flour, sugar, skimmed milk powder, salt and baking powder) were placed into a food mixer (Thermomix® TM31, Vorwerk, Germany) and mixed to obtain a homogeneous powdery mix (1.5 minutes/ 50 rpm).
2. Liquid ingredients (water, oil and whole liquid egg) were added to the food mixer along with the dry ingredients and were all mixed for 1 minute at 105 rpm to generate a homogeneous mixture.
3. The produced mixture was whisked for 10 minutes at 550 rpm to incorporate air and to thus obtain cake batter.
4. 250 g of cake batter (approximately 1 cm high) were placed into a pre-greased metal mold (8x8x15cm) to be baked.
5. The metal molds were placed in the middle of the oven (530x450x340, grill power 1200W, internal volume 32L, Rotisserie, DeLonghi, Italy) plate, which was preheated to 180ºC. The baking time was 35 minutes.

2.4. Characterization of cakes

In order to ensure that the heat treatments applied to the wheat flour influenced the physical properties of the end product, the following were studied: final height (A), mass loss during baking process (ΔMb), texture profile analysis (TPA) and internal crumb bubble size (*Bz*). Mass loss during the baking process was calculated by the difference between the weight of the pre-baking batter and

that of the finished cake (cooled at room temperature for 1 h), expressed as %. The TPA was performed following the method by (Miñarro et al. 2012). Six 12.5 mm-thick cross-sectional slices were obtained from the center of each cake. These slices were grouped to be analyzed in pairs to form 25-mm slices. Finally, three analyses of each cake were done with five cakes from each heat treatment. A TPA was run in a TA-TX2 texture analyzer (Stable Micro Systems, Surrey, UK). A 25-kg load cell (diameter of 35 mm) was used. Assay speed was set at 1.7 mm/s to compress the cake crumb center to 50% of the initial height of the slices (25 mm). The time between compressions was 5 s. The studied parameters were: hardness (*H*), springiness (*S*), cohesiveness (*C*), gumminess (*G*) and chewiness (*Ch*). The cake height and crumb internal structure were studied by 2D image segmentation. Once baking had finished, four 1-cm-thick slices were obtained from the center of each cake. One side of each slice was captured with a scanner (Aficio™ MP C300-Ricoh. Tokyo. Japan) to be analyzed by the 2D image segmentation method described previously by (Verdú et al. 2015). Five cakes were baked from each treated flour, thus 20 crumb images were obtained. A large number of samples was necessary to ensure recognition patterns on the internal crumb structure images since wide variability is normally presented. Images were acquired at a resolution of 300 dpi. A black background was used in all the captures to improve contrast, and to enhance the cell wall structure and porosity measurements.

2.5. Statistical analysis

The heat treatment effect on wheat flour was evaluated by the SW-NIR spectra with the multivariate unsupervised statistical procedure PCA (Principal Component Analysis). This method is used to describe and reduce the dimensionality of a large set of quantitative variables to a low number of new variables, called principal components (PCs), which are the result of linear combinations of the original variables. The number of PCs was selected after considering the change in tendency on the screen plot, and also the accumulated percentage of explained variability above 75%.

The physical parameters of cakes (A, ΔMb, *H, S, C, G, Ch* and *Bz*) were studied by a one-way variance study (ANOVA). In those cases in which the effect was significant (P-value < 0.05), means were compared with Fisher's least significant difference (LSD) procedure.

Support Vector Machines (SVM) were used to study the relationship between the hyperspectral data of the treated flours and the physical parameters of cakes. They were used to carry out nonlinear regressions between both data sets. SVR are a powerful supervised learning methodology, based on the statistical learning theory, that are commonly used for spectral analyses (Boser et al. 1992).

The procedures were run with PLS Toolbox 6.3 (Eigenvector Research Inc., Wenatchee, Washington, USA), which is a toolbox extension in the Matlab 7.6 computational environment (The Mathworks, Natick, Massachusetts, USA).

3. Results

3.1. SW-NIR data acquisition and processing

Figure V.1 shows the scores in the PCA space according to the time and temperature factors of the heat treatment (77.4% of captured variance). Data evolution occurred mainly across axis PC1 (Principal Component 1, 54% of captured variance), influenced by the above factors. The control sample was situated on the positive extreme of PC1, whereas all the other samples were displaced gradually to the zero value and to the negative zone, where both heat treatment temperature and time increased. When a combinatorial effect of both factors was evaluated, the samples treated at 80ºC for the three times were placed near the control sample in the positive PC1 zone, while the treatment at 130ºC was located in the negative PC1 zone for all three treatment times. Therefore, the hyperspectral information was obtained by the image technique report differences in the PCA space, where differences in samples placement could be related to the various heat treatments applied.

In order to facilitate the observation made of the effect of temperature and time of treatments on the hyperspectral information, a plot that included the evolution of the PC1 scores according to these factors was constructed. Figure V.2 shows the mean PC1 scores value for each heat treatment according to both factors. When the PC1 values for each temperature were adjusted to an equation, the slope showed an increase in the change rate among

the treatment times depending on temperature (80ºC = 5.10^9; 100ºC = 8.10^9; 130ºC = 1.10^{10}). Thus one example of the observed behavior was the mean score value for treatment 100ºC/10 min, which fell between those obtained from 80ºC for 20 and 30 min. Similarly, the score value for the 100ºC/20 min treatment was situated between those at 130ºC for 10 and 20 min, while the 100ºC/30 min treatment appeared to overlap the 130ºC/20 min one.

With the aim of evaluating which spectra zone explained these changes in flour due to heat treatment, the PCA loadings were analyzed. Loadings were calculated according to the correlation between the original variables (wavelengths) and the principal components. Therefore, the original variables with a higher value in either the positive or negative correlation to the studied component meant a heavy weight in the explanation of the variability explained by that principal component. As there were two variables, temperature and time, and after considering the differences between slopes in the above studied PCA, a decision was made to obtain three new PCAs based on the same data set, but a different one for each individual temperature. Here the objective was to view the evolution

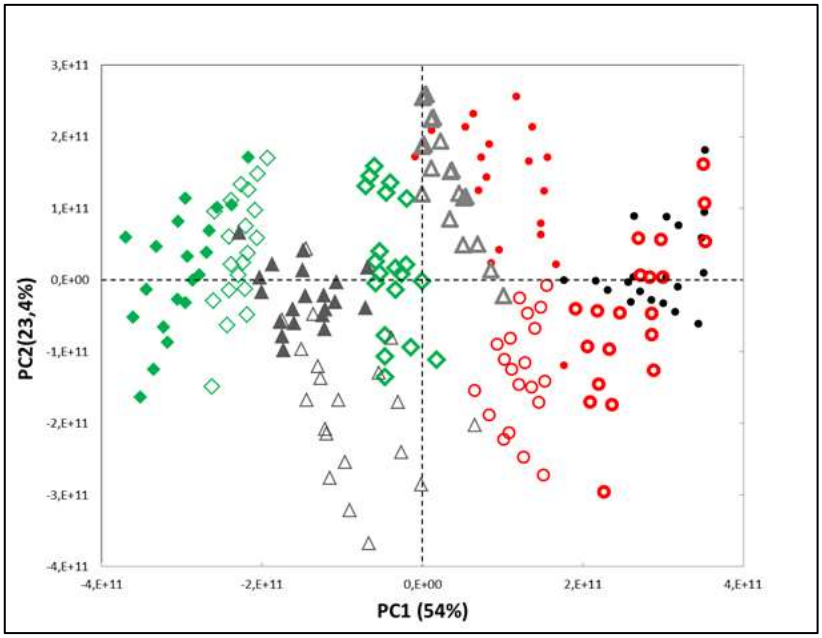

Figure V.1. The PCA space obtained based on the reflectance of the SW-NIR imaging from wheat flour samples with different heat treatments. Colors of series correspond to different heat treatments temperatures: black, control flour (●); red 80ºC (○ 80ºC/10 min; ○ 80ºC/20 min; ● 80ºC/30 min); gray 100ºC (Δ 100ºC/10 min; Δ 100ºC/20 min; ▲ 100ºC/30 min); green, 130ºC (□ 130ºC/10 min; □ 130ºC/20 min; ■ 130ºC/30 min).

of the importance of the original variables influenced by an increase in temperature. Therefore, three new different PCAs were generated: PCA1 (80ºC: 10, 20 and 30 min), PCA2 (100ºC: 10, 20 and 30 min) and PCA3 (130ºC: 10, 20 and 30 min). These PCAs were compared in loading weight terms. Figure V.3 shows the loadings for component PC1, which gave the widest variance in the three new PCAs, and

generated a spontaneous data clustering according to treatment time.

It is important to note that all the loadings presented the same tendency for the spectra zones. The loadings of the visible spectra zones (400-700 nm) were situated mainly toward the positive values, whereas the SW-NIR zone (700-1000 nm) was situated toward the negative ones. This distribution meant that the wavelengths from both spectra zones provided inverted contributions to the variability explanation collected in PC1. The differences observed between the spectra zones obtained from the different heat treatments affected the loadings of each wavelength by increasing or decreasing the weight of the specific zone spectra in the explanation of the variability collected in PC1.

Hence the influence of heat treatments on flour reflectance was observed by evaluating the progress of the loadings from PC1, presented by each temperature (Figure V.3A, 3B and 3C). First, high loadings for the wavelengths were observed from the visible zone, which meant that this spectra zone helped account for most of the variability obtained in PC1; specifically the wavelengths around 600 nm presented the common maximum value for them all, regardless of temperature. Different values among the temperatures were observed within the 411-490 nm range. Therefore, this zone recorded the variations influenced by temperature.

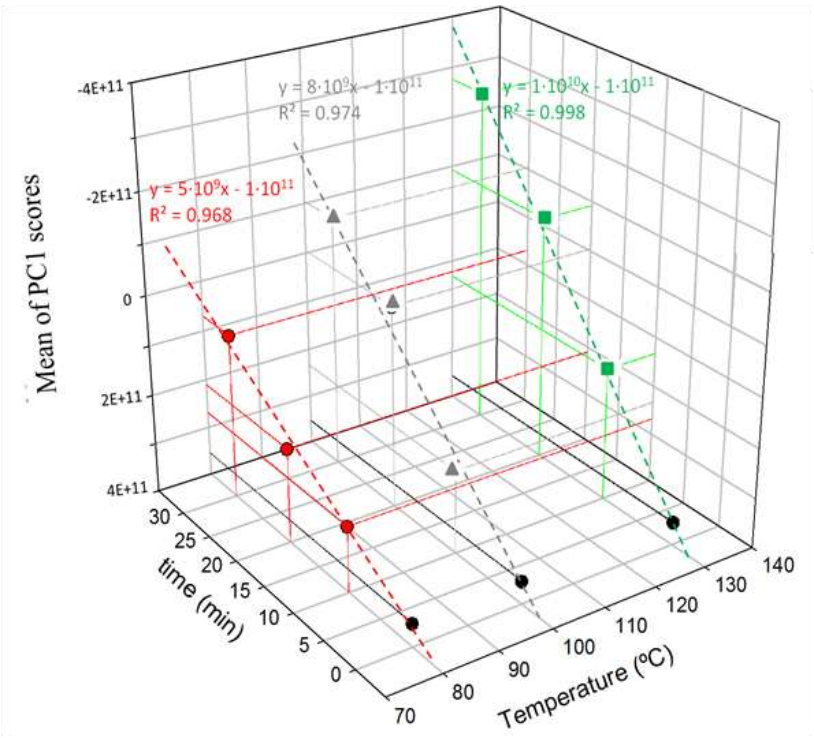

Figure V.2. Representation of the mean of the scores for each temperature and heat treatment time, and the correlation index and the equation of the described line. Colors of the series correspond to different heat treatment temperatures: black, control flour (●); red 80ºC (○ 80ºC/10 min; ○ 80ºC/20 min; ● 80ºC/30 min); gray 100ºC (Δ 100ºC/10 min; Δ 100ºC/20 min; ▲ 100ºC/30 min); green 130ºC (□ 130ºC/10 min; □ 130ºC/20 min; ■ 130ºC/30 min). Points of the control flour were positioned only in relation to the mean score axis.

In the SW-NIR zone, the common maximum contribution was observed at around 780 nm for them all, regardless of temperature. There were also zones where differences among the temperatures were observed. These spectrum zones presented different areas where changes were differentiated (700-770 and 800-900) and related with the various functional groups (Murray, 2004). The interval between 700 and 770 nm presented variations among temperatures and corresponded to the 3rd overtone of O-H, and also to a recognized water influential zone (Sinelli et al. 2006). It also represented the 4th overtone of C-H, in addition to a CH_2 influential zone (Li Vigni and Cocchi 2013). This zone could be related with modifications in the state of water compared to the other presented components (Chen et al. 2006), such us starch, in this case given the presence of OH, CH_2 and C-H in its structures. In this work, no changes in the concentrations of the flour components were made because only a physical treatment was applied to flours. So any changes in the reflectance in these wavelengths could be attributed to differences in the water and the rest of components states between the treated samples and the control sample. The 800-900 nm interval also presented differences among temperatures, and in relation to the 3rd overtone of N-H; in other words, primary and secondary amines (Kimiya et al. 2013). The variations in loadings within this range were similar to the above range. Their weight increased toward negative values with a rise in temperature. The

most marked change noted among temperatures was detected for 859 and 892 nm. The interpretation of this change in loadings could refer to the modifications undergone by proteins during heat treatment. The interaction between the amine groups from proteins and radiation could be modified when heat treatment was stronger because the original tridimensional structure of flour proteins (secondary, tertiary or quaternary) could have altered.

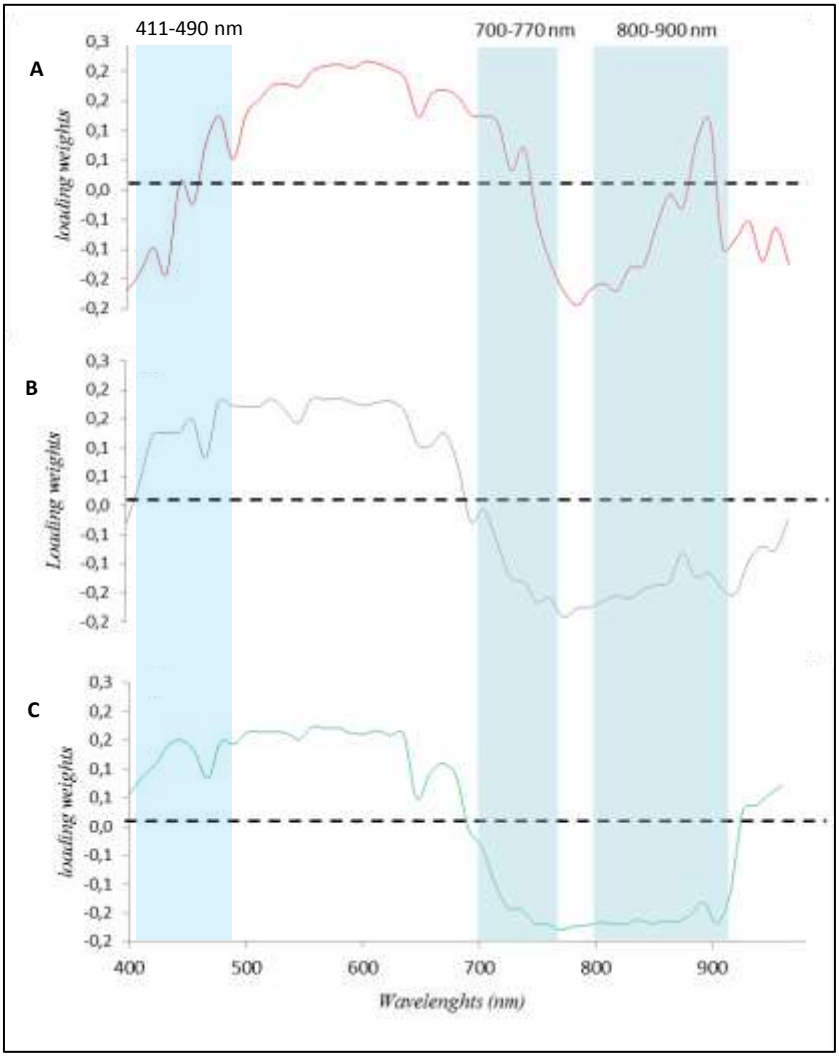

Figure V.3. Loadings of PC1 for each heat treatment temperature. A: PCA1 isolated loadings of the 80ºC heat treatments; B: PCA2 isolated loadings of the 100ºC heat treatments, C: PCA3 isolated loadings of the 130ºC heat treatments. Water marks indicate the regions with marked changes between treatments.

3.2 Reducing number of wavelengths

Having established that the hyperspectral information was able to characterize differences in heat treatments, dimensionality was reduced through wavelength selection. The aim of wavelength selection was to select the optimal wavelengths that contained important information on quality attributes, and to make as few errors as possible for qualitative discriminations or quantitative determinations (Wu & Sun 2013). The elimination of irrelevant variables can predigest calibration modeling and improve results in accuracy and robustness terms (Wu et al. 2008). Thus as reducing the number of wavelengths to obtain the same result for spontaneous heat treatments differentiation (Figure V.1) was the objective, we found that some wavelengths included mainly irrelevant information and did not improve model performance.

The wavelength selection criterion was based on the previous observations of loadings in Figure V.3. As the characterization of heat treatments was influenced by the contribution level for specific wavelengths, those wavelengths with a higher contribution increment according to temperature were searched. To this end, loadings increment (*ΔLoadings*) was calculated between the lower temperature (80ºC) loading values and the other treatments, thus two loadings incremented the values for each wavelength (Figure V.4). Maximum increments were observed within the previously defined wavelength ranges. Although almost all the wavelengths

increased, the most important ones fell within the ranges previously established in Figure V.3. The most marked peaks within these ranges were assumed to be the variables with the highest contribution to characterize heat treatments. The number of wavelengths was minimum to equate the result generated with the complete spectra (Figure V.1). Six wavelengths were finally selected, as indicated in Figure V.4 (433, 456, 713, 736, 859 and 892 nm).

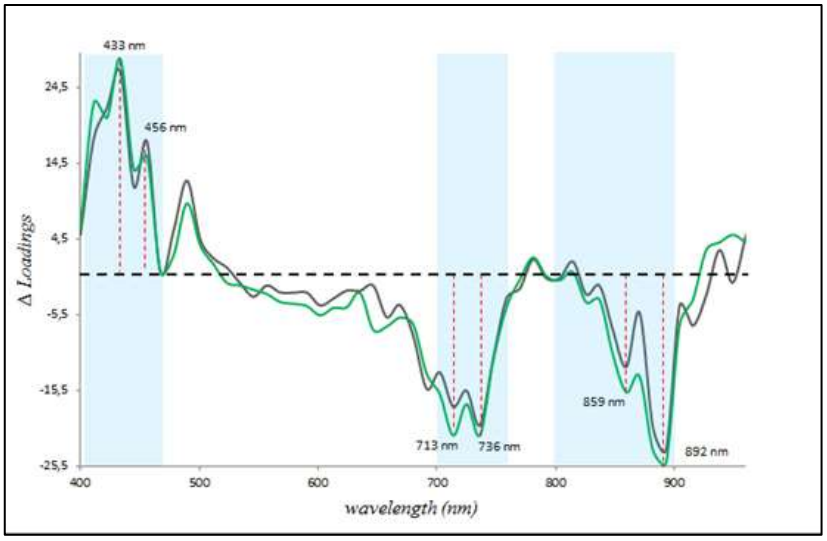

Figure V.4. Wavelength selection. Red dashed lines represent the selected wavelengths. Colored series represent the increments of the PC1 loadings of heat treatments at 100 and 130ºC compared to 80ºC. Gray: loadings increment for the 100ºC heat treatment, Green: PCA3 loadings increment for the 130ºC heat treatment. Water marks indicate the regions with maximum increments across the spectrum.

As observed in Figure V.5, the same spontaneous clustering distribution of samples across PC1 was observed by employing only these six selected wavelengths. The relative position of the treated flours across PC1 was the same in both cases. Even the results maintained the effect observed in Figure V.2 for the increase in slope for the change rate among the treatment times according to temperature. It was possible to condense the information from 54 to 6 wavelengths through wavelength selection by studying the loadings method.

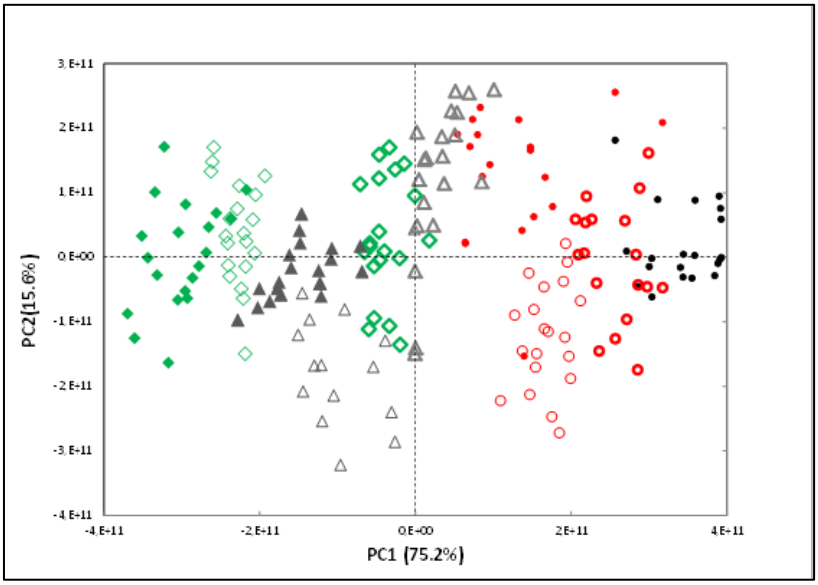

Figure V.5. The PCA space obtained based on the reflectance of the six selected wavelengths. Colors of the series correspond to different heat treatment temperatures: black, control flour (●); red 80ºC (○ 80ºC/10 min; ○ 80ºC/20 min; ● 80ºC/30 min); gray 100ºC (△ 100ºC/10 min; △ 100ºC/20 min; ▲ 100ºC/30 min); green, 130ºC (□ 130ºC/10 min; □ 130ºC/20 min; ■ 130ºC/30 min).

3.3 Relationship between information from the SW-NIR analysis and sponge cake properties

After ensuring that the hyperspectral information was capable of recognizing the changes that took place in flours during heat treatments, cakes were produced using those treated flours to ensure that the influence of the heat-treated flour on cakes reported

by other authors (Chesterton et al. 2015; Meza et al. 2011) was repeated in this case.

The results of the physical cake properties are included in Table V.2, where the influence of the heat treatment of flour on several cake properties is seen. Mass loss during the baking process (ΔMb) showed a drop, together with an increase of both temperature and time during the heat treatment, but not in all cases. The cakes made with the flours treated at 80ºC presented statistical differences compared with the controls in all three cases, and their ΔMb lowered. The effect was inverse when treated for 30 min at 100 and 130. No differences were observed for height (A), except for 130ºC/30 min, which presented the lowest value. For *Bz*, the tendency of the results was similar to ΔMb. The flour treated at 80ºC obtained lower *Bz* values compared to the control. For the flours treated at 100ºC and 130ºC, which came close to the values of the control, those treated for 20 min and 10 min obtained the lowest *Bz* values. Differences in texture properties were also observed. The hardness, gumminess and chewiness of cakes increased when compared to the control, which they also did with the flour treated for 10 min, and regardless of the temperature used. However these parameters reduced at 20 and 30 minutes, and lower values were obtained for 130ºC/20 min and 30 min. Cohesiveness lowered for 80ºC and 100ºC at all the tested times, but an increment at 130ºC/30 min was observed. No differences were found in springiness

compared to the control, except for 130ºC/30 min. Overview, the results of the physical cake properties proved that the tested heat treatments modified samples, exactly as previous authors have described.

Table V.2. Results of physical properties of cakes.

Heat-treatement		Texture and internal estructure of cakes							
Temperature (Cº)	time (min)	ΔMb	A	Bz	H(g)	S	C	G	Ch
Control	-	11.8 ± 0.3 b	8.7 ± 0.4 b	2.9 ± 0.3 e	61.6 ± 2.3 b	0.84 ± 0.01 a	0.67 ± 0.01 c	41.7 ± 1.8 b	35.4 ± 1.8 b
80	10	10.5 ± 0.3 a	8.7 ± 0.3 a	2.2 ± 0.3 c	80.1 ± 8 d	0.86 ± 0.09 ab	0.66 ± 0.01 ab	53.1 ± 4.9 d	45.9 ± 7.2 d
	20	10.3 ± 0.3 a	8.5 ± 0.1 b	2,0 ± 0.2 b	75.8 ± 7.7 c	0.87 ± 0.05 ab	0.66 ± 0.01 bc	50.8 ± 4.9 c	44.2 ± 5.7 cd
	30	10.2 ± 0.3 a	8.4 ± 0.2 b	1.9 ± 0.1 b	71.6 ± 7.4 c	0.87 ± 0.01 ab	0.67 ± 0.01 c	48.4 ± 5 c	42.5 ± 4.3 cd
100	10	10.3 ± 0.1 a	8.4 ± 0.1 b	1.5 ± 0.1 a	78.5 ± 6.5 d	0.88 ± 0.01 ab	0.67 ± 0.01 c	53.1 ± 4.4 d	47 ± 3.4 d
	20	10.8 ± 0.2 a	8.7 ± 0.2 b	1.9 ± 0.1 a	71.1 ± 5.4 b	0.88 ± 0.01 ab	0.67 ± 0.01 c	47.9 ± 3.7 b	42.3 ± 3.1 bc
	30	11.3 ± 0.3 b	8.6 ± 0.2 b	2.3 ± 0.2 cd	63.6 ± 4.3 b	0.88 ± 0.01 ab	0.67 ± 0.01 bc	42.7 ± 3,0 b	37.6 ± 2.8 b
130	10	10.2 ± 0.3 a	8.7 ± 0.3 b	1.6 ± 0.1 a	67.9 ± 3.7 bc	0.86 ± 0.01 ab	0.65 ± 0.01 a	44.7 ± 2.8 bc	38.9 ± 2.5 bc
	20	10.8 ± 0.3 b	8.5 ± 0.2 b	2,0 ± 0.1 d	52.9 ± 4.8 ab	0.88 ± 0.01 a	0.68 ± 0.01 c	35.9 ± 3.4 ab	31.5 ± 3.1 a
	30	11.4 ± 0.2 b	8.6 ± 0.2 a	2.4 ± 0.2 d	38,0 ± 5.9 a	0.89 ± 0.01 b	0.71 ± 0 d	27 ± 4 ab	24.2 ± 3.6 a

Values and standard deviations of cakes properties; ΔMb = mass loss during the baking process (%); A= height (cm); Bz = bubble size (m2.10-6), H = hardness (g); S = springiness; C = cohesiveness; G = gumminess; Ch = chewiness. Values followed by different letters were significantly different at $P < 0.05$ in columns.

Finally, in order to prove the dependency noted between the reduced hyperspectral information and the set of cake properties, non linear regression was carried out based on the SVM technique. For this purpose, the complete data of the physical cake properties,

and the scores obtained from the PCA performed using the selected wavelengths (Figure V.5), were used as X and Y inputs, respectively. Non linear regression was done based on nu-SVM and the radial basis function as the kernel type, where 58 support vectors were used. The R^2 of calibration was 0.992, while that of cross-validation was 0.985. This result reported a model that could evidence the relationship and dependency between the hyperspectral information and cake features. Figure V.6 shows the correlation between the observed PCA scores obtained with the hyperspectral information and those predicted from the physical cake properties. Despite the number of samples being insufficient for developing a model to predict the behavior of cakes, it sufficed to conclude that the used SW-NIR image system was able to obtain information from which it was possible to characterize heat treatment on cake wheat flours, which could be used to develop robust prediction models to process the control and optimization of end products.

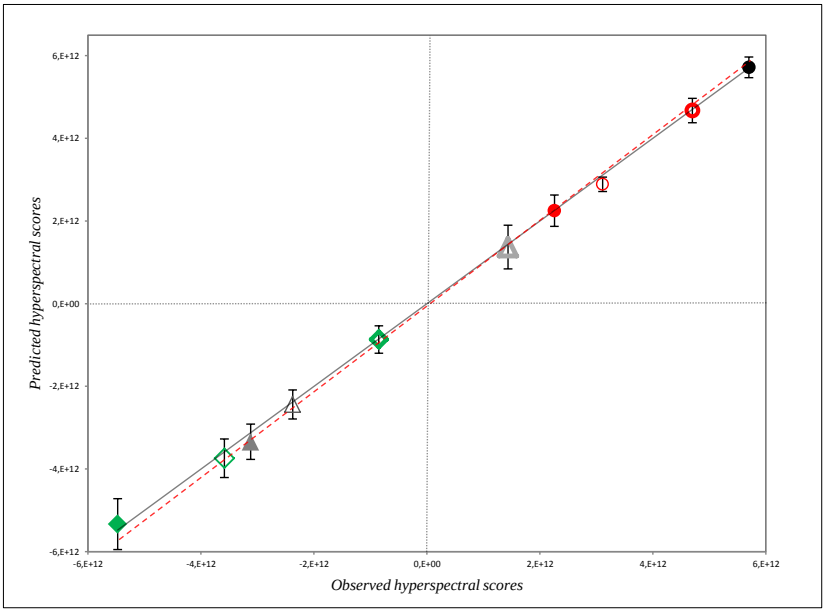

Figure V.6. Observed scores from the hyperspectral information PCA and those predicted from physical cake properties. Colors of the series correspond to different heat treatment temperatures: black, control flour (●); red 80ºC (○ 80ºC/10 min; ○ 80ºC/20 min; ● 80ºC/30 min); gray 100ºC (Δ 100ºC/10 min; Δ 100ºC/20 min; ▲ 100ºC/30 min); green, 130ºC (□ 130ºC/10 min; □ 130ºC/20 min; ■ 130ºC/30 min). The black line means fit 1:1 and the red line means data fit. Vertical bars mean standard deviation.

4. Conclusions

The SW-NIR imaging system was capable of obtaining information about the diffuse reflectance spectrum from the treated flour and of characterizing different heat treatments according to time and temperature. The effect of the different heat treatments applied to

flour led to a difference in the specific wavelength reflectance, which may relate to the main modifications undergone by flour components. The wavelengths that contributed the most, and were implied in the differentiations, were detected. The selection of wavelengths allowed us to optimize the analysis, which reduced from 54 to 6 wavelengths. Dependency between the hyperspectral information of flour and cake properties with these flours was observed. These results indicated that the SW-NIR imaging analysis was capable of obtaining information about the changes that took place during heat treatments with flour, which can be used to determine and adjust process variables in order to improve the behavior of flours in different cake production phases. This method could be the basis to develop a non destructive analysis tool to help control and optimize online flour heat treatments.

5. Bibliography

Boser, B. E., Guyon, I. M., & Vapnik, V. N. (1992). A Training Algorithm for Optimal Margin Classifiers. In *Proceedings of the 5th Annual ACM Workshop on Computational Learning Theory* (pp. 144–152).

Chen, Z.-P., Morris, J., & Martin, E. (2006). Extracting chemical information from spectral data with multiplicative light

scattering effects by optical path-length estimation and correction. *Analytical chemistry*, *78*(22), 7674–81.

Chesterton, a. K. S., de Abreu, D. a. P., Moggridge, G. D., Sadd, P. a., & Wilson, D. I. (2013). Evolution of cake batter bubble structure and rheology during planetary mixing. *Food and Bioproducts Processing*, *91*(3), 192–206.

Chesterton, a. K. S., Wilson, D. I., Sadd, P. a., & Moggridge, G. D. (2015). A novel laboratory scale method for studying heat treatment of cake flour. *Journal of Food Engineering*, *144*, 36–44.

Jiranuntakul, W., Puttanlek, C., Rungsardthong, V., Puncha-arnon, S., & Uttapap, D. (2011). Microstructural and physicochemical properties of heat-moisture treated waxy and normal starches. *Journal of Food Engineering*, *104*(2), 246–258.

Kimiya, T., Sivertsen, A. H., & Heia, K. (2013). VIS/NIR spectroscopy for non-destructive freshness assessment of Atlantic salmon (Salmo salar L.) fillets. *Journal of Food Engineering*, *116*(3), 758–764.

Lee, C. J., Kim, Y., Choi, S. J., & Moon, T. W. (2012). Slowly digestible starch from heat-moisture treated waxy potato starch:

Preparation, structural characteristics, and glucose response in mice. *Food Chemistry*, *133*(4), 1222–1229.

Li Vigni, M., & Cocchi, M. (2013). Near infrared spectroscopy and multivariate analysis to evaluate wheat flour doughs leavening and bread properties. *Analytica chimica acta*, *764*, 17–23.

Meza, B. E., Chesterton, A. K. S., Verdini, R. a., Rubiolo, A. C., Sadd, P. a., Moggridge, G. D., & Wilson, D. I. (2011). Rheological characterisation of cake batters generated by planetary mixing: Comparison between untreated and heat-treated wheat flours. *Journal of Food Engineering*, *104*(4), 592–602.

Miñarro, B., Albanell, E., Aguilar, N., Guamis, B., & Capellas, M. (2012). Effect of legume flours on baking characteristics of gluten-free bread. *Journal of Cereal Science*, *56*(2), 476–481.

Neill, G., Al-Muhtaseb, A. H., & Magee, T. R. a. (2012). Optimisation of time/temperature treatment, for heat treated soft wheat flour. *Journal of Food Engineering*, *113*(3), 422–426.

Sağol, S., Turhan, M., & Sayar, S. (2006). A potential method for determining in situ gelatinization temperature of starch using initial water transfer rate in whole cereals. *Journal of Food Engineering*, *76*(3), 427–432.

Scanlon, M. G., & Zghal, M. C. (2001). Bread properties and crumb structure. *Food Research International*, *34*(10), 841–864.

Shibata, M., Sugiyama, J., Tsai, C. L., Tsuta, M., Fujita, K., Kokawa, M., & Araki, T. (2011). Evaluation of viscoelastic properties and air-bubble structure of bread containing gelatinized rice. *Procedia Food Science*, *1*, 563–567.

Sinelli, N., Benedetti, S., Bottega, G., Riva, M., & Buratti, S. (2006). Evaluation of the optimal cooking time of rice by using FT-NIR spectroscopy and an electronic nose. *Journal of Cereal Science*, *44*(2), 137–143.

Singh, C. B., Jayas, D. S., Paliwal, J., & White, N. D. G. (2009). Detection of insect-damaged wheat kernels using near-infrared hyperspectral imaging. *Journal of Stored Products Research*, *45*(3), 151–158.

Sun, Q., Han, Z., Wang, L., & Xiong, L. (2014). Physicochemical differences between sorghum starch and sorghum flour modified by heat-moisture treatment. *Food chemistry*, *145*, 756–64.

Toit, D. (2009). NEAR INFRARED HYPERSPECTRAL IMAGING AND CHEMOMETRICS FOR EXPLORATION AND CLASSIFICATION OF

WHOLE WHEAT KERNELS Department of Food Science, (December).

Verdú, S., Ivorra, E., Sánchez, A. J., Barat, J. M., & Grau, R. (2015). Relationship between fermentation behavior, measured with a 3D vision Structured Light technique, and the internal structure of bread. *Journal of Food Engineering*, *146*, 227–233.

Wang, S., Karrech, A., Regenauer-Lieb, K., & Chakrabati-Bell, S. (2013). Digital bread crumb: Creation and application. *Journal of Food Engineering*, *116*(4), 852–861.

Wu, D., He, Y., & Feng, S. (2008). Short-wave near-infrared spectroscopy analysis of major compounds in milk powder and wavelength assignment. *Analytica Chimica Acta*, *610*, 232–242.

Wu, D., & Sun, D.-W. (2013). Advanced applications of hyperspectral imaging technology for food quality and safety analysis and assessment: A review — Part I: Fundamentals. *Innovative Food Science & Emerging Technologies*, *19*, 1–14.

Xing, J., Symons, S., Hatcher, D., & Shahin, M. (2011). Comparison of short-wavelength infrared (SWIR) hyperspectral imaging system with an FT-NIR spectrophotometer for predicting alpha-amylase activities in individual Canadian Western Red Spring (CWRS) wheat kernels. *Biosystems Engineering*, *108*(4), 303–310.

CAPÍTULO VI

Hyperspectral image control of the heat-treatment process of oat flour to model composite bread properties

Samuel Verdú, Francisco Vásquez, Eugenio Ivorra, Antonio J. Sánchez, José M. Barat, Raúl Grau

Abstract

A hyperspectral image analysis was used to characterize heat treatment in oat flour, performed by treating oat flour at 80, 100 and 130ºC for 30 min. Images from both original oat and treated flours were captured, and hyperspectral information was collected. Oat flours were used to obtain composite flours based on two different substitution levels (10 and 20%) of wheat flour. Composite breads were produced from the obtained flours. A battery of analyses was run to characterize them in terms of physical properties. The hyperspectral information of oat flours was analyzed by multivariate statistics and a pattern evolution-depending temperature was observed. Similarly, a set of the physical properties of breads was analyzed based on multivariate statistics, and a pattern of temperature-dependent evolution, in addition to the substitution level, was also recognized. Multivariate non linear regressions were done between both data sets to study their relationship and high values in the calibration and cross-validation results obtained. The changes undergone by oat flour during treatment were characterized with hyperspectral information, which could represent a non destructive monitoring tool to then regulate it until oat flours are obtained that confer composite bread adequate properties.

Keywords: oats flour, heat treatment, hyperspectral image, composite breads, process monitoring

1. Introduction

The cereal processing and transformation industry is one of the most important sectors in the food industry. Type of grains, and derived flours and products, require vast numbers of operations and specific processes, which finally offer a wide variety of transformed products: bread, cakes, snacks, transformed flours, gluten-free products, enriched products, etc. This is the result of the impact that grain components, such as proteins, soluble and insoluble fibers, minerals, oils, etc., have on maintaining and improving human health, which has been an important scientific work area in recent decades (Cleary, et al., 2007). Mixing and enriching grain-derived products have led to improved nutritional quality and safety, and to organoleptic features like texture, taste and palatability. In the same way, properties about their behavior during the food-making process have been modified to facilitate easy handling during processing (Angioloni & Collar, 2011). Many grain combinations of bread that originates from composite flours production have been developed and tested (Eriksson et al., 2014; Rehman et al.,2007; Ronda et al., 2015; Verdú et al., 2015).

In this work, composite flour based on wheat and oats has been examined. Oat flour is becoming an important element as raw material in the cereal-derived industry because of the health benefits obtained from its derived products (Butt et al., 2008). This grain is an interesting resource for preparing composite derivates because we can find β-glucanin its composition. This component is a hydrocolloid, which represents a hydrosoluble fiber with beneficial effects on

human health, according to recent works (Whitehead et al., 2014). There are also reports that a high concentration of oat flour in composite flour induces changes that could alter dough properties, and could thus modify the properties of both intermediate operations (e.g. dough rheology and transport, dough fermentation process rates, etc.) and quality features compared to pure wheat breads (Gill et al., 2002). Therefore, it is usual to find solutions based on chemical modifications, limited concentrations of added oat flours, modification of process parameters during the bread-making process, etc.

In line with this, one of the most widely used procedures is heat treatment of flours at different temperatures and from distinct moisture contents. This is a physical treatment method utilized to modify the functional properties of native starch, including pasting characteristics, granule morphology, amylose leaching, textural properties, etc., which are particularly favorable for food applications (Jiranuntakul et al., 2011; Lee et al., 2012; Sun et al., 2014). However, the heterogeneity of grain flours produced by cultivar type, mixes of varieties, climate conditions during growth, etc., imply difficulties in obtaining a standard optimal combination of time and temperature which reports the stable behavior of product features during the process. To this end, the automatic and non destructive control of each flour batch during heat treatments can improve knowledge about flour state for it to be optimized until the product presents

optimal properties. In this work, the hyperspectral image technique is proposed as a non destructive control method in order to test its capability to characterize oat flour evolution during heat treatment, and to study its relationship to flour's behavior in composite bread properties.

2. Material and Methods

2.1 Experiment procedure

Figure VI.1 shows the scheme of the experiment procedure. Step 1 was based on treating oat flour at three different temperatures, 80, 100 and 130ºC, for 30 min to finally obtain four oat flour types. In Step 2 the hyperspectral image analysis of the flours obtained in Step 1 was done and the obtained data were processed. Step 3 involved the production of composite flours. For this purpose, pure wheat flour was substituted at two levels, 10 and 20% (w/w), using the four oat flour types. Then eight different composite flour types, plus one of pure wheat flour, used as a control, were obtained. Step 4 involved bread production for which the composite and pure wheat flours obtained in Step 3 were employed. In Step 5 the composite bread properties were analyzed by different physico-chemical procedures. Step 6 was based on the joint study of the hyperspectral information of flours and bread properties in order to test the capacity of the former to characterize the heat treatment process of oat flour, and to determinate relationships with bread behaviors.

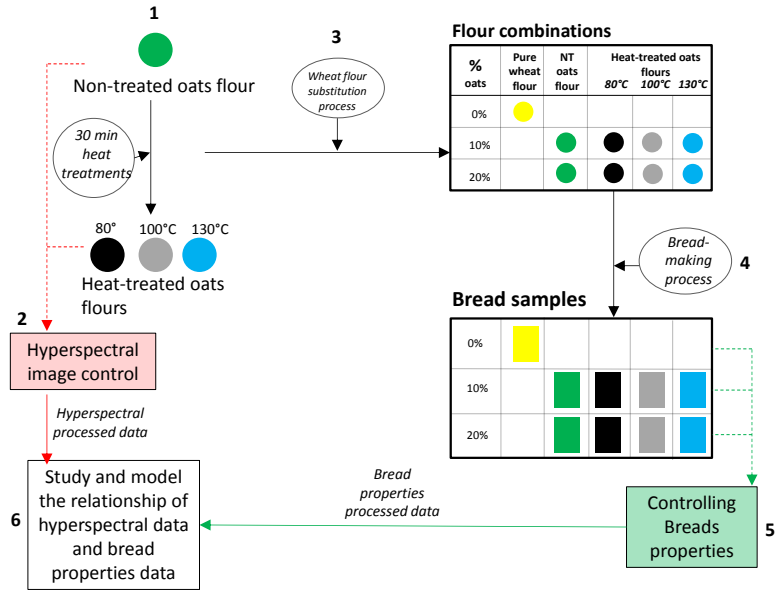

Figure VI.1. Scheme about the complete experiment procedure. Numbers 1- 6 indicate the steps followed, where 1: heat treatment of oat flour for 30 min at 80, 100 and 130 °C; 2: collecting the hyperspectral image data of oat flours; 3: obtaining combined flours based on the substitution of pure wheat flour at 0, 10 and 20% (w/w) for oat flour and its heat-treated versions; 4:bread-making process from the combined flours; 5: collecting bread properties data; 6: studying the relationship between the hyperspectral data of flours vs. produced bread properties data. NT oat flour: non treated oat flour.

2.2 Raw materials

The commercial oat flour was obtained from a local producer (La Carabasseta, Valencia, Spain). Its composition was 11.3±0.1% of proteins, 8.0±0.1% of fat, 12.6±0.6% of moisture and 0.92±0.1% of

ash (w.b). The commercial wheat flour (WF) was supplied from a different local producer (Molí de Picó-Harinas Segura S.L. Valencia, Spain). Its composition was as follows: 12.7±0.6% of proteins, 1.0±0.03% of fat, 13.09±0.5% of moisture, and 0.32±0.1% of ash (w.b). The alveographic parameters were also facilitated by the seller, which were P = 94±2 (maximum pressure (mm)), L = 128±5 (extensibility (mm)), W = 392±11 (strength (J-4)) and P/L= 0. 73. In order to maintain particle size homogeneity, oat flours were analyzed and remilled in a stainless steel grinder, whenever necessary (Retsch GmbH, ZM 200, Haan, Germany), until particle size distribution was achieved with no significant differences with the used wheat flour. The particle size of flours was measured 6 times by laser scattering in a Mastersizer 2000 (Malvern, Instruments, UK), equipped with a Scirocco dry powder unit. The results were expressed as maximum size in µm at 10%, 50% and 90% (d (0.1), d (0.5) and d (0.9), respectively) of the total volume of the analyzed particles as their averages (D [4, 3]). The average results were d (0.1) = 25.5±1.1, d (0.5) = 92.0±0.6, d (0.9) = 180.6±0.8 and D [4, 3] = 99.4±1.2. Having ensured homogeneous particle size, composed flours were obtained by substituting two distinct percentages of wheat flour with the different oats flour. Those percentages were 10 and 20% (w/w).

The other ingredients used to make bread were sunflower oil (maximum acidity 0.2º Koipesol Semillas, S.L., Spain), pressed yeast (Saccharomyces cerevisiae, Lesafre Ibérica, S.A., Spain), white sugar (≥ 99.8% of saccharose, Azucarera Ebro, S.L., Spain) and salt (refined

marine salt ≥ 97% NaCl Salinera Española S.A., Spain), which were purchased in local stores.

2.3 Heat treatment of oat flour

For the purpose of obtaining a register from different treatment intensities, three distinct heat treatments were carried out at 80, 100 and 130ºC for 30 minutes with forced convection hot air. Here the work of Neill et al., (2012) was taken as a reference. The time for stabilizing the oven temperature was 1.5 minutes as a maximum for the lower heat treatment (80ºC). Temperature was monitored with a digital thermometer (range 0-300 ºC, resolution 0.1ºC, precision ± 0.2 ºC). Each treatment was carried out by extending 300 g of untreated flour on a layer of a maximum 0.5 cm thickness, which was placed onto a metal plate covered with baking paper. During this process, moisture reduced from 15% to 10.5% (wet basis) as a maximum for 130ºC. Loss of moisture was calculated gravimetrically based on the mass difference between weights after and before heat treatment. In order to recover the original moisture values, flours were placed into a chamber (KBF720 Binder Tuttlingen Germany) with controlled humidity and temperature (15% R.H. and 25 ºC). Flours remained inside the chamber for 48 h as this time was required to recover moisture in a case of maximum loss, which was 130ºC. Finally, in order to homogenize any oversized particles produced during the process, oat flours were analyzed and remilled in the stainless steel

grinder until particle size distribution was accomplished with no significant differences with the non treated flours.

2.4 Hyperspectral image data acquisition and processing

Heat-treated oat flours captures were carried out with a Photonfocus CMOS camera, model MV1-D1312 40gb 12 (Photonfocus AG, Lachen, Switzerland), using a SpecimImSpector V10 1/2" filter (Specim Spectral Imaging, LTD., Oulu, Finland), which worked as a linear hyperspectral camera. The illuminant was an ASD illuminator reflectance lamp (ASD Inc, Boulder, USA), which produces constant illumination over the full working spectral range. The sample preparation protocol was based on Verdú et al., (2015). Fifteen grams of each flour (control oats flour and all three heat-treated oats flours) were placed into a glass Petri dish (10-cm diameter) and a homogeneous surface and height were maintained (approx. 0.75 cm). Six samples of each oat flour were prepared. Four images of each sample were acquired by rotating 1.04 radians each time around its normal axis. Twenty-four image acquisitions of each flour were obtained. Spectra were collected directly at room temperature. The position of the illuminant and camera in relation to the sample was always constant in order to control lighting conditions and to obtain constant image size. In order to avoid any heat transfer to samples, the distance between the illuminant and samples was 0.5 m. The distance between the camera and samplea was 0.15 m. The obtained

image (scanned line) comprised 256 gray levels (8 bits). The diffuse reflectance spectrum was collected with 53 different wavelengths (each wavelength was digitalized with 8 bits). These wavelengths were distributed at intervals of 11.2 nm within the 400-1000 nm range. The scanned line comprised 1312 points, so an image was recorded with a resolution of 1312 x 1082 pixels. Image reflectance calibration and preprocessing were performed as described in (Verdú et al., 2015). The camera was operated by developed software based on SDK Photonfocus-GigE_Tools, and programming language C++ was used.

2.5 Bread-making process

The formulation used to prepare bread dough was that according to previous works (Verdú et al., 2015) and was as follows: 56% flour (pure wheat flour or combined flours), 2% refined sunflower oil, 2% commercial pressed yeast, 4% white sugar 1.5% salt and 34.5% water. The process was carried out by mixing all the ingredients in a food mixer (Thermomix® TM31, Vorwerk, Germany) according to the following method: in the first phase, liquid components (water and oil), sugar and salt were mixed for 4 minutes at 37 ºC. Yeast was added in the next phase to be mixed at the same temperature for 30 seconds. In the last step flour was added and mixed with the other ingredients according to a default bread dough mixing program to make homogeneous dough. The program system centers on mixing

ingredients with random turns of the mixer helix in both directions (550 revolutions/minute) to obtain homogeneous dough. This process was applied for 4.5 minutes at 37 ºC. Then 450 g of dough were placed in the metal mold (8x8x30cm) for fermentation. Height was approximately 1 cm.

Dough fermentation was carried out in a chamber with controlled humidity and temperature (KBF720, Binder, Tuttlingen, Germany). The fermentation process conditions were 37 °C and 90% relative humidity (RH). Samples were fermented for 1 h. The baking process was carried out at the end of fermentation. Metal molds were placed in the middle of the oven (530x450x340, grill power 1200W, internal volume 32L, Rotisserie, DeLonghi, Italy) plate, which was preheated to 180 ºC. Baking time was 35 minutes.

2.6 Characterization of bread properties

In order to evaluate the effect of wheat substitution and heat treatments of oat flour on bread properties, some of most relevant ones were studied.. In this phase, bread volume was measured by the millet seed displacement method (Griswold, 1962), and then the specific volume (*Sv*) was calculated as the ratio between volume (mL) and bread weight (g). The baking process was also studied based on the produced mass loss (ΔM_b). It was concluded by the difference between the pre-baking dough weight (g) and the finished bread

weight (g) (cooled previously at room temperature for 1 h). The water activity of raw crumbs (a_w) was determined in an Aqualab® dew point hygrometer (DECAGÓN Aqualab CX-2, Pullman, WA, USA). The texture profile analysis (*TPA)* was performed following the method used by Miñarro, Albanell, Aguilar, Guamis, & Capellas, 2012 , where two 12.5-mm-thick cross-sectional slices were obtained from the center of each bread. The texture profile analysis was carried out in a TA-TX2 texture analyzer (Stable Micro Systems, Surrey, UK). A 25-kg load cell (35-mm diameter) was used. The assay speed was set at 1.7 mm/s to compress the bread crumb center at 50% of its previous height. The time between compressions was 5 s. The studied parameters were hardness (*H*), springiness (*S*), cohesiveness (*C*), gumminess (*G*), chewiness (*Ch*) and resilience (*R*). Ten bread replies of each formula were performed and analyzed.

2.7 Statistical methods

Many variables obtained from both the hyperspectral information of flours and bread properties, a multivariable statistical procedure was applied to process them. To this end, a multivariate unsupervised statistical PCA (Principal Component Analysis) was used for the two different blocks: hyperspectral data results and bread properties results. This method was used to describe and reduce the dimensionality of a large set of quantitative variables to a small number of new variables, called principal components (PCs), which

are the result of linear combinations of the original variables. The number of PCs was selected after considering the change in tendency on the screen plot, and also the accumulated percentage of explained variability above 75%.

Bread properties (ΔM_b, a_w and TPA (*H, S, C, G, Ch*)) were also studied by a one-way variance study (ANOVA). In those cases in which the effect was significant (P-value < 0.05), means were compared by Fisher's least significant difference (LSD) procedure.

Support Vector Machines (SVM) were used to model the relationship between the hyperspectral data of the oat flours and the set of bread properties. They were used to carry out non linear regressions between both data sets. SVR are a powerful supervised learning methodology based on the statistical learning theory, which are commonly used for spectral analyses (Boser et al., 1992). Several SVM were done, first by employing the score values generated in the bread properties data PCA, which were taken as the descriptor of bread global characteristics since this parameter collects information about the differences among breads influenced by all the properties simultaneously. The remaining SVM were done between the hyperspectral data and each analyzed physical variable. Procedures were performed with PLS Toolbox, 6.3 (Eigenvector Research Inc., Wenatchee, Washington, USA), a toolbox extension in the Matlab 7.6 computational environment (The Mathworks, Natick, Massachusetts, USA).

3. Results

3.1 Hyperspectral image data acquisition

The data obtained from the hyperspectral image control (Step 2) of flours were processed and analyzed. For this purpose, information collected by the camera was studied according to the heat treatment temperature. A PCA was then used to reduce data dimensionality and to observe the spontaneous unsupervised clustering of samples within maximum variance dispersion. Figure VI.2 shows the PCA space where the scores of samples are represented. It was the result of two PCs, which explain 94.8% of total data set variance. PC1 collected 83.1% and PC2 collected 13.7% of total variance.

A clustering tendency of samples was observed following the pre-established class division (types of flours). Each oat flour class was sited separately from the rest. Thus an evolution following increase in temperature from the NT oat flour (positive PC1 zone) to the maximum treatment temperature (negative PC1 zone) was observed along the PC1 axis. Thus we can initially conclude that the information obtained from the hyperspectral image control allowed us to characterize the processing of oat flours according to temperature.

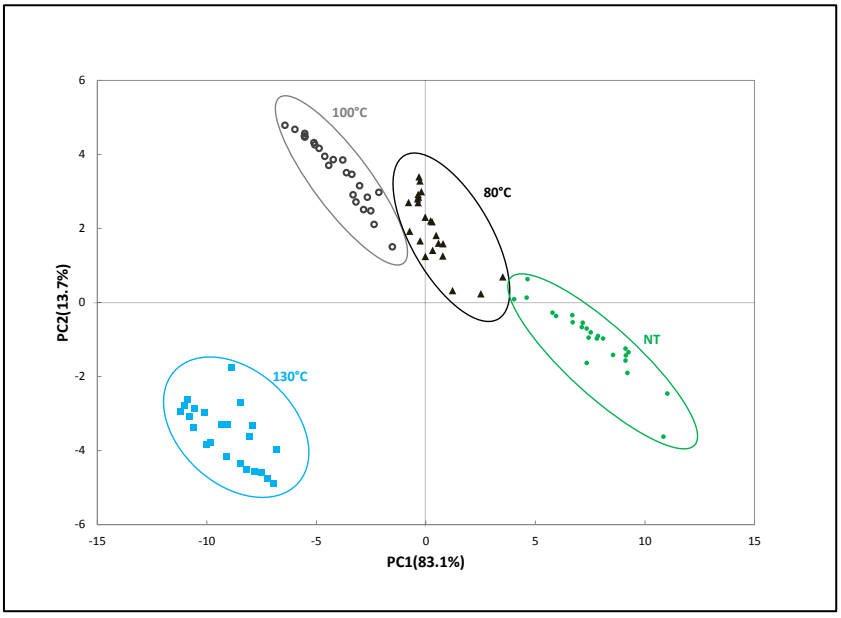

Figure VI.2. Study of the hyperspectral image data of oat flours. The PCA space with samples scores representation. ●: NT (non treated oat flour); ▲: oat flours treated at 80 ºC; ○: oat flours treated at 100 ºC; ■: oat flours treated at 130 ºC. Circumferences mark classes.

3.2 Characterization of bread properties

The bread properties acquired from using combined flours, based on the different oat flours and the pure wheat flour, were analyzed. Table VI.1 shows the bread properties results for the studied physicochemical parameters. In spite of oat proteins not possessing characteristic wheat gluten properties (Hüttner et al., 2010) to maintain gas, the specific volume was not significantly modified with the addition of NT oat flour at any tested substitution level. However, the oat flour treated at 100ºC produced a maximum value at both

the 10% and 20% substitutions. Water activity presented an increment in all the 10% substitution cases, while reduction was observed for the 20% substitution cases with no clear temperature effect. Mass loss during the baking process for the breads obtained using NT oat flour presented increments up to 3% compared to the pure wheat at each substitution level. For this parameter, mass reduction loss was clear following the increase in the treatment temperature of oat flour, and values were obtained with no significant differences at 130ºC for both substitution levels. Hardness presented a decrease when adding the NT oat flour at both substitution levels. Temperature produced a sharper decrease for the 10% level, while the inverse behavior was observed for the 20% substitution. Springiness presented no clear evolution compared to the pure wheat bread, and values were similar. Gumminess displayed a parallel behavior to hardness. A decrease was noted when adding the NT oat flour at both substitution levels, and a decrease was also observed for the 10% level, but the inverse behavior was observed for the 20% substitution due to temperature. Chewiness lowered for the 10% substitution, while values near to the pure wheat ones were obtained for the flour treated at 130ºC at 20% substitution. Resilience presented a reduction at both substitution levels when the NT oat flour was added. However, an increase occurred almost up to the pure wheat values with increased treatment temperature. Cohesiveness increased with the addition of oat flour and did not appear to be affected by treatment temperature. The modifications

observed on textural properties were in line with known effects of partial lack of gluten and presence of β-glucan in composite breads (Flander et al., 2011).

In order to observe whether the set of bread properties presented a recognizable pattern according to treatment temperature, all the parameters were studied together. For this purpose, the PCA was done according to the parameters in Table VI.1. Figure VI.3 shows the biplot space based on the PCA done using the bread properties data set. Two PCs were selected, where PC1 collected 42.7% and PC2 34.5% of total data variance (77.2%).

The situation of bread samples (cases) and properties (variables) in the biplot space revealed a relationship among them, hence the weight of each property in the explanation of global bread characteristics. Two different tendencies pertained to the 10% and 20% substitution levels. Samples were ordered following an increase in treatment temperature from the NT oat flour to the 130ºC-treated flours. Pure wheat bread appeared on the edge of the positive PC1 zone. Samples presented an equal tendency across PC2, which was inversed across PC1.

Table VI.1. Bread properties results

	%	specific volume	a_w	mass loss	hardness	springiness	gumminess	chewiness	resilence	cohesiveness
Pure wheat	0	2.22 ± 0.08 a	0.9579 ±0.0008 bc	12.5 ± 0.53 a	6.25 ± 0.54 d	0.94 ±0.05 a	5.1 ± 0.4 c	5.5 ± 0.57 c	0.46 ±0.01 d	0.78 ± 0.00 a
NT Oats	10	2.16 ± 0.08 a	0.9701 ±0.0031 d	15.68 ± 0.3 c	4.82 ± 0.66 cd	0.99 ±0.043 b	4.0 ± 0.54 b	2.5 ± 0.58 a	0.35 ±0.04 a	0.78 ± 0.01 a
Oats 80°C		2.44 ± 0.08 b	0.9575 ±0.0003 bc	13.68 ± 0.31 b	4.02 ± 0.97 cd	0.98 ±0.02 a	3.34 ± 0.78 ab	3.31 ± 0.79 ab	0.42 ±0.01 c	0.83 ± 0.01 bc
Oats 100°C		2.64 ± 0.09 cd	0.9589 ±0.0041 cd	13.44 ± 0.37 b	3.22 ± 0.45 b	0.95 ±0.09 a	2.7 ± 0.38 a	2.58 ± 0.49 a	0.44 ±0.01 c	0.83 ± 0.01 bc
Oats 130°C		2.34 ± 0.2 b	0.9622 ±0.0040 d	12.64 ± 0.33 a	3.21 ± 0.57 bc	0.99 ±0.02 b	2.74 ± 0.46 a	2.71 ± 0.48 a	0.46 ±0.01 d	0.85 ± 0.01 c
NT Oats	20	2.10 ± 0.1 a	0.9525 ±0.0021 a	15.0 ± 0.20 c	1.30 ± 0.61 a	0.98 ±0.04 b	2.5 ± 0.48 a	1.2 ± 0.47 a	0.40 ±0.04 b	0.84 ± 0.01 c
Oats 80°C		2.56 ± 0.07 bc	0.9525 ±0.0019 a	14.24 ± 0.25 b	2.57 ± 0.47 b	0.96 ±0.1 a	2.16 ± 0.36 a	2.14 ± 0.37 a	0.41 ±0.01 b	0.84 ± 0.01 c
Oats 100°C		2.74 ± 0.06 d	0.9521 ±0.0028 a	13.78 ± 0.27 b	3.45 ± 0.8 b	0.98 ±0.01 a	2.85 ± 0.63 a	2.79 ± 0.61 a	0.41 ±0.01 b	0.82 ± 0.01 b
Oats 130°C		2.49 ± 0.13 bc	0.9548 ±0.0017 ab	12.42 ± 0.61 a	5.47 ± 0.57 cd	0.97 ±0.01 a	4.59 ± 0.47 bc	4.53 ± 0.45 bc	0.44 ±0.01 c	0.84 ± 0.01 c

NT: non treated oat flour. Values followed by different letters are significantly different at $P < 0.05$ in columns

To interpret those distributions, the loadings of variables for both PCs were studied. PC1 had high loading values for hardness (*H*), chewiness (*Ch*) and gumminess (*G*) in the positive zone, while cohesiveness (*C*) was found in the negative one. Those breads that contained 10% of NT oat flour and 20% of the 130ºC-treated oat flours came the closest to pure wheat flour as regards these properties. For PC2, mass loss (ΔM_b) in the positive zone and resilience (*R*) in the negative one were the variables with high loadings. Regarding these properties, both substitution levels with the 130ºC-treated oats came the closest to pure wheat flour, while those that contained the NT oats flour differed the most. Water activity (a_w) and springiness (*S*) presented intermediate loadings for both PCs, while specific volume (*Sv*) presented the lowest one.

Overall, increased temperature principally reduces mass loss and water activity in bread, but increases resilience at both substitution levels until it comes close to pure wheat flour. Chewiness, gumminess, hardness and cohesiveness were influenced inversely by temperature as regards the substitution level. The effect of heat treatment on oat flours led to amended bread properties compared to the breads substituted for the NT oat flour, which were almost pure wheat breads for some properties.

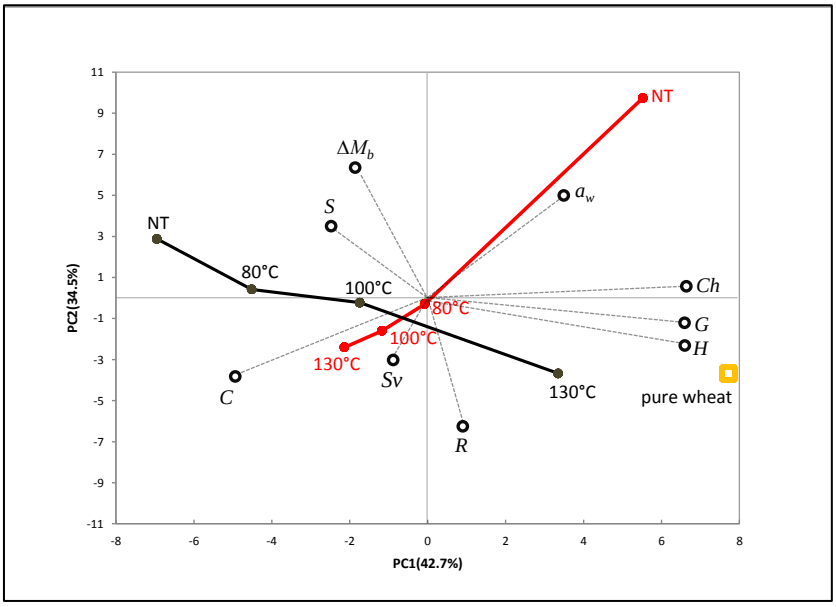

Figure VI.3. Study of the bread properties data set. Biplot PCA space based on sample' mean scores and variable loadings representation. NT: non treated oat flour; *H*: hardness; *S*: springiness; *C*: cohesiveness; *G:* gumminess; *Ch:* chewiness; *R:* resilience; *Sv*: specific volume; a_w: water activity; ΔM_b: mass loss. Circumferences mark variables. Red: 10% substituted samples; Black: 20% substituted samples. Yellow square: pure wheat bread.

3.3 Studying the relationship of hyperspectral data and bread properties data

The relationship between the hyperspectral data and bread properties was studied by testing the dependence between both datasets. The dependency of the global bread properties was studied by taking the score value generated in the bread properties data PCA

as their descriptor (Figure VI.3). This was done because this value collects any differences among those breads influenced by all properties simultaneously, and it is a feasible parameter to compare them globally. Therefore, the mean of the PC1 scores of the hyperspectral image information of the PCA (Figure VI.2) was plotted as the Z axis in the bread properties data PCA (Figure VI.3). Figure VI.4 shows the resultant plot. Dispersion of points into a generated tridimensional space presented an organized sequence for the hyperspectral image data, with two different recognizable tendencies described according to each substitution level. Having observed these results, a decision was made to test the capability of the hyperspectral image information to form models with the bread properties data. The objective here was to know whether it was possible to obtain acceptable regression levels between both data set blocks or not.

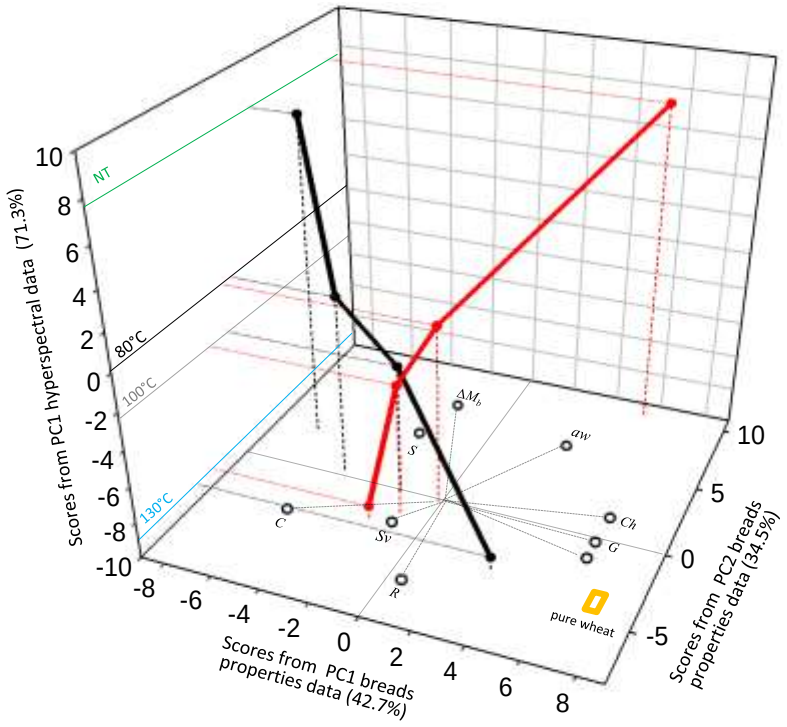

Figure VI.4. Plot of the relationship between the bread data and the hyperspectral image data. Y axis: mean scores from the PC2 bread properties data; X axis: mean scores from the PC1 bread properties data; Z axis: mean scores from the PC1 hyperspectral data. Black circumferences mark the bread properties variables on the XY plane. Red: 10% substituted samples; Black: 20% substituted samples. Yellow square: pure wheat bread. Lines across the Z axis: Green: NT (non treated oat flour); Black: oat flours treated at 80 ºC; Gray: oat flours treated at 100 ºC; Blue: oat flours treated at 130 ºC.

Since a non linear relationship is observed in Figure VI.4, Support Vector Machines (SVM) were used to obtain the regression calibration and cross-validation coefficients. The hyperspectral image data were used as independent variables (X) and the scores of the bread properties PCA as the dependent variable.

Calculations were made by taking into account the scores of both PCs from the bread properties PCA, as well as substitution levels, which resulted in four regressions to be studied (the PC1/PC2 scores from the 10% substitution and the PC1/PC2 scores from the 20% substitution). The results for all four regressions were successful, although PC1 presented slightly better values (Table VI.2) at both substitution levels. The 10% substitution presented cross-validation coefficients 0.95 and 0.91 for PC1 and PC2, respectively. Likewise, 20% presented 0.98 and 0.97 for PC1 and PC2, respectively.

Having observed the results about the relationships globally with bread properties, the dependency of each variable was also singly tested. Those single dependencies between the hyperspectral image and bread properties are included in Table VI.2. The obtained fit was also successful, although the cross-validation values were lower than those obtained for PC1 and PC2 for the majority. With 10% substitution, maximums R^2 *CV* were obtained for mass loss, chewiness and resilience with 0.97, followed by gumminess. The lowest one was specific volume and cohesiveness, with 0.81 and

Table VI.2. Results of the regressions calculated between the hyperspectral image data of the oat flours and bread properties data.

% sustitution	SVM regresion parameters	Scores PC1	Scores PC2	Sv	a_w	ΔM_b	H	S	C	G	Ch	R
10	Number of SVs	35	36	36	38	35	21	33	41	36	36	35
	RMSEC	0.04	0.1	0.09	0.0	0.01	0.13	0.05	0.08	0.07	0.01	0.02
	RMSECV	0.09	0.7	4.03	0.0	0.1	0.19	0.07	0.1	0.09	0.16	0.04
	R^2 Cal	0.97	0.95	0.99	0.99	0.99	0.96	0.93	0.99	0.97	0.99	0.99
	R^2 CV	0.95	0.91	0.81	0.86	0.97	0.92	0.86	0.82	0.94	0.97	0.97
20	Number of SVs	36	39	92	89	92	89	71	95	95	59	83
	RMSEC	0.03	0.003	2.60	0.00	0.10	0.18	0.00	0.00	0.14	0.16	0.01
	RMSECV	0.05	0.04	6,00	0.00	0.20	0.36	0.03	0.05	0.24	0.25	0.02
	R^2 Cal	0.99	0.98	0.96	0.99	0.98	0.98	0.9	0.91	0.98	0.98	0.99
	R^2 CV	0.98	0.97	0.83	0.96	0.94	0.94	0.63	0.64	0.95	0.95	0.98

PC1 and PC2: scores from the bread properties PCA*; Sv*: specific volume; a_w: water activity; *H*: hardness; *S*: springiness; *C*: cohesiveness; *G:* gumminess; *Ch:* chewiness; *R:* resilience; ΔM_b: mass loss; *Number of SVs*: number of support vectors used in the regression to calculate; *RMSEC*: root mean square error of calibration; *RMSECV*: root mean square error of cross-validation; R^2 *Cal*: calibration coefficient; R^2 *CV*: cross-validation coefficient.

0.82, respectively. For the 20% substitution level, the maximum was resilience with 0.98, followed by chewiness and gumminess with 0.95. The lowest ones were springiness and cohesiveness with 0.63 and 0.64, respectively.

The results proved the relationship between the hyperspectral image data obtained at different heat treatment temperatures applied to the oat flours, and also to the properties of the breads made with these flours. These dependencies are interesting because of the possibility of building a general model to obtain knowledge about

bread properties by studying the heat treatment process of oat flour, in which more heat treatment temperatures and substitution levels can be included. Therefore, the capability to monitor the heat treatment process of oat flour that corresponded to the hyperspectral image technique was proved. It could be used as a control tool for the multigrain bread-making process to, for example, manipulate the properties of several oat flours to guarantee end product homogeneity.

4. Conclusions

A heat treatment process on oat flour was effectively characterized by the hyperspectral image technique. This characterization reported information that allowed changes in oat flours to be monitored during the process, from non treated oat flour to the 130ºC-treated flour. The pattern between the hyperspectral information analysis and the response of composite breads in physical properties terms was observed. This relationship presented both high correlation and cross-validation values when non linear regression testing was carried out between them. The information obtained from the hyperspectral image system during heat treatment gave a direct relationship with oat flour behavior during the bread-making process. This could represent a non destructive control tool to monitor this process, and to regulate treatment until oat flours that provide bread with the desired properties are obtained.

5. Bibliography

Angioloni, A., & Collar, C. (2011). Nutritional and functional added value of oat, Kamut ®, spelt, rye and buckwheat versus common wheat in breadmaking. *Journal of the Science of Food and Agriculture*, *91*, 1283–1292.

Boser, B. E., Guyon, I. M., & Vapnik, V. N. (1992). A Training Algorithm for Optimal Margin Classifiers. In *Proceedings of the 5th Annual ACM Workshop on Computational Learning Theory* (pp. 144–152).

Butt, M. S., Tahir-Nadeem, M., Khan, M. K. I., Shabir, R., & Butt, M. S. (2008). Oat: Unique among the cereals. *European Journal of Nutrition*, *47*, 68–79.

Cleary, L. J., Andersson, R., & Brennan, C. S. (2007). The behaviour and susceptibility to degradation of high and low molecular weight barley ??-glucan in wheat bread during baking and in vitro digestion. *Food Chemistry*, *102*, 889–897.

Eriksson, E., Koch, K., Tortoe, C., Akonor, T. P., & Oduro-Yeboah, C. (2014). Evaluation of the physical and sensory characteristics of bread produced from three varieties of cassava and wheat composite flours. *Food and Public Health*, *4*, 214–222.

Flander, L., Suortti, T., Katina, K., & Poutanen, K. (2011). Effects of wheat sourdough process on the quality of mixed oat-wheat bread. *LWT - Food Science and Technology*, *44*, 656–664.

Gill, S., Vasanthan, T., Ooraikul, B., & Rossnagal, B. (2002). Wheat bread quality as influenced by the substitution of waxy and regular barley flours in their native and cooked forms. *Journal of Cereal Science*, *36*, 239–251.

Hüttner, E. K., Bello, F. D., & Arendt, E. K. (2010). Rheological properties and bread making performance of commercial wholegrain oat flours. *Journal of Cereal Science*, *52*, 65–71.

Jiranuntakul, W., Puttanlek, C., Rungsardthong, V., Puncha-arnon, S., & Uttapap, D. (2011). Microstructural and physicochemical properties of heat-moisture treated waxy and normal starches. *Journal of Food Engineering*, *104*(2), 246–258.

Lee, C. J., Kim, Y., Choi, S. J., & Moon, T. W. (2012). Slowly digestible starch from heat-moisture treated waxy potato starch: Preparation, structural characteristics, and glucose response in mice. *Food Chemistry*, *133*(4), 1222–1229.

Miñarro, B., Albanell, E., Aguilar, N., Guamis, B., & Capellas, M. (2012). Effect of legume flours on baking characteristics of gluten-free bread. *Journal of Cereal Science*, *56*(2), 476–481.

Neill, G., Al-Muhtaseb, A. H., & Magee, T. R. a. (2012). Optimisation of time/temperature treatment, for heat treated soft wheat flour. *Journal of Food Engineering*, *113*(3), 422–426.

Rehman, S. U., Paterson, A., Hussain, S., Anjum Murtaza, M., & Mehmood, S. (2007). Influence of partial substitution of wheat flour with vetch (Lathyrus sativus L) flour on quality characteristics of doughnuts. *LWT - Food Science and Technology*, *40*(1), 73–82.

Ronda, F., Perez-Quirce, S., Lazaridou, A., & Biliaderis, C. G. (2015). Effect of barley and oat β-glucan concentrates on gluten-free rice-based doughs and bread characteristics. *Food Hydrocolloids*, *48*, 197–207.

Sun, Q., Han, Z., Wang, L., & Xiong, L. (2014). Physicochemical differences between sorghum starch and sorghum flour modified by heat-moisture treatment. *Food Chemistry*, *145*, 756–64.

Verdú, S., Ivorra, E., Sánchez, A. J., Barat, J. M., & Grau, R. (2015). Study of high strength wheat flours considering their physicochemical and rheological characterisation as well as fermentation capacity using SW-NIR imaging. *Journal of Cereal Science*, *62*, 31–37.

Verdú, S., Vásquez, F., Ivorra, E., Sánchez, A. J., Barat, J. M., & Grau, R. (2015). Physicochemical effects of chia (Salvia Hispanica) seed flour on each wheat bread-making process phase and product storage. *Journal of Cereal Science*, *65*, 67–73.

Whitehead, A., Beck, E. J., Tosh, S., & Wolever, T. M. S. (2014). Cholesterol-lowering effects of oat b -glucan : a meta-analysis of randomized controlled trials 1 – 4. *The American Journal Of Clinical Nutrition*, *100*, 1413–1421.

CAPITULO VII

Physicochemical effects of chia (Salvia Hispanica) seed flour on each wheat bread-making process phase and product storage

Journal of Cereal Science, Volume 65, September 2015, Pages 67-73
Samuel Verdú, Francisco Vásquez, Eugenio Ivorra, Antonio J. Sánchez, Jose M. Barat, Raúl Grau
Versión para tesis doctoral

Abstract

Some chia seed flour effects relating to different bread-making process phases and variables were studied by distinct image analysis and physicochemical techniques. Wheat flours with three different degrees of substitution (5%, 10% and 15%) were tested. In technological terms, the aim was to study the influence and properties of chia flour on several relevant parameters, such as pasting properties, growth kinetics and internal crumb structure during dough fermentation; and baking process, mass loss, water activity and texture profile of the end product during its storage. Some changes in pasting properties were observed. The effects obtained by image analysis techniques proved that addition of chia improved gas retention in dough and cut the time required to reach maximum dough development. A delay in hardness and water loss during storage of breads was also observed. Bread presented reduced water activity, and contained the same amount of moisture compared with the control. The mucilage provided by chia has properties that can explain these observed effects given the influence on water-holding capacity and its interactions with gluten proteins throughout the gluten matrix-forming process.

Keywords: Chia, bread-making process, image analysis, wheat flour

1. Introduction

Some relevant factors affect productivity in the cereal by-product industry due to changes between the properties and the behavior of the flour sort and other ingredients used in production phases. Flour features, such as flour origin and quality, cultivation and milling method, and cereal variety are some of the most influential factors. Variability conferred by raw materials directly affects the process and product variables (Cocchi et al. 2005), which are necessarily controlled to obtain high yields and homogeneous characteristics in both the production chain and product quality. Some of the most affected properties derive from the rheology of dough and batters, such as gas retention capacity, water interactions and flow behaviors. How different strategies act with these factors has been studied to solve the problems that appear in some phases of industrial processes (Ahlborn et al. 2005). Work has been done mainly in those cases in which flours present defects or low technological quality to reach the properties of reference products, such as wheat flour with a small amount of gluten, flours without gluten for gluten-free products, modifying properties during storage, etc. (Lazaridou et al. 2007). In relation to the above objectives, one of the most studied areas is the development of new ingredients, among which, several of the most important ones are compounds that are situated in any plant part, like grains, which improve gas retention in the dough matrix and water activity modification, among others (Houben et al. 2012). The nature of those compounds is diverse, but the most

influential ones can form hydrocolloid structures. Hydrocolloids can induce some structural changes in the main flour components from the bread-making process to product storage. So they are usually added to dough to improve its viscoelastic properties, as well as the structure, mouthfeel, acceptability and shelf life of bakery products (Ahlborn, et al. 2005). Hydrocolloids are used either alone or combined to achieve specific synergies between their respective functional properties. Numerous types of hydrocolloids are obtained from the flour of whole grains and have been analyzed in this approach to take advantage of the other active compounds and nutrients in these products (Del Rio et al. 2013). One grain with interesting properties for this area is chia seeds (*Salvia hispanica*). Chia is an annual herb of the *Labiatae* family and was one of the basic nourishments of Central American civilizations in pre-Columbian times (Ayerza & Coates, 2005). Some studies have shown the potential uses of chia based on its compositional profile (defatted chia seeds have 22% of fiber and 17% of protein). These contents are similar to those of other oilseeds currently used in the food industry (Cumby et al. 2008; Vázquez-Ovando et al., 2010). The consumption of chia provides numerous health benefits, such as a high content of oil, protein and bio-active peptides, antioxidants, minerals and dietary fiber (Ixtaina et al. 2008). Some works have been published with information about dough behavior and organoleptic acceptance, with degrees of substitution between 4-5% with both chia by-products and whole seed flour (Iglesias & Haros, 2013; Moreira et al.,

2013). This percentage of substitution is based on the daily bread intake recommended by the World Health Organization, which would result in considerably improved nutrient contribution if all bread consumed contained 5% of chia. Those results report interesting technological properties apart from nutritional improvement. The effect of high substitution degrees could be interesting from a technological application point of view for the development of new formulas based on gluten-free flours, and for possible improvements to different bread-making process phases. From this technological viewpoint, the most important component of these seeds is fiber content, which includes a polysaccharide gum with high-molecular-weight mucilage. It has been proposed that the structure of the basic mucilage unit is a tetrasaccharide with 4-O-methyl-a-D-glucoronopyranosyl residues which occurs in branches of β-D-xylopyranosyl in the main chain (Lin et al. 1994). This compound presents a high water-holding capacity and forms an active hydrocolloid. The work of Iglesias & Haros (2013) observed how this compound could improve the dough volume rate due to the formation of hydrophilic complexes between their ionic groups and proteins as gluten, which favors gluten matrix formation. For all these reasons, chia seeds present interesting features for testing some aspects of the bread-making process, and to evaluate their plausible applications in order to improve some of these aspects. Therefore, the purpose of the present study was to report further information about how substituting wheat flour for chia seed flour at the 5%, 10%

and 15% degrees affects some important technological features; e.g., pasting properties of flour mixtures; dough fermentation process; baking loss; physicochemical properties (texture profile, mass loss and water activity) during storage of the end product for 0, 1, 3 and 7 days.

2. Material and Methods

2.1. Raw materials and dough preparation

The commercial wheat flour used was obtained from a local producer (Molí del Picó-Harinas Segura S.L. Valencia, Spain) whose chemical composition was: 14.7±0.6% of proteins, 1.1±0.03% of fat, 14.5±0.5% of water, and 0.32±0.1 of ash (w.b). The alveographic parameters were also facilitated by the company, which were *P* = 94±2 (maximum pressure (mm)), *L* = 128±5 (extensibility (mm)), *W* = 392±11 (strength (J^{-4})) and 0.73 of *P/L*. Chia flour was obtained from a commercial black chia seed format (BIOCESTA S.L., Valencia Spain) by milling in a stainless steel grinder (Retsch GmbH, ZM 200, Haan, Germany) to obtain a particle size distribution as close to the used wheat flour as possible. The particle size of flours was measured 6 times by laser scattering in a Mastersizer 2000 (Malvern, Instruments, UK) equipped with a Scirocco dry powder unit. The results are expressed as a maximum size in µm at 10%, 50% and 90% (*d (0.1)*, *d (0.5)* and *d (0.9),* respectively) of the total volume of the analyzed particles as their averages (*D [4, 3]*). The wheat flour results were *d (0.1)* = 25.5±1.1, *d (0.5)* = 92.0±0.6, *d (0.9)* = 180.6±0.8 and D

[4, 3] = 99.4±1.2. The chia flour results were *d (0.1)* = 23.9±1.9, *d (0.5)* = 95.3±1.2, *d (0.9)* = 181.9±1.3 and *D [4, 3]* = 100.1±1.1. Chia flour contained 2±1% of proteins, 30.4±0.9% of fat, 8±0.3% of moisture and 4.1±0.8% of ash (w.b). Four flour mixtures, which presented 0%, 5%, 10% and 15% wheat flour substitution degrees for chia flour, were prepared to carry out the study.

The control formulation used to prepare dough was the following: 56% flour, 2% refined sunflower oil (maximum acidity 0.2º Koipesol Semillas, S.L., Spain), 2% commercial pressed yeast (*Saccharomyces cerevisiae*, Lesafre Ibérica, S. A., Spain), 4% white sugar (≥ 99.8% of saccharose, Azucarera Ebro, S.L., Spain), 1.5% salt (refined marine salt ≥ 97% NaCl, Salinera Española. S.A., Spain) and water 34.5%. This formulation slightly increased the amount of water, following degree of substitution, to 1% in the case of 15% mixture, due to the low moisture of chia to maintain a constant ratio between moisture (provided by wheat, chia and the added water) and dry matter (provided by wheat and chia), observed in the control sample (0.89 g water/g dry matter). Bread dough was made according to a closed process with no modifications between mixes to observe the effect on a possible continuous industrial process. The process was carried out by mixing all the ingredients in a food mixer (Thermomix® TM31, Vorwerk, Germany) according to the following method: in the first phase, liquid components (water and oil), sugar and NaCl were mixed for 4 minutes at 37 ºC. Pressed yeast was added in the next phase to be mixed at the same temperature for 30 seconds. Finally, flour was

added and mixed with the other ingredients according to a default bread dough mixing program, which provides homogeneous dough. The program system centers on mixing ingredients with random turns of the mixer helix in both directions (550 revolutions/minute) to obtain homogeneous dough. This process was applied for 4.5 minutes at 37 ºC. Then 450 g of dough were placed in the metal mold (8x8x30cm) for fermentation. Height was approximately 1 cm.

2.2. Characterization of flour mixing dough by a viscometer Rapid Viscosity Analyser (RVA)

The pasting properties of the flour mixtures were analysed using the viscosity profile obtained by the viscometer RVA (Rapid Visco Analyser Super 4, Newport Scientific). For this purpose, the method approved by AACC (America Association of Cereal Chemists), whose reference is "General Pasting Method for Wheat or Rye Flour of Starch Using the Rapid Visco Analyser. AACC 2000, number: 76-21"), was used. Samples of 3 g±0.01g were weighed and the amount of water incorporated was 25 g±0.01g. The test started at 50 °C and 960 RPM, and was slowed down to 160 RPM at 10 s. Temperature was maintained during the first minute. The temperature from 50 °C to 95 °C was increase during the next 4 minutes to reach 95 °C at minute 5 in a second step. The third step involved maintaining a temperature of 95 °C until minute 7.5. The fourth step was to lower the temperature to 50 °C, which was reached at minute 11. The last step

was to maintain a temperature of 50 °C until minute 13. Measurements were taken in triplicate.

2.3. Fermentation process and its continuous monitoring

The fermentation process was carried out in a chamber with controlled humidity and temperature (KBF720 Binder Tuttlingen, Germany). The conditions were 37 °C and 90% of Relative Humidity (RH). Dough growth evolution was monitored by a device installed and calibrated inside the chamber. This device was based on an image analysis of Structured Light (SL), following the method described previously by Ivorra et al. (2014). Only the points between mold edges were analyzed by this method. During the process, one picture per second was captured until the required analysis time according to the phase study. The 3D information calculated from each image during the process focused on maximum height (*H*: the maximum Z edge value) and transversal area (*A*: the integration of the Z-values along the X direction of the sample). Data acquisition and data processing were carried out using an own code developed in the Matlab computational environment (The Mathworks. Natick. Massachusetts, USA). The behavior of the dataset average during fermentation was modeled by the SL method, obtained from dough samples per mixture and adapted to the Gompertz prediction model. The Gompertz function is a nonlinear sigmoid growth function which

was developed by Gompertz (1825) to calculate the mortality rate of microorganisms. The equation is as follows:

$$A = a \cdot \exp((-\exp\,(\frac{V}{A} \cdot (Lt - t) + 1\,)) \quad (1)$$

where *t* is time, *A* is area during the process, α is the area observed during process, *V* is the maximum growth rate, and *Lt* represents the latency time before dough development begins. Model parameters were determined by a nonlinear regression procedure and were obtained by minimizing the sum of squares from prediction errors.

2.4. Study of internal dough structure in the fermentation phase

In order to study the chia effect on crumb evolution during the process, dough fermentation was interrupted at 25%, 50%, 75% and 100% compared to its maximum developing time (*Ft*). Thus the study of maximum fermentation development was firstly analyzed (until dough depletion). In each sample, dough was baked and sliced to be studied by 2D image segmentation. The baking process took place in an oven (Rotisserie, DeLonghi, Italy) at 180ºC for 30 minutes. Once baking finished, six 1 cm-thick slices were obtained from the center of the bread. In order to study crumbs, both sides of each slice were captured in a scanner (Aficio™ MP C300-Ricoh. Tokyo, Japan) to be

then analyzed by 2D image segmentation (Verdú et al., 2014; Datta et al. 2007; Esteller et al. 2006). Three bread products of each mixture and fermentation time were examined, which meant that 36 crumb images were obtained. Images were acquired at a resolution of 300 dpi. A black background was used in all the captures to improve contrast and to enhance both cell wall structure and porosity measurements.

2.5. Study of the end product

To study the effect of chia on several of the most relevant bread properties, various assays were carried out at different times before and after packing to test their evolution. Baking loss (ΔM_b) was first determined. In this phase, mass loss during the baking process was concluded by the difference between the pre-baking dough weight and the finished bread weight (both bread products were cooled at room temperature for 1 h). Then samples were packed in a low-density polyethylene bag, similar to that used in commercial presentations, and were stored under environmental conditions (23 ºC and 72% R.H. approximately). The assay was carried out for 1, 3 and 7 days of storage. Mass loss of whole breads, the texture profile analysis (*TPA*) and water activity (a_w) of crumbs were performed for each time.

Mass loss (ΔM_t) was analyzed by paying attention to the weight at the beginning and at each sampling time. *TPA* was performed

following the method used by Miñarro et al. (2012), where two 12.5 mm-thick cross-sectional slices were obtained from the center of each bread product. The texture profile analysis was carried out in a TA-TX2 texture analyzer (Stable Micro Systems, Surrey, UK). A 25kg load cell (35 mm diameter) was used. The assay speed was set at 1.7 mm/s to compress the bread crumb center to 50% of its previous height. The time between compressions was 5 s. The studied parameters were: hardness (*D*), springiness (*S*), cohesiveness (*C*), gumminess (*G*), chewiness (*Ch*) and resilience (*R*). Water activity of crumbs (a_w) was determined in an Aqualab® dew point hygrometer (DECAGÓN Aqualab CX-2, Pullman, WA, USA).

2.6 Statistical analysis

The results of pasting properties, fermentation parameters (*A, V, Ft*), bubble size and baking loss were studied by a one-way variance study (ANOVA). A multifactor ANOVA was used to study the main effects and interactions on the evolution of the parameters studied during storage (texture, mass loss and water activity). In those cases where the effect was significant (P-value < 0.05), the average was compared by Fisher's least significant difference (LSD).

3. Results and Discussion

3.1. Characterization of flour mixtures by Rapid Viscosity Analysis

The results of the pasting properties obtained by RVA and the profiles of the different mixtures samples are shown in Figure VII.1. The corresponding pasting parameters are summarized in Table VII.1. The pasting times of the samples lowered due to degree of chia substitution, and significant differences were observed for the 10% and 15% substitution mixtures. Peak viscosity presented an inverse behavior and became higher with increasing chia substitution, where the 10% and 15% mixtures continued to show significant differences compared to the control and 5% mixture despite the peak time presenting this inverse behavior. Trough, breakdown and setback also showed a clear increment with degree of substitution.

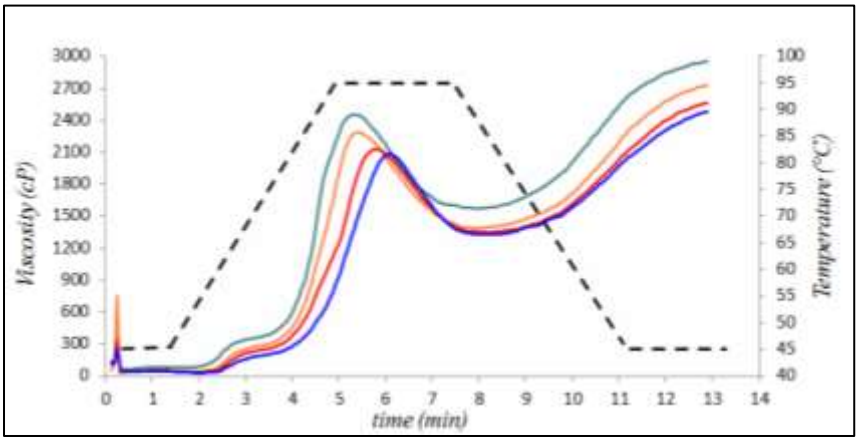

Figure VII.1. Pasting profile of control wheat flour –; 5% –; 10% –; 15% – of substitution, temperature – –

Initially, reduced water availability due to the presence of chia compounds should make starch gelatinization difficult. Thus the pasting temperature should present the opposite behavior to that observed in the results. One possible explanation is that chia mucilage, in combination with water and heat, produces increased viscosity at a lower temperature compared to starch. Therefore, the increase in viscosity at the beginning of the assay, at the 10% and 15% degrees of substitution could be attributed more to mucilage hydration than to starch gelatinization. The peak time results were also affected for the same reason, which lowered. This indicates a higher degree of substitution. Yet despite the reduction in peak time, peak viscosity increased with degree of substitution. These behaviors proved that chia components mainly affected the viscosity of mixtures, independently of wheat, because the degree of substitution incremented the viscosity level. Similarly, final viscosity was another parameter that showed considerable changes. This implies that the changes in pasting properties observed in the behaviors of the mixtures could be produced by chia seed mucilage. This component has a high water-holding capacity and hydration features (Inglett et al. 2014) and this phenomenon had no major influence on starch granule gelatinization. However, the rapid formation of hydrocolloids, when they came into contact with water, was the main factor responsible for the variations in the viscosity parameters observed.

Table VII.1. Pasting characteristics of different mixtures

% Substitutio	Pasting time	Peak viscosity	Trough	Breakdown	Final visc	Setback	Peak time
Control	68.5 ± 0.6 c	2245 ± 15 a	1421 ± 49 a	823 ± 10 a	2660 ± 56 a	1238 ± 10 a	6.1 ± 0.1c
5%	67.7 ± 0.1 c	2289 ± 98 a	1430 ± 14 a	859 ± 12 a	2738 ± 12 a	1308 ± 21 b	5.8 ± 0.1b
10%	66.1 ± 0.1 b	2472 ± 26 b	1530 ± 65 b	942 ± 4 b	2965 ± 58 b	1435 ± 70 c	5.5 ± 0.2a
15%	63.9 ± 0.6 a	2639 ± 91 c	1673 ± 10 c	966 ± 19 b	3173 ± 49 c	1500 ± 15 d	5.3 ± 0.1a

Different letter within columns means significant differences at $p \leq 0.05$

3.2. Fermentation process

Figure VII.2A shows the results obtained by the Gompertz fitting model of fermentation curves generated by a 3D device. The parameters obtained from each mixture are presented in Table VII.2. Maximum dough growth, represented by parameter *A*, did not present significant differences among samples, except for the 15% mixture, which was significantly higher than the rest.

Velocity features (*V*) were similar in the 5% and 10% mixtures. The control sample gave the lowest value, while the 15% mixture obtained the highest one, and both showed significant differences with the 5% and 10% mixtures. *Lt* (time latency) also presented significant differences between the control and mixtures, with values up to 3-fold lower than the chia mixtures. The control obtained the highest *Ft* (maximum development time) value, followed by the 5%, 10% and 15% mixtures in ascending order, and the differences among them were significant. The highest values in the 10% and 15% mixtures were for the average bubble size data (Table VII.2), where

these mixtures gave significant differences compared to the other samples at *Ft.*

In order to evaluate the influence of chia in the fermentation phase, the resultant data of the fermentation curves, which took the control curve as a reference, were studied. Thus the time when each mixture reached the same *A* value of the control was determined (*Ac*). This time factor was called *tAc*. Once each mixture *tAc* was obtained, it was calculated how long it took to reduce in each mixture to reach *Ac*. This parameter was called *ΔtAc*. The results showed that *tAc* reduced according to the increase in the degree of substitution. After analyzing the *ΔtAc* results, the 5% mixture reached 23.2% *Ac* faster than the control, 33.3% for the 10% mixture, while the 15% mixture obtained the highest value and reduced the time to 44.3%.

Table VII.2. Results of fermentation process characterization

			Control	5%	10%	15&
Curve parameters	A ($m^2.10^{-4}$)		12,9 ± 1,1 a	13,1 ± 1,2 a	13,5 ± 1,5 a	15,8 ± 0,9 b
	V ($m^2.10^{-4}$/min)		32,9 ± 3,5 a	45,4 ± 4,1 b	47,5 ± 2,4 b	50,9 ± 1,3 c
	Ft (min)		81 ± 3,2 b	77 ± 2,1 b	68 ± 3,1 a	65 ± 2,9 a
Bubble size ($m^2.10^{-6}$)	T1		1,1 ± 1,0 b	1,2 ± 1,3 b	1,8 ± 1,9 b	0,8 ± 0,97 a
	T2		3,7 ± 1,2 b	3,4 ± 1,4 b	5,0 ± 1,9 b	3,4 ± 1,06 a
	T3		4,1 ± 2,3 a	4,2 ± 2,0 a	7,1 ± 2,2 b	5,3 ± 1,44 a
	T4		4,9 ± 1,9 a	5,2 ± 2,0 a	7,7 ± 2,5 a	7,2 ± 1,78 a
Nº of bubbles/$m^2.10^{-4}$	T1		13,4 ± 1,0 a	13,2 ± 1,3 a	14,4 ± 1,9 b	13,0 ± 0,97 a
	T2		5,9 ± 1,2 a	8,2 ± 1,4 b	7,4 ± 1,9 b	10,5 ± 1,06 c
	T3		6,4 ± 2,3 b	6,9 ± 2,0 b	5,1 ± 2,2 a	7,5 ± 1,44 b
	T4		7,4 ± 1,9 a	7,5 ± 2,0 a	6,7 ± 2,5 a	7,5 ± 1,78 a
Time parameters comparing to control	tA_c (min)		81	72	59,1	46,2
	ΔtA_c (%)		-	11,1	30,4	43,0

Different letters within rows mean significant differences at $p \leq 0.05$

Several authors have reported studies about different chia flour properties, which have proven the improvement of gas retention in the dough matrix through variations in their pasting properties; for example, in products prepared with gluten-free flours (Moreira et al., 2013). Some changes in the rheological properties of dough resulted mainly from the polymeric structure of chia mucilage, whose capacity to form hydrocolloids increases water retention, and thus the surface tension of the matrix. This property could improve the volume of dough through the formation of hydrophilic complexes between their ionic groups and gluten proteins to favor the gluten matrix formation and, therefore, to help avoid gas from leaking (Iglesias & Haros, 2013).

Therefore, the improvement of gas retention could lead to increased growth velocity, and reaching *Ac* required less time. The 15% of degree of substitution, and probably higher degrees, could keep enough gas to overcome *Ac* for the same initial dough mass. Likewise, the effect of this property on bubble size was increased mechanical resistance to the matrix walls, which confers more porous matrix to the gluten network, and permits greater stability and further expansion during the fermentation process (Bárcenas & Rosell, 2005). Consequently, the structure coalescence delay took place, followed by collapsing dough.

The number of bubbles in the different mixtures was similar to that in the control. However for the highest substitution mixtures, 10% and 15%, bubble size was significantly larger at T4 (100% of dough

growth). Those results are in agreement with Iglesias & Haros (2013), whose study did not report differences in bubble size between the wheat flour control and the 5% mixture. However, the significantly larger bubble size in the 10% and 15% mixtures, and the fact that, at the same time, no differences were found in their number of bubbles $/m^2 \cdot 10^{-4}$, could explain their high *A* at *Ft* values in the other samples due to a reduced gas leak. Therefore some changes in crumb structure were observed from degrees of substitution above 5%, which also had a direct effect on *A*.

3.3. End product

3.3.1. Baking process phase

Figure VII.2B represents the middle increment of mass (ΔM_b) in % in relation to the baking process phase of each mixture at *tAc*. This baking-loss was due mainly to the water loss which resulted from heat treatment. The results show reduced baking loss when incrementing the degree of substitution. The 10% and 15% mixtures presented significant differences to the control, but not to the 5% mixture, and significant differences were found among them. The chia compounds property on water retention, as previously postulated by some authors, was also observed in this phase of the process. In line with this, the studies into chia mucilage by Muñoz et al. (2012) reported that it is able to hydrate 27 times its own weight. Likewise, the results obtained by Vázquez-Ovando et al. (2009), but

on a fiber-rich fraction of defatted chia, confirmed its good water-holding capacity, among other aspects.

In order to study the observed effect and the results based on the literature in detail, diverse parameters were calculated for the different compositional fractions of each mixture and bread product, and how the process affected them. Table VII.3 summarizes the calculated parameters and ratios. Firstly, although fat influenced several dough properties, the final dry matter without fat (*DMf)* of each mixture was calculated following the assays on matter balances by Vázquez-Ovando et al., (2009) as proteins, starch and other carbohydrates, such as fiber, are the main influential components of flour in terms of the interactions of dough in water (Wilhelm et al. 2005). In order to obtain an overview of the variations in this parameter with degree of substitution, the decrease in *%DMf* was calculated compared to the control flour. Thus the results showed that *DMf* lowered when degree of substitution increased and, therefore, the decrease in *%DMf* varied from 1.3% for the 5% mixture to 3.8% in the 15% mixture. Those variations were produced because chia flour has more than 10 times the amount of lipids compared to wheat flour and, consequently, due to a lower proportion of the remaining dry matter. Secondly, moisture of bread products was calculated (*Xw)*. It was observed how bread moisture augmented with an increasing degree of substitution. To link these two parameters, the grams of water contained in each bread product per gram of *DMf* (*g Water of bread / g DMf*) were calculated. The results

indicated that although there was less dry matter in highly substituted flour, water retention per gram rose when the degree of substitution was higher. Thus this last parameter was estimated as a % in relation to the control *(%gWater / g DMf increment).* The 15% mixture contained 80.9% ore water per gram of dry matter of flour mixture than the control flour. It was, followed by the 10% mixture with 64.7% and the 5% mixture with 26.4%. The contribution of chia to water retention in the matrix allowed baking loss to lower with the same g of water/ g of dry matter ratio of the control sample.

Table VII.3. Parameters of dry matter of flour mixtures and their effect on baking process.

%	*DMf*	*Xw of bread*	*g Water of bread / g DMf*	*%DMf reduced*	*%Xw increment*	*%gWater / g DMf increment*
Control	0.84	0.20 ± 0.01 a	0.10 ± 0.01 a	-	-	-
5%	0.83	0.21 ± 0.02 ab	0.12 ± 0.02 b	1.3	5.8	26.4
10%	0.82	0.22 ± 0.01 bc	0.16 ± 0.01 cd	2.5	13.5	64.7
15%	0.81	0.24 ± 0.00 c	0.18 ± 0.01 d	3.8	18.1	80.9

DMf : Fraction of dry matter without fat of each flour mixture. *Xw of bread*: moisture of bread after baking process. *g Water of bread / g DMf* : ratio between grams of water in bread per each gram of dry matter without fat of flour mixture. *%DMf reduced*: Reduction of dry matter without fat by the increase of % substitution compared to control flour. *%Xw increment*: Increment of moisture in bread after baking in each flour mixture compared to control flour. *% g Water / g DMf increment*: Increment of grams of water in bread per each gram of dry matter without fat of flour mixture compared to control flour. -Different letters within columns mean significant differences at $p \leq 0.05$.

3.3.2 Texture, mass loss and water activity of bread

End product package evolution over time was analyzed. All bread products were firstly fermented until *tAc* to evaluate differences with the control at the same degree of dough development. Table VII.4 shows the results of the mass loss and texture parameters of *TPA* at four different time points: days 0, 1, 3 and 7.

On day 0, hardness did not present any important difference between the control and the chia mixtures, nor on day 1. On day 3, high levels of hardness were observed for them all (more than 1400 g), where the highest value went to the control compared to the chia mixtures. After seven days, the hardness of the control increased to reach values of around 2600g, while the values of the chia mixtures were maintained from day 3 with no statistical differences. Significant differences were found for springiness between the 15% mixture and the other mixtures on day 3, between the 5% mixture and the other mixtures on day 0, and for the 5% and 15% mixtures on day 1. Cohesiveness presented significant differences for the 10% and 15% mixtures, principally on day 0. The chewiness of the 5% mixture obtained significantly lower values compared to the control for days 3 and 7, and the 10% and 15% mixtures presented a significantly high value on day 1 compared to the control. However, significant differences with lower values compared to the control on days 5 and 7 were observed. Obviously the fact that all the samples presented textural properties on day 3 is unfavorable for consumption from an

organoleptic point of view. However, the observation made until day 7 allowed us to note the effect of chia under extreme conditions.

Mass loss also differed between mixtures and control. From day 1 onward, the control lost the largest amount of water than the chia mixtures. Thus the control presented a mass loss of 2% on day 7 compared to the mass on day 0, while the chia 5%, 10% and 15% mixtures lost 0.7%, 0.6% and 0.5% respectively. A significant effect for the "storage day" main effect was observed for all the variables, except springiness. The "degree of substitution" main effect also had a significant effect, but only for hardness and a_w. The interactions between the main effects with a significant effect were observed in hardness, cohesiveness and a_w, although with a lower F-ratio compared to the main effects.

This effect could also derive from water-retention capacity of chia mucilage. Water in the bread matrix was better maintained in the mucilage structures, which made its outward leak difficult (Capitani et al. 2012). Furthermore, these high levels of moisture could allow to make water available to delay starch retrogadation and could, therefore, influence texture features. This could explain the differences among hardness, gumminess and chewiness throughout storage, and would agree with Bárcenas et al. (2005), whose results concluded that the incorporation of hydrocolloids into bread dough improves the crumb texture profile by reducing crumb hardness.

The moisture retention property could also be counterproductive from the standpoint of conservation features. So a decision was made to study this water availability with a water activity analysis. This parameter was studied because the sole determination of moisture content does not inform about the nature of water; that is, whether it is bound, free, inert or occluded (Mathlouthi, 2001). This is a critical factor that affects a product's shelf life, which controls food behavior during processing and storage (Anese et al. 1996; Yang & Paulson. 2000). Figure VII.2C shows the tendencies of the evolution of a_w and X_w during the storage time of mixtures.

Table VII.4. Results of end product analysis with time. Texture Profile Analysis (TPA) and mass-loss.

%	time (days)	Hardness(g)	Springiness	Cohesiveness	Gumminess	Chewiness	Mass-loss(%)
Contol	0	298.6 ± 22.1 a	1.0 ± 0.05 c	0.9 ± 0.01 a	2.6 ± 0.2 a	2.6 ± 0.1 a	-
	1	571.4 ± 139.7 b	9.0 ± 0.2 b	0.8 ± 0.03 b	4.3 ± 0.9 b	3.9 ± 1.4 b	1.6 ± 0.1 b
	3	1889.2 ± 210.3 d	1.0 ± 0.01 a	0.7 ± 0.04 cd	12.7 ± 1.4 e	12.0 ± 1.3 e	1.8 ± 0.03 c
	7	2630.4 ± 387.2 e	0.9 ± 0.03 a	0.6 ± 0.05 e	15.9 ± 2.1 f	14.7 ± 3.6 f	2.0 ± 0.05 d
5%	0	262.1 ± 22.7 a	1.0 ± 0.03 c	0.9 ± 0.01 a	1.4 ± 0.2 a	1.4 ± 0.2 a	-
	1	494.0 ± 37.7 b	0.8 ± 0.01 b	0.8 ± 0.02 b	3.9 ± 0.1 b	3.5 ± 0.2 b	0.52 ± 0.01 a
	3	1427.0 ± 85.2 c	0.9 ± 0.01 b	0.7 ± 0.01 d	9.5 ± 0.7 c	8.9 ± 0.7 bc	0.6 ± 0.01 a
	7	1325.6 ± 37.7 c	0.9 ± 0.01 a	0.6 ± 0.02 e	8.5 ± 0.1 c	7.6 ± 0.2 c	0.6 ± 0.01 a
10%	0	260.4 ± 10.8 a	1.0 ± 0.03 c	0.9 ± 0.01 b	2.2 ± 0.2 a	2.2 ± 0.1 a	-
	1	688.6 ± 73,0 b	0.9 ± 0.01 b	0.8 ± 0.02 bc	5.3 ± 0.9 bc	5.0 ± 0.9 c	0.5 ± 0.01 a
	3	1452.1 ± 89.1 c	0.9 ± 0.01 b	0.7 ± 0.01 d	10.1 ± 1.4 d	9.5 ± 0.5 d	0.5 ± 0.01 a
	7	1403.8 ± 176.1 c	0.9 ± 0.01 a	0.6 ± 0.02 e	9.1 ± 2.1 d	8.4 ± 0.7 d	0.6 ± 0.05 a
15%	0	360.7 ± 85.2 a	1.0 ± 0.01 c	0.9 ± 0.01 b	3,0 ± 0.7 a	3.0 ± 0.7 a	-
	1	688.32 ± 33.5 b	1.0 ± 0.03 b	0.8 ± 0.01 c	6.6 ± 0.4 c	6.5 ± 0.5 c	0.4 ± 0.01 a
	3	1457.1 ± 53,0 c	1.0 ± 0.03 a	0.7 ± 0.01 d	10.7 ± 0.4 d	10.1 ± 0.5 d	0.5 ± 0.01 a
	7	1481.9 ± 207.5 c	0.9 ± 0.09 a	0.7 ± 0.01 e	9.7 ± 1.3 d	9.1 ± 1.1 d	0.5 ± 0.02 a

Different letters within columns mean significant differences at $p \leq 0.05$.

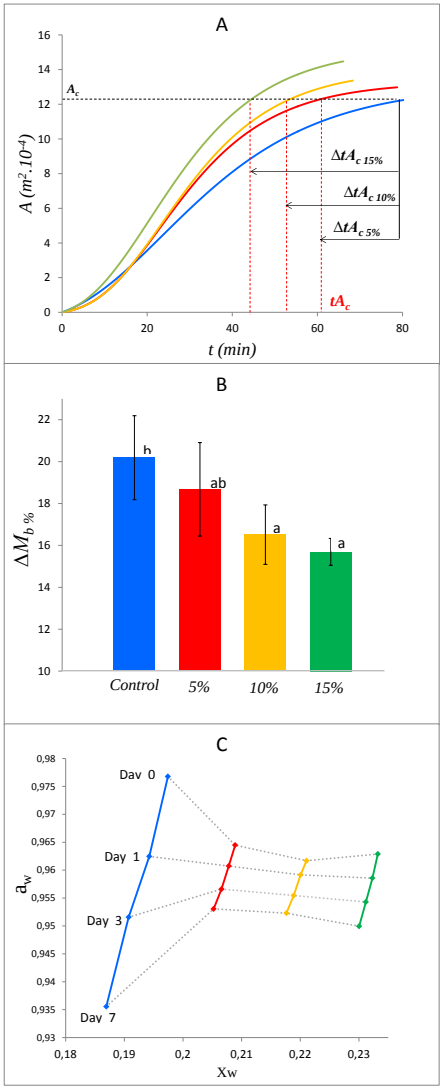

Figure VII.2. A: Fermentation curves resulted from Gompertz curve-fitting procedure. B: Percentage of mass-loss during baking process (ΔM_b). Bars express standard deviation and letters on the columns mean significant differences at $p \leq 0.05$. C: Evolution of X_w and a_w during the storage of breads. Colors mixtures correspond as follows: Control –;5% –; 10% –; 15% –; control area (*Ac*) – –; time to reach control area (*tAc*) – –.

From day 0 to 7, the a_w values showed marked differences between the control and chia mixtures. On day 0, the control had a higher a_w than the rest of the samples, which had between 5.8% and 13.1% less *Xw* (Table VII.3). The reduction of a_w for the control between the study time (days) was also more intense. The chia mixtures underwent some considerably slighter changes in this parameter throughout storage time. Finally, moisture reduction in the control brought about a sharper drop in the a_w values than the chia mixtures.

The most interesting phenomenon noted during storage was the property of chia to maintain the a_w levels close to an initial value despite the large amount of water they retained in the matrix. The results agree with previously reported studies by Muñoz et al. (2012), who observed the chia mucilage properties of increasing the linked water in matrix to further reduce the availability of it being used by other reactions, which could prolong storage time and, therefore, the shelf life.

4. Conclusions

The parameters of the different bread-making phases studied herein were modified by substituting wheat flour with chia seed flour. Those modifications can be associated with the effect of the hydrophilic compounds of chia, which has good water-holding capacity, and can develop stable hydrocolloids and improve the gluten net. These properties imply increased viscosity, mainly for 10% and 15% mixtures, and can amend the other pasting properties of flours. In

the same way, the kinetics of dough fermentation was modified to cut the time to reach the control's maximum volume to 40%. Bread properties also were modified and less water was lost during both the baking process and storage. Chia also had effect on degree of water activity, which remained the same despite containing a larger amount of crumb moisture. Texture presented the least influenced properties, and retardation of hardness at prolonged times was mainly observed. The results concluded that the degrees of substitution, up to 15%, could be used to improve not only nutritional provision, but also the technological properties of wheat flours. More studies are needed to evaluate consumers' acceptance of these degrees of substitution and the properties of each fraction of chia seed components.

5. Acknowledgements

We wish to thank the Polytechnic University of Valencia and the Generalitat Valenciana for the financial support they provided through the Projects PAID-05-011-2870 and GVPRE/2008/170, respectively.

6. Bibliography

Ahlborn, G. J., Pike, O. A., Hendrix, S. B., Hess, W. M., & Huber, C. S. (2005). Sensory, mechanical, and microscopic evaluation of

staling in low-protein and gluten-free breads. Cereal Chemistry, 82, 328-335.

Anese, M., Shtylla, I., Torreggiani, D., Maltini, E. (1996). Water activity and viscosity-relations with glass transition temperatures in model systems. Thermochimica Acta, 275, pp. 131–137.

Ayerza, R., Coates, W., (2005). Chia: Rediscovering a Forgotten Crop of the Aztecs. The University of Arizona Press, Tucson, AZ, USA.

Barcenas M. E, Rosell CA (2005) Effect of HPMC addition on the microstructure, quality and aging of wheat bread. Food Hydrocolloids. 19:1037–1043

Capitani, M.I., Spotorno, V., Nolasco, S.M.,. Tomás M.C. Physicochemical and functional characterization of by-products from chia (Salvia hispanica L.) seeds of Argentina. LWT - Food Science and Technology, 45 (2012) 94-102

Cocchi, M., , Corbellinib M, Focaa,G., Lucisanoc, M., Paganic, M. A., Lorenzo T. & Alessandro, U. (2005). Classification of bread wheat flours in different quality categories by awavelet-based feature selection/classification algorithm on NIR spectra. Analytica Chimica Acta, 544, 100–107.

Cumby, N., Zhong, Y., Naczk, M., & Shahidi, F. (2008). Antioxidant activity and waterholding capacity of canola protein hydrolysates. Food Chemistry, 109, 144-148.

Datta, A. K., Sahin, S., Sumnu, G., & Keskin, O. (2007). Porous media characterization of breads baked using novel heating modes. Journal of Food Engineering, 79, 106–116.

Del Rio, D., Rodriguez-Mateos, A., Spencer, J. P. E., Tognolini, M., Borges, G., & Crozier, A. (2013). Dietary (poly)phenolics in human health: Structures, bioavability, and evidence of protective effects against chronic diseases. Antioxidant & Redox Signaling, 18, 1818–1892.

Esteller, M. S., Zancanaro, O., Jr., Santos-Palmeira, C. N., & da Silva-Lannes, S. C. (2006).The effect of kefir addition on microstructure parameters on physical properties of porous white bread. European Food Research Technology, 222, 26–31.

Houben, A., Höchstötter, A., & Becker, T. (2012). Possibilities to increase the quality in gluten-free bread production: An overview. European Food Research Technology, 235, 195–208.

Iglesias-Puig, E, Haros, M. Evaluation of performance of dough and bread incorporating chia (Salvia hispanica L.). European Food Research Technology (2013) 237:865–874

Inglett G.E, Chen, D., Liu, S., Lee, S. Pasting and rheological properties of oat products dry-blended with ground chia seeds. LWT - Food Science and Technology 55 (2014) 148-156.

Ivorra, E., Verdú, S, Sánchez A., Barat, J.M., Grau., R. (2014). Continuous monitoring of bread dough fermentation using a 3D vision Structured Light technique. Journal of Food Engineering, 130 8–13

Ixtaina VY, Nolasco SM, Tomas MC (2008) Physical properties of chia (Salvia hispanica L.) seeds. Ind Crop Prod 28:286–293.

Lazaridou, A., Duta, D., Papageorgiou, M., Belc, N., & Biliaderis, C. G. (2007). Effects of hydrocolloids on dough rheology and bread quality parameters in gluten-free formulations. Journal of Food Engineering, 79, 1033-1047.

Lin KY, Daniel JR, Whistler RL (1994) Structure of chia seed polysaccharide exudate. Carbohyd Polym 23(1):13–18

Mathlouthi, M. (2001) Water content, water activity, water structure and stability of foodstuffs. Food Control, 12, pp. 409–417.

Miñarro B., Albanell , E., Aguilar , N., Guamis B., Capellas , M., (2013). Effect of legume flours on baking characteristics of gluten-free bread. Journal of Cereal Science ,56 (2012) 476-481.

Moreira, R., Chenlo, F., Torres, M.D. Effect of chia (Sativa hispanica L.) and hydrocolloids on the rheology of gluten-free doughs based on chestnut flour. LWT - Food Science and Technology 50 (2013) 160e166

Muñoz, L. A , Cobos, A., Diaz, O., Aguilera, J.M. Chia seeds: Microstructure, mucilage extraction and hydration. Journal of Food Engineering 108 (2012) 216–224.

Vázquez-Ovando, A., Rosado-Rubio, G., Chel-Guerrero, L., Betancur-Ancona, D., 2009. Physicochemical properties of a fibrous fraction from chia (Salvia hispanica L.). LWT – Food Science and Technology, 42 (1), 168–173.

Vázquez-Ovando, J. A., Rosado-Rubio, J. G., Chel-Guerrero, L. A., & Betancur- Ancona, D. A. (2010). Dry processing of chia (Salvia hispanica L.) flour: chemical and characterization of fiber and protein. CYTA Journal of Food, 8, 117-127.

Verdú, S., Ivorra, E., Sánchez, A.J., Barat, J.M., Grau, R. (2014). Relationship between fermentation behaviour, measured with a 3D vision Structured Light technique, and the internal structure of bread. Journal of Food Engineering, 146 (2015) 227–233.

Wilhelm, L.R., Suter, D.A, Brusewitz, G.H., 2005. Physical properties of food materials. Food and Process Engineering Technology.

American Society of Agricultural, St. Joseph, Michigan, pp. 23–52.

Yang, L., Paulson, A.T. (2000). Effects of lipids on mechanical and moisture barriers properties of edible gellan film. Food Research International, 33, pp. 571–578.

CONCLUSIONES GENERALES

Las técnicas de análisis de imagen hiperespectral y tridimensional han sido aplicadas con éxito en base al objetivo marcado en la tesis, pudiendo monitorizar, caracterizar y controlar determinadas operaciones específicas dentro de la industria harinera y de sus derivados, así como en el control de calidad de materia prima y producto acabado. La adaptación del sistema de análisis de imagen tridimensional, basado en luz estructurada, al proceso de fermentación de masas panarias permitió realizar un estudio de dicha operación mediante la monitorización en continuo del mismo. Dicha monitorización fue llevada a cabo en base a los descriptores específicos desarrollados, a partir de los cuales se consiguió una caracterización de la materia prima utilizada en relación a su comportamiento, así como sus implicaciones con respecto a las características de producto y su evolución durante la fermentación (CAPÍTULO I y II). El establecimiento de las bases de la monitorización mediante la técnica de luz estructurada permitió también estudiar el comportamiento de masas panarias reformuladas con la incorporación de nuevos ingredientes (CAPÍTULO VII). Por otra parte, la adaptación del sistema de análisis de imagen hiperespectral al tipo de muestra utilizada permitió caracterizar las harinas en base a sus espectros de reflectancia difusa. Se establecieron relaciones entre la información espectral y su composición fundamental, así como con el comportamiento durante el proceso de fermentación (CAPÍTULO III). Dichas relaciones fueron estudiadas y aplicadas a la inspección de harina y pan de trigo, con el objetivo de detectar cereales diferentes,

consiguiendo así una sensibilidad de detección de adulteraciones de hasta un 2.5% con avena, maíz y sorgo (CAPÍTULO IV). La información espectral también resultó útil en la caracterización del proceso de tratamiento térmico tanto en harinas de trigo para bizcochos (CAPÍTULO V) como en harina de avena para la elaboración de panes multicereal (CAPÍTULO VI), pudiendo relacionar los cambios observados con pautas de variación en el procesado posterior y características del producto final. Así pues, el resultado del trabajo es satisfactorio pues se han cumplido los objetivos establecidos en primera instancia. En su mayoría, los trabajos realizados son la base de otros que se están llevando a cabo en la actualidad, con el objetivo de avanzar en cada una de las aplicaciones específicas para poder ser implementadas de forma real en líneas de inspección y/o transformación industriales.

PUBLICACIONES REALIZADAS DURANTE EL PERIODO DE REALIZACIÓN DE LA TESIS DOCTORAL

REVISTAS INTERNACIONES

Samuel Verdú, Eugenio Ivorra, Antonio J. Sánchez, Jose M. Barat, Raúl Grau. Relationship between fermentation behavior, measured with a 3D vision Structured Light technique, and the internal structure of bread. Journal of Food Engineering, Volume 146, February 2015, Pages 227-233.

Samuel Verdú, Eugenio Ivorra, Antonio J. Sánchez, Joel Girón, Jose M. Barat, Raúl Grau. Comparison of TOF and SL techniques for in-line measurement of food item volume using animal and vegetable tissues. Food Control, Volume 33, Issue 1, September 2013, Pages 221-226.

Samuel Verdú, Francisco Vásquez, Eugenio Ivorra, Antonio J. Sánchez, Jose M. Barat, Raúl Grau. Physicochemical effects of chia (Salvia hispanica) seed flour on each wheat bread-making process phase and product storage. Journal of Cereal Science, Volume 65, September 2015, Pages 67-73.

Samuel Verdú, Francisco Vásquez, Raúl Grau, Eugenio Ivorra, Antonio J. Sánchez, José M. Barat. Detection of adulterations with different grains in wheat products based on the hyperspectral image technique: The specific cases of flour and bread. Food Control, Volume 62, April 2016, Pages 373-380.

Samuel Verdú, Eugenio Ivorra, Antonio J. Sánchez, José M. Barat, Raúl Grau. Study of high strength wheat flours considering their physicochemical and rheological characterisation as well as fermentation capacity using SW-NIR imaging. Journal of Cereal Science, Volume 62, March 2015, Pages 31-37.

Eugenio Ivorra, Samuel Verdú Amat, Antonio J. Sánchez, José M. Barat, Raúl Grau. Continuous monitoring of bread dough fermentation using a 3D vision Structured Light technique. Journal of Food Engineering, Volume 130, June 2014, Pages 8-13.

Eugenio Ivorra, Joel Girón, Antonio J. Sánchez, Samuel Verdú, Jose M. Barat, Raúl Grau Detection of expired vacuum-packed smoked salmon based on PLS-DA method using hyperspectral images. Journal of Food Engineering, Volume 117, Issue 3, August 2013, Pages 342-349.

Eugenio Ivorra, Antonio J. Sánchez, Samuel Verdú, José M. Barat, Raúl Grau. Shelf life prediction of expired vacuum-packed chilled smoked salmon based on a KNN tissue segmentation method using hyperspectral images. Journal of Food Engineering, In Press, Accepted Manuscript, Available online 9 January 2016.

CONGRESOS

Samuel Verdú, Francisco Vasquez, Eugenio Ivorra, Antonio Sánchez, José M. Barat, Raúl Grau. Uso del análisis de imagen hiperespectral SW-NIR para la detección de cereales diferentes de trigo en miga de pan. Congreso Internacional Seguridad Alimentaria ACOFESAL 2015. Universidad Politécnica de Valencia.

Samuel Verdú, Francisco Vasquez, Eugenio Ivorra, Antonio Sánchez, José M. Barat, Raúl Grau Use of 3D image analysis for studying the Salvia Hispaica flour effect over fermentation kinetics of wholemeal dough. 1st International Congress of students of Food Science and Technology. Universidad de Valencia

Samuel Verdú, Esteban Fuentes, Eugenio Ivorra, Joel Girón, Antonio Sánchez, José M. Barat, Raúl Grau. Estudio de la influencia de la incorporación de Salvia Hispanica en la panificación. 9 Congreso Iberoamericano de Ingeniería de Alimentos. Valencia 2014. Universidad Politécnica de Valencia.

Edwin Baldeón, Guadalupe Hernandez, Samuel Verdú, Miguel Alcañiz, Rafa Masot, José M. Barat, Raúl Grau. Determinación de la capacidad antioxidante de extractos de aliso (alnus acuminata) mediante la técnica de lengua electrónica voltamétrica. 9 Congreso Iberoamericano de Ingeniería de Alimentos. Valencia 2014. Universidad Politécnica de Valencia.

Joel Girón, Samuel Verdú, Eugenio Ivorra, Antonio J. Sánchez , Jose M. Barat, Raúl Grau. “Evaluación de la técnica de imagen multiespectral SW-NIR como posible herramienta para la clasificación de lomo de cerdo” . VII Congreso Español de Ingeniería de Alimentos. Ciudad real 2012. Universidad de Castilla la Mancha.